

Preface

The Institute of Chemical Technology in Prague will be celebrating the 50th anniversary of its existence as an independent technical university.

The Department of Mathematics has decided to contribute to this celebration by organizing a scientific colloquium. This Colloquium is the continuing tradition of the first and second Colloquium held in 1980 and 1986.

One of the purposes of this Colloquium is to promote contacts between mathematicians from Czech Republic and Slovak Republic teaching at Technical Universities namely Universities with orientation at chemical technology and chemical engineering.

We had the pleasure, at our Colloquia, to welcome several outstanding mathematicians from other countries. This year five guests from abroad (USA, Germany, Belgium, Slovak Republic) will participate as well, all of them dealing with nonlinear dynamical systems.

The printed Proceedings of this Colloquium can be divided into 4 parts. These simultaneously characterize the major activities of the Department of Mathematics ICT Prague:

- Theory and applications of nonlinear dynamical systems
- Methods of discrete mathematics (graphs, groups, number theory)
- Applications of statistical methods in chemistry, biology and medicine
- Education in mathematics at Technical Universities.

We would like to sincerely thank ICZ holding for sponsoring the publication of this Proceedings.

We would also like to thank chief editor of ICT Publishing House, Mrs. Eva Dibuszová, and coworkers for their suggestions and kind assistance.

Alois Klíč
Head of the Department of Mathematics

Organization

3rd Scientific Colloquium on Mathematics is organized by the Department of Mathematics of the Institute of Chemical Technology, Prague in cooperation with Center for Nonlinear Dynamics, Faculty of Chemical Engineering of the Institute of Chemical technology, Prague and with Center For Discrete Mathematics (DIMATIA), Charles University.

Organizing Committee

Organizing Chair: Drahoslava Janovská (Institute of Chemical Technology, Prague)
Member of Committee: Zdeňka Crkalová, Miroslava Dubcová, Alois Klíč, Milan Kubíček, Miloslav Loučka (Institute of Chemical Technology, Prague), Ivo Marek (Charles University, Prague), Daniel Turzík, Pavel Veselý (Institute of Chemical Technology, Prague)

List of Participants

G. Allgower Colorado State University, Fort Collins, USA
allgower@math.colostate.edu
V. Baláž Slovak Technical University, Bratislava
vbalaz@chelin.chtf.stuba.sk
P. Brunovský Comenius University in Bratislava
brunovsk@pc2.iam.fmph.uniba.sk
Z. Crkalová Institut of Chemical Technology, Prague
zdenka.crkalova@vscht.cz
M. Dellnitz University of Paderborn, Germany
dellnitz@uni-paderborn.de
J. Doležalová Technical University of Ostrava
jarmila.dolezalova@vsb.cz
M. Dubcová Institut of Chemical Technology, Prague
dubcovam@vscht.cz
W. Govaerts University of Gent, Belgium
Willy.Govaerts@rug.ac.be
R. Grepl Military Academy, Brno
V. Hapalová Institut of Chemical Technology, Prague
L. Heřmánek Institut of Chemical Technology, Prague
hermanekl@vscht.cz
Š. Hošková Military Academy, Brno
hoskova@scova.vabo.cz

D. Janovská	Institut of Chemical Technology, Prague janovskd@vscht.cz
V. Janovský	Faculty of Mathematics and Physics, Charles University, Prague janovsky@karlin.mff.cuni.cz
Š. Janská	Institut of Chemical Technology, Prague janskas@vscht.cz
F. Jaroš	Institut of Chemical Technology, Prague jarosf@vscht.cz
H. Kartáková	Institut of Chemical Technology, Prague
F. Katrnožka	Institut of Chemical Technology, Prague
A. Klíč	Institut of Chemical Technology, Prague klica@vscht.cz
M. Kohout	Institut of Chemical Technology, Prague kohoutm@tiger.vscht.cz
J. Kosek	Institut of Chemical Technology, Prague jkk@vscht.cz
P. Kreml	Technical University of Ostrava pavel.kreml@vsb.cz
J. Kubanová	University of Pardubice jana.kubanova@upce.cz
J. Kuben	Military Academy, Brno kuben@scova.vabo.cz
M. Kubíček	Institut of Chemical Technology, Prague kubicek@vscht.cz
V. Kvasnička	Slovak Technical University, Bratislava kvasnic@cvt.stuba.sk
B. Linda	University of Pardubice bohdan.linda@upce.cz
M. Loučka	Institut of Chemical Technology, Prague louckam@vscht.cz
M. Malec	Institut of Chemical Technology, Prague
I. Marek	Faculty of Mathematics and Physics, Charles University, Prague marek@ms.mff.cuni.cz
J. Maxová	Faculty of Mathematics and Physics, Charles University, Prague jana@kam.ms.mff.cuni.cz
J. Míčka	Institut of Chemical Technology, Prague
J. Nešetřil	Faculty of Mathematics and Physics, Charles University, Prague nesetril@ms.mff.cuni.cz
J. Pavlík	Institut of Chemical Technology, Prague pavlikp@vscht.cz
P. Pokorný	Institut of Chemical Technology, Prague pavel.pokorny@vscht.cz

Š. Porubský	Institut of Chemical Technology, Prague Stefan.Porubsky@vscht.cz
J. Pospíchal	Slovak Technical University, Bratislava pospich@cvt.stuba.sk
R. Potůček	Military Academy, Brno radovan.potucek@vabo.cz
M. Šabo	Slovak Technical University, Bratislava sabo@cvt.stuba.sk
I. Schreiber	Institut of Chemical Technology, Prague schrig@vscht.cz
H. Schwetlick	Institut für Numerische Mathematik, Technische Universität Dresden, Germany schwetlick@math.tu-dresden.de
B. Šikulová	Military Academy, Brno bela.sikulova@scova.vabo.cz
J. Taufer	Czech Technical University in Prague taufer@fd.cvut.cz
D. Turzík	Institut of Chemical Technology, Prague turzikd@vscht.cz
H. Vaníčková	Institut of Chemical Technology, Prague
P. Veselý	Institut of Chemical Technology, Prague veselyp@vscht.cz
Š. Varga	Slovak Technical University, Bratislava varga@cvt.stuba.sk

Contents

A two - parameter numerical study of the neuron model of Plant

W. Govaerts and A. Dhooge

Department of Applied Mathematics and Computer Science, University of Gent,
Krijgslaan 281 - S9, B - 9000 Gent, Belgium

Abstract We study numerically a model of R. E. Plant for the R - 15 pacemaker neuron of Aplysia, the sea hare. This model exhibits a periodically spiking behaviour in a relevant range of two parameters. In this two - dimensional range the behaviour changes continuously, except for a number of tiny regions, called bifurcation islands. In these islands the dynamic behaviour is much more complicated. We locate the islands numerically and compute the bifurcation phenomena, in particular fold bifurcations and period - doubling bifurcations. Such calculations are clearly near the limits of computability.

1 Introduction

The study of models for the electrochemical activity of neurons is a challenge for mathematicians working in dynamical systems and bifurcation theory. The highly nonlinear response of nerve cells indeed allows a complicated spiking and bursting behaviour that is very sensitive to parameter changes.

It is generally recognized that spiking and bursting are related to the presence of slow and fast variables. This is implicit in the qualitative explanations of these phenomena. The idea was worked out especially well in [17]. For a good introduction see [22]. Mathematically this is studied in the framework of *singularly perturbed problems*, see e.g. [9] and references in that paper.

Many authors have studied the relation between the form of the bursts (maximal spike value, length of the interspike intervals) and the bifurcations through which the bursts are generated. An extensive discussion can be found in [11]. The transition from n to $n + 1$ spikes was studied in [1] in a model with an external forcing term. A detailed study of a model of an excitable membrane is given in [19]. It is shown that the transition may either be continuous, in which case the period of the bursting solution increases significantly and then decreases again, or it may give rise to chaotic dynamics.

In a sequel to this, [20] discusses the transition from bursting to continuous spiking.

An interesting feature of several neural models is the presence of so - called *bifurcation islands* in parameter space. This means that small, well - located regions are found where many bifurcations are very close. This includes folds, cascades of period doubling bifurcations and homoclinic orbits. Moreover, the

location of these islands presents obvious regularities. Such islands were also found in non - neural models [12], [21]. From a mathematical point of view they seem to be related to the unfoldings of higher codimension homoclinic orbits and not necessarily related to the presence of fast and slow dynamics. See [21], [15].

Numerically, spiking and bursting lead to stiff differential equations and difficult boundary value problems. The computation of bifurcation points in dynamical systems therefore is an essential tool in the study of neural models. The sophisticated software tools available nowadays allow to describe and compute many of the simpler phenomena that are common in neural models; for the more complicated phenomena a lot remains to be done. Recent attempts include the use of high degree Taylor expansions and automatic differentiation [2].

The computation of periodic orbits and the continuation of such orbits as parameters change is the main entrance to the study of the dynamics of neural models. Stable periodic orbits can lose their stability in three different ways (fold, flip and Neimark - Sacker); they can disappear entirely in many other ways. For an informal numerically - oriented discussion of the latter possibilities see [9]. Recently, the interest in the *blue sky catastrophe* as a possible way of terminating a branch of periodic orbits was revived [18].

For background on dynamical systems theory we refer to [7] and [13]. For numerical methods for bifurcations from dynamical equilibria see [5].

The contribution of the present paper is modest : a particular model (due to R. E. Plant) is studied numerically and compared with other models. We show how to find the bifurcation islands and, partially, how to compute their boundaries. We draw several practical conclusions with respect to the understanding of the interesting dynamics of the model and to its efficient numerical handling.

2 A brief review of the AB - neuron model

The **Anterior Burster** neuron of the stomatogastric ganglion of the spiny lobster *Panulirus interruptus* is a conditional bursting neuron. It presents several characteristic patterns of rhythmic activity, including bursting oscillations, periodic action potentials and slow oscillations without action potentials.

A two - parameter bifurcation study of the AB - neuron was performed in [8], using a six - variable dynamical systems model. The model contains six channels, three of which are similar to those of the classical Hodgkin - Huxley model [10]. One of the additions is a new potassium channel, called the *A* - channel and modelled similarly to the sodium channel in the Hodgkin - Huxley model but with a large maximal conductance g_A . Next there are two calcium - activated channels, namely a calcium and a potassium channel, with maximal conductances g_{Ca} and g_{KCa} respectively.

The state variables are v, c, n, h, z, h_A . Here v denotes the potential difference across the membrane and n, h, z, h_A are gating variables related to the conductances of the ion channels. The slow variable c is a measure for the calcium concentration in the AB - neuron. The full equations are given in the Appendix.

In [8] the parameters g_{KCa} and g_A are the bifurcation parameters. Figure 1 (drawn by using CONTENT [14]) represents the most interesting region in (g_{KCa}, g_A) - space. The cusp - like curve in the upper left quadrant that ends in the point denoted CP (for "Cusp") is a curve of fold points. The other curves in Figure 1 are, in fact, all part of one curve of Hopf points. This curve intersects itself in a DH (Double Hopf) point with two different pairs of pure imaginary eigenvalues. The periodic orbits born along the Hopf curve are stable between the GH (Generalized Hopf) points at approximately (0.38, 83.8) and (0.30, 50.7) on the one hand, and between the GH point at approximately (0.27, 62.6) and the DH point on the other hand.

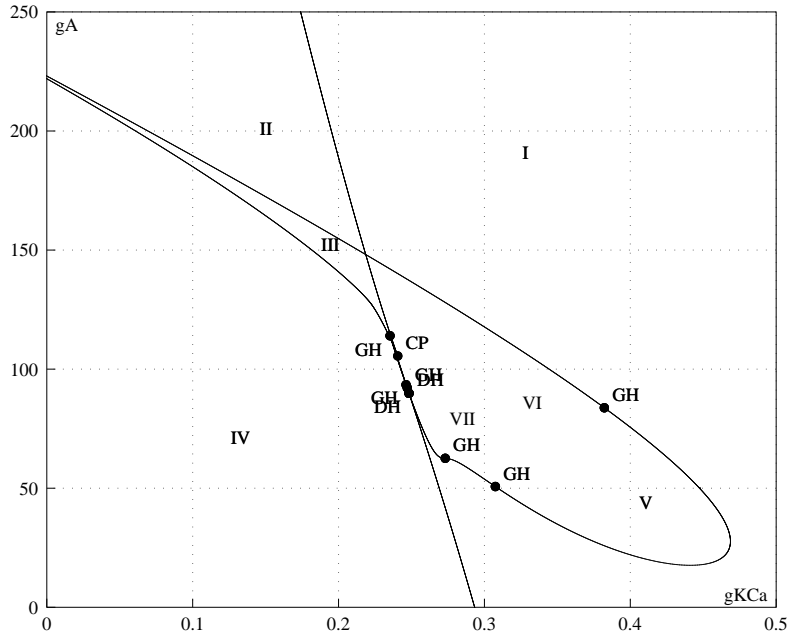


Figure 1: The AB neuron : regions with different dynamic behaviour.

The symbols I - VII in Figure 1 denote regions with specific types of dynamic behaviour :

I : quiescent, i.e. stable steady states.

II : 1 stable steady state, 2 unstable steady states, action potentials.

III : 3 unstable steady states, action potentials.

IV : 1 unstable steady state, action potentials.

V : 1 unstable steady state, slow oscillations.

VI : 1 unstable steady state, bursting behaviour.

VII : 1 unstable steady state, irregular (chaotic ?) behaviour.

The boundaries of the regions I, II, III are those suggested by Figure 1. The regions IV, V, VI and VII together fill the rest of the picture but the boundaries between any two of them are not on the picture; these boundaries are curves of bifurcations of periodic orbits and their precise nature requires further investigations.

The number of spikes in region VI increases roughly from lower right to upper left, starting with a single spike per burst and increasing to many. In Figure 2 we give a picture of a periodic bursting case with four spikes. The parameter values are $g_{KC_a} = 0.321606$, $g_A = 77.95$.

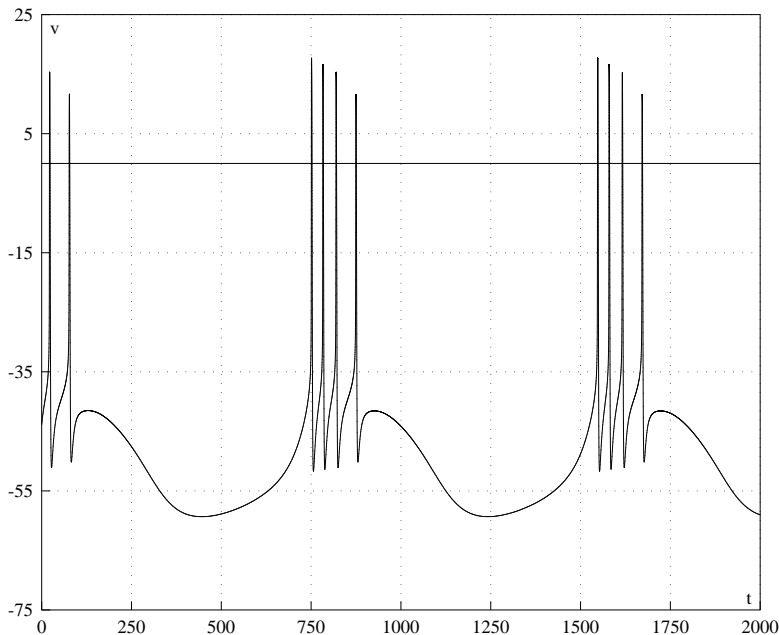


Figure 2: Periodic bursting in the AB neuron, $g_{KC_a} = 0.321606$, $g_K = 77.95$

The results on spiking and bursting in [8] were obtained by simulation, i.e. time integration. It is found that region VI consists of narrow, nearly parallel stripes in which the number of spikes is fixed. It is not too clear what the boundaries between the stripes represent mathematically; anyway the convergence to stable periodic orbits is difficult near these boundaries.

The software packages AUTO [3] and CONTENT [14] allow to compute periodic orbits as periodic boundary value problems. In [6] the transition from region V to region VI, as indicated in Figure 1 is studied by fixing $g_A = 56.25$ and following with CONTENT the curve of periodic orbits that originates at the Hopf curve in Figure 1 for g_{KC_a} approximately equal to 0.45; g_{KC_a} is the free parameter along this curve. For $g_{KC_a} = 0.386$ we find a periodic orbit with no spikes. For $g_{KC_a} = 0.382$ the orbit has a single spike.

While following the curve of periodic orbits for decreasing values of g_{KC_a} , CONTENT discovers several bifurcation points between values $g_{KC_a} = 0.386$ and $g_{KC_a} = 0.382$. The following array gives the values of g_{KC_a} and the correspond-

ing bifurcations.

$$\begin{aligned}
 0.3851913 &: LP \\
 0.3851987 &: NS \\
 0.3851987 &: LP \\
 0.3851984 &: PD \\
 0.3836543 &: PD
 \end{aligned} \tag{1}$$

Here LP denotes a Limit Point of Cycles (generically a turning point), NS a Neimark - Sacker (torus) bifurcation and PD a period - doubling (flip) bifurcation. The periodic orbit is initially stable while g_{KCa} decreases from 0.386 to 0.3851913 (the first LP point). There it loses stability and g_{KCa} increases until the second LP point is reached. Very close to the second LP point there is in addition an NS point. After the second LP point g_{KCa} decreases again and for $g_{KCa} = 0.3851984$ the first PD point is reached. The orbit regains stability at the second PD point at $g_{KCa} = 0.3836543$. So it is unstable between the first and last values for g_{KCa} given in (1). On the other hand, there is another curve of periodic orbits, with nearly double period, between the two PD points in (1).

In the region where the second spike is developed a remarkably similar series of bifurcation points is found. The preceding computations lead to an interesting conclusion. The new spikes in the bursting process (at least the first and second spikes) evolve gradually from the smooth part of the orbits but this happens after the orbits have lost their stability. They regain stability when the new spike is fully developed. In the intermediate regions the stability is partly taken over by other periodic orbits with spikes; in some small parameter ranges the two stable periodic orbits may coexist. Also, irregular (chaotic?) behaviour is found in small parameter ranges.

In Figure 3 we present the stable periodic orbit that exists for $g_{KCa} = 0.361194$ and is found by simple orbit integration after the transients have died out. This is clearly a period - doubled orbit; interestingly it presents alternating bursts with one and with two spikes. A similar phenomenon was remarked already in [16].

3 The model of Plant

3.1 The equations

This model has evolved over a sequence of studies motivated by experimental data from the R - 15 pacemaker neuron of Aplysia, the sea hare. This is a genus of large sluglike mollusks, often colorful, with finlike swimming lobes on the foot, four tentacles and a rudimentary internal test; some forms emit dark fluid when disturbed.

A model was studied in [16] and further used in [17] in their dissection of the dynamical system in a fast and a slow process to explain bursting. The solution set of the fast subsystem is studied with the slow variables treated as parameters.

The model in [16] was used in numerical studies of bursting in [16] and [4]. It contains five state variables V, x_T, x_K, y_I, c and the dynamic equations are given by

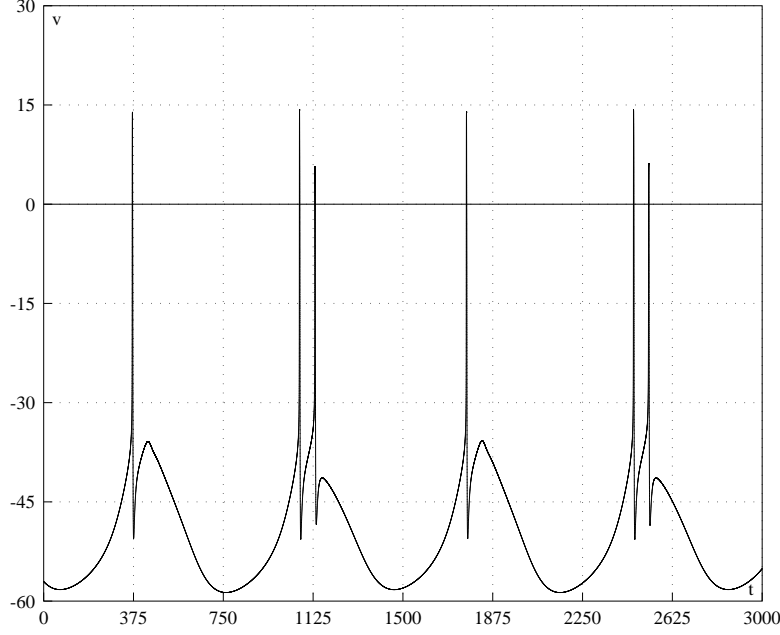


Figure 3: A stable periodic orbit with two bursts, $g_{KC_a} = 0.361194$, $g_A = 56.25$.

$$\begin{aligned}
\dot{V} &= (g_I s_I(V)^3 y_I + g_T x_T)(V_I - V) + \\
&\quad (g_K x_K^4 + \frac{g_{PC}}{K_P + c})(V_K - V) + \\
&\quad g_L(V_L - V) \\
\dot{x}_T &= \frac{s_T(V) - x_T}{\zeta \tau_{xT}} \\
\dot{x}_K &= \frac{s_K(V) - x_K}{\zeta \tau_{xK}(V)} \\
\dot{y}_I &= \frac{z_I(V) - y_I}{\tau_{yI}(V)} \\
\dot{c} &= v\rho(K_c x_T(V_{C_a} - V) - c).
\end{aligned} \tag{2}$$

Here $V_I = 30$, $V_K = -75$, $V_{C_a} = 140$ and $V_L = -40$ are the equilibrium potentials. Other parameters are $g_K = 0.3$, $g_P = 0.03$, $K_P = 0.5$, $g_L = 0.003$, $\tau_{xT} = 235$, $\zeta = 1$, $K_c = 0.0085$, $\rho = 0.0003$.

We further define

$$a = \frac{V_{Na}^H - V_K^H}{V_I - V_K}, \quad b = \frac{V_{Na}^H V_K - V_I V_K^H}{V_I - V_K}$$

where $V_{Na}^H = 115$, $V_K^H = -12$ are the Hodgkin - Huxley equilibrium potentials. Setting $V_s = aV + b$ we define the auxiliary functions

$$\alpha_m(V) = 0.1 \frac{50 - V_s}{e^{(50 - V_s)/10} - 1}, \quad \beta_m(V) = 4e^{\frac{25 - V_s}{18}},$$

$$\alpha_n(V) = \frac{0.01(55 - V_s)}{e^{(55-V_s)/10} - 1}, \quad \beta_n(V) = 0.125e^{\frac{45-V_s}{80}},$$

$$\alpha_h(V) = 0.07e^{\frac{25-V_s}{20}}, \quad \beta_h(V) = \frac{1}{e^{(55-V_s)/10} + 1}.$$

The voltage - dependent functions in (2) are

$$s_I(V) = \frac{\alpha_m(V)}{\alpha_m(V) + \beta_m(V)}, \quad s_T(V) = \frac{1}{e^{0.15(-50-V)} + 1},$$

$$s_K(V) = \frac{\alpha_n(V)}{\alpha_n(V) + \beta_n(V)}, \quad \tau_{xK}(V) = \frac{12.5}{\alpha_n(V) + \beta_n(V)},$$

$$z_I(V) = \frac{\alpha_h(V)}{\alpha_h(V) + \beta_h(V)}, \quad \tau_{yI}(V) = \frac{12.5}{\alpha_h(V) + \beta_h(V)}.$$

In this model c is a slow variable; the other variables are fast. We note that there are two sodium channels, a fast one with maximal conductance g_I and a slow one with maximal conductance g_T . In our study g_I, g_T will be the bifurcation parameters.

The model of Plant presents a bursting behaviour. Specifically, Plant [16] describes a bifurcation study in which $g_T = 0.01$ and g_I is the bifurcation parameter. For $g_I = 0$ the system has a periodic orbit without spikes; the spikes gradually develop for increasing values of g_I . The study is repeated with AUTO [3] by Doedel in [4] and provided as a demonstration example in AUTO. Up to four spikes appear in the bursts before the periodic orbit ends in a homoclinic bifurcation. The transition from n to $n + 1$ spikes occurs continuously along an unstable branch. The loss and gain of stability is accompanied by cascades of period - doubling bifurcations. There is a small interval where the original periodic orbit is unstable and the period doubled orbit is stable. There is an even smaller interval where both are stable simultaneously and there is also a small interval where none of them is stable. For practical purposes, the g_I - interval between 0 and the parameter value of the homoclinic orbit is divided into 5 intervals characterized by a fixed number of spikes; these interval are separated by tiny intervals in which the dynamic behaviour is more complicated and which are characterized by the presence of limit point and period doubling bifurcations.

3.2 The two - parameter picture

We now describe a two - parameter bifurcation study with g_I and g_T as free parameters. A basic understanding is obtained by repeating the experiment in [4] for a number of nearby values of g_T , in fact for $g_T = 0.01 + 0.0101r$, $r = 0, 1, \dots, 9$. In each case a number of bifurcation islands is crossed and the continuation ends when a homoclinic orbit is reached. As noted in [4] these computations are near the limits of computability. It is necessary to work with a large number of mesh intervals ($ntst = 200$) in every orbit and many collocation points ($ncol = 7$) in each interval. In Figure 4 each dot indicates the first bifurcation point encountered on a general bifurcation island (in nearly all, but not all cases an LP

- point). The diamonds indicate the cases in which the main branch contains a homoclinic orbit. The bifurcation islands form long thin stripes that are bounded on the left side (i.e. all bifurcations disappear). They consist of two parts. Their left (upper) part does not contain homoclinic orbits on the main branch. Let us call it the G - (general) part. Their right (lower) part does. Let us call this the H - (homoclinic) part.

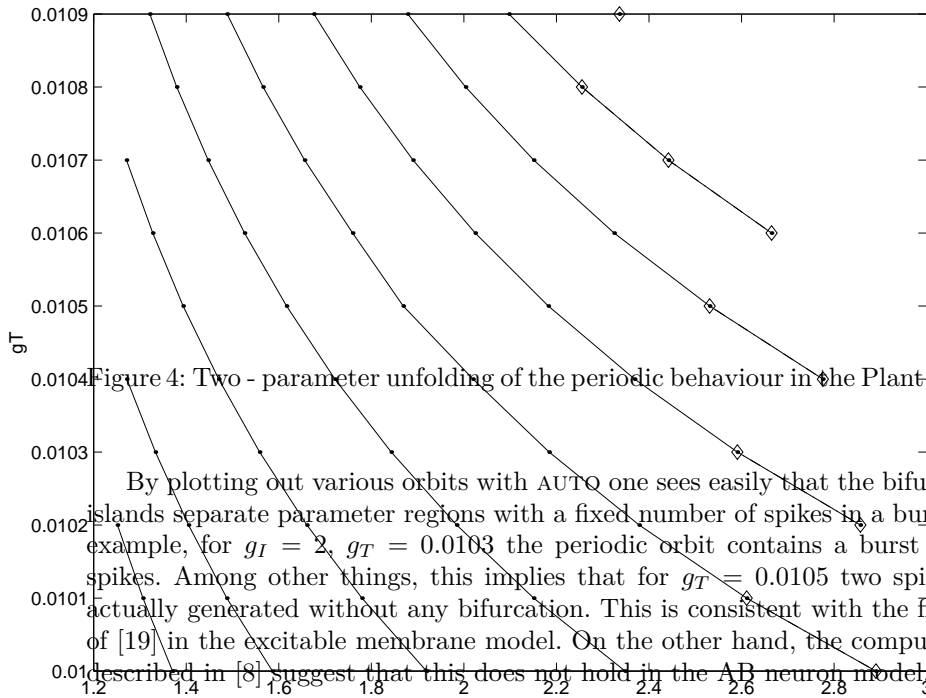


Figure 4: Two - parameter unfolding of the periodic behaviour in the Plant model.

By plotting out various orbits with AUTO one sees easily that the bifurcation islands separate parameter regions with a fixed number of spikes in a burst. For example, for $g_I = 2$, $g_T = 0.0103$ the periodic orbit contains a burst with 4 spikes. Among other things, this implies that for $g_T = 0.0105$ two spikes are actually generated without any bifurcation. This is consistent with the findings of [19] in the excitable membrane model. On the other hand, the computations described in [8] suggest that this does not hold in the AB neuron model.

The width of the islands is not uniform; it generally increases with increasing values of g_I but does not seem to depend sensitively on g_T . In Table 1 the all bifurcations found for $g_T = 0.0106$ and corresponding values of g_I are given. The

	LP	LP	PD
Island1	1.327585	1.327546	1.328431
Island2	1.525935	1.524596	1.528061
Island3	1.759647	1.752833	1.763818
Island4	2.024667	2.007976	2.031372
Island5	2.324688	2.298980	2.334119
Homoclinic	2.664931		

Table 1: Bifurcations found for $g_T = 0.0106$.

exact boundaries of the islands and the separation between the G and the H parts are not in Figure 4; computation of these is another, hard task (cf. §3.3). Nevertheless some conclusions can be drawn.

First, it is possible to let g_I and g_T depend on a single parameter s so that the point $(g_I(s), g_T(s))$ navigates in Figure 4 between two bifurcation islands with a fixed number of spikes and without ever losing stability or meeting a bifurcation point.

In the above experiments most of the computing time is spent while crossing the islands. So a strategy for avoiding the islands is also of numerical interest if the computation of the periodic orbits outside the islands is the main objective. This is a reasonable assumption because the islands contain cascades of period doubling bifurcations and dynamic behaviour that is chaotic for all practical purposes.

Second, by a similar strategy it is possible to compute periodic orbits, say for $g_T = 0.1$, to the right of the homoclinic orbit by circumnavigating the homoclinic barrier of the H - parts of the islands. This is an obvious advantage of the two - parameter approach. It may also be important in a numerical study of the exact nature of the homoclinic bifurcation.

3.3 The bifurcation islands

In [19] it is noted that in the case of a continuous transition from n to $n+1$ spikes the period of the bursting solution increases significantly and then decreases again. It turns out that a similar phenomenon can be found in the Plant model while crossing the bifurcation islands. To illustrate this we present in Table 2 some data for the case $g_T = 0.0105$ (type, value of g_I and period are given). A close inspection of the more detailed output of AUTO confirms the guess that in the second, third and fourth bifurcation islands the period attains a local maximum in the second LP point. The first bifurcation island is an exception : the period is then close to a local minimum but clearly distinct from it. From Table 2 it is also clear that the rise of the period increases with g_I .

The behaviour of the critical eigenvalue near the first LP point in each island is what is to be expected, i.e. it moves smoothly from values less than 1 to values greater than 1. Similarly, in each PD point it moves smoothly from values less than -1 to values greater than -1 .

On the other hand, the bifurcation behaviour near the second LP point of each island requires further investigation. In each case the critical multiplier

Type	g_I	Period
LP	1.393632	$1.065224E + 4$
LP	1.393345	$1.064764E + 4$
PD	1.394848	$1.067611E + 4$
LP	1.616700	$1.077235E + 4$
LP	1.613841	$1.079117E + 4$
PD	1.619519	$1.078832E + 4$
LP	1.879804	$1.094704E + 4$
LP	1.869031	$1.131077E + 4$
PD	1.884961	$1.092101E + 4$
LP	2.182518	$1.117894E + 4$
LP	2.161429	$1.322351E + 4$
PD	2.190399	$1.108153E + 4$

Table 2: Bifurcations found for $g_T = 0.0105$ (omitting the LP point that precedes the homoclinic orbit).

behaves in an erratic way near this point, moving from values greater than 1 to values less than -1 . For example, near the LP point at $g_I = 1.869031$ it moves from $1.132975E+6$ to $-1.071468E+6$ in the next (very close) continuation point. This points to numerical difficulties caused by the presence of a more complicated bifurcation. This is confirmed by a sketch drawn in [3] that suggests that either the LP point coincides with a PD point or is very close to it. We recall that in a similar situation in the AB neuron model two PD points were found that are connected by a period - doubled orbit [6].

Computing the boundaries of the islands and the separation between the G and the H parts is an obvious challenge. The computations in §3.2 suggest that the boundaries are formed by curves of LP points or PD points. We did some computational experiments, starting from bifurcation points found for $g_T = 0.0105$. Starting from the first LP point on this curve ($g_I = 1.393632$) we were able to continue numerically (using AUTO) the curve of LP points in the direction of increasing values of g_T and find the first LP point for $g_T = 0.0106$. The continuation broke down before the value $g_T = 0.0107$ was reached. This is not surprising because the first bifurcation island for $g_T = 0.0107$ contains only two PD points.

In the opposite direction we found the first LP points for $g_T = 0.0104, 0.0103, 0.0102, 0.0101, 0.01$. It was also possible to continue numerically the second LP point ($g_I = 1.393345$).

These computations took many hours on a SUN Ultra - 5 workstation. The total computing time for the results in Figure 4 was approximately 120 hours.

We were not successful when trying the numerical continuation of an LP point on the fourth bifurcation island crossed for $g_T = 0.0105$. Such tasks probably need even higher number of mesh intervals and more accurate computations and must be near the limits of computability.

Appendix. The equations of the AB - neuron model are given by

$$\begin{aligned}
\dot{v} &= -\frac{1}{C_m}(g_{Na}m^3h(v-v_{Na}) + g_{Ca}\frac{z}{0.5+c}(v-v_{Ca}) + g_Kn^4(v-v_K) + \\
&\quad g_{KCa}\frac{c}{0.5+c}(v-v_K) + g_Am_A^3h_A(v-v_K) + g_l(v-v_l)) + \frac{1}{C_m}I_{ext} \\
\dot{c} &= \rho\left(\frac{k_{Ca}z(v_{Ca}-v)}{1+2c} - c\right) \\
\dot{n} &= \lambda_n(a_n(1-n) - b_n n) \\
\dot{h} &= \lambda_h(a_h(1-h) - b_h h) \\
\dot{z} &= \frac{z_v - z}{\tau_z} \\
\dot{h}_A &= (h_{A_i} - h_A)k_A
\end{aligned} \tag{3}$$

where

$$\begin{aligned}
a_m &= \frac{\frac{127}{105}v + \frac{201}{7}}{10 - 10e^{-\frac{201}{70} - \frac{127}{1050}v}}, \\
b_m &= 4e^{-\frac{188}{63} - \frac{127}{1890}v}, \\
m &= \frac{a_m}{a_m + b_m}, \\
a_h &= \frac{7}{100}e^{-\frac{94}{35} - \frac{127}{2100}v}, \\
b_h &= \frac{1}{1 + e^{-\frac{83}{35} - \frac{127}{1050}v}}, \\
a_n &= \frac{\frac{127}{105}v + \frac{166}{7}}{100 - 100e^{-\frac{83}{35} - \frac{127}{1050}v}}, \\
b_n &= \frac{1}{8}e^{-\frac{59}{140} - \frac{127}{8400}v}, \\
m_A &= \frac{1}{1 + e^{\frac{v-v_a}{s_a}}}, \\
h_{A_i} &= \frac{1}{1 + e^{\frac{v-v_b}{s_b}}}, \\
z_v &= \frac{1}{1 + e^{-\frac{15}{100}(v-z_b)}}.
\end{aligned}$$

Here v denotes the potential difference across the membrane and n, h, z, h_A are gating variables similar to M, N, H in the Hodgkin - Huxley model. In our experiments $I_{ext} = 0$; the values of 20 other parameters are fixed and given in Table 3. The remaining parameters g_{KCa} and g_A are the bifurcation parameters.

References

1. J. C. Alexander, E. J. Doedel and H. G. Othmer, *On the resonance structure in a forced excitable system*, SIAM J. Appl. Math. 50 (1990) 1373 - 1418.
2. W. G. Choe and J. Guckenheimer, *Computing periodic orbits with high accuracy*, Computer methods in applied mechanics and engineering, 170 (1999) 331 - 341.

param	value	unit	param	value	unit
ρ	0.003	ms^{-1}	s_b	6	mV
λ_n	0.8	ms^{-1}	v_{Na}	30	mV
λ_h	0.8	ms^{-1}	v_{Ca}	140	mV
k_A	1	ms^{-1}	v_K	-75	mV
τ_z	23.5	ms	v_l	-40	mV
k_{Ca}	0.0078	mV^{-1}	g_l	0.0854	μS
z_b	-50	mV	g_K	8.0	μS
v_a	-12	mV	g_{Ca}	0.04	μS
v_b	-62	mV	g_{Na}	15	μS
s_a	-26	mV	C_m	1	nF

Table 3: Fixed parameters of the AB neuron model.

3. E. J. Doedel, A. R. Champneys, T. F. Fairgrieve, Yu. A. Kuznetsov, B. Sandstede and X. J. Wang, *AUTO97 : Continuation and Bifurcation Software for ordinary differential Equations (with HomCont), User's Guide*, Concordia University, Montreal, Canada 1997.
4. E. Doedel, *Nonlinear numerics*, Int. J. Bifurcat. Chaos 7 (1997) 2127 - 2143.
5. W. Govaerts, *Numerical methods for bifurcations of dynamical equilibria*, SIAM, Philadelphia 2000.
6. W. Govaerts, *Numerical study of bifurcation phenomena in nerve cells*, in: W. Sulis and I. Trofimova (eds.) *Nonlinear dynamics in Life and Social Sciences*, IOS Press, Amsterdam 2001, pp. 232 - 243.
7. J. Guckenheimer and P. Holmes, *Nonlinear Oscillations, Dynamical Systems, and Bifurcations of Vector Fields*, Applied Mathematical Sciences **42**, Springer Verlag 1983.
8. J. Guckenheimer, S. Gueron and R. Harris - Warrick, *Mapping the dynamics of a bursting neuron*, Phil. Trans. R. Soc. Lond. B 341 (1993) 345 - 359.
9. J. Guckenheimer, R. Harris - Warrick, J. Peck and A. Willms, *Bifurcation, bursting and spike frequency adaptation*, J. Comput. Neuroscience 4 (1997) 257 - 277.
10. A. Hodgkin and A. Huxley, *A qualitative description of membrane current and its application to conduction and excitation in nerves*, J. Physiol. 117 (1952) 500 - 544.
11. E. M. Izhikevich, *Neural excitability, spiking and bursting*, Int. J. Bifurcation and Chaos, 10 (2000) no. 6, 1171 - 1266.
12. E. Knobloch, D. R. Moore, J. Toomre and N. O. Weiss, *Transitions to chaos in two - dimensional double - diffuse convection*, J. Fluid Mech. 166 (1986) 409 - 448.
13. Yu. A. Kuznetsov, *Elements of Applied Bifurcation Theory*, Applied Mathematical Sciences **112**, Springer Verlag, 1995, 1998.
14. Yu. A. Kuznetsov and V. V. Levitin, *CONTENT : A multiplatform environment for analyzing dynamical systems*, Dynamical Systems Laboratory, CWI, Amsterdam 1995 - 1997 (<ftp.cwi.nl/pub/CONTENT>).
15. B. E. Oldeman, B. Krauskopf and A. R. Champneys, *Death of period - doublings: locating the homoclinic - doubling cascade*, Physica D. 146 (2000) 100 - 120.
16. R. E. Plant, *Bifurcation and resonance in a model for bursting neurons*, J. Math. Biol. 11 (1981) 15 - 32.
17. J. Rinzel and Y. S. Lee, *Dissection of a model for neuronal parabolic bursting*, J. Math. Biol. 25 (1987) 653 - 675.

18. L. Shilnikov and D. Turaev, *A new simple bifurcation of a periodic orbit of "blue sky catastrophe" type*, Weierstrass Institute für Angewandte Analysis und Stochastik, Preprint No. 560, Berlin 2000.
19. D. Terman *Chaotic spikes arising from a model of bursting in excitable membranes*, Siam J. Appl. Math. 51 (1991) 1418 - 1450.
20. D. Terman *The transition from bursting to continuous spiking in excitable membrane models*, J. Nonlinear Sci. 2 (1992) 135 - 182.
21. S. Wiczorek, B. Krauskopf and D. Lenstra, *A unifying view of bifurcations in a semiconductor laser subject to optical injection*, Optics Communications 172 (1999) 279 - 295.
22. H. R. Wilson, *Spikes, Decisions and Actions*, Oxford University Press, Oxford 1999.

Cellular Exclusion Algorithms

G. Allgower, K. Georg and M. Erdman

Colorado State University, Fort Collins, USA

Abstract Cellular exclusion algorithms can be used to find all of the real zero points lying in a prescribed n -cell C for a class of maps $F : C \rightarrow \mathbb{R}^n$. Analogously, they may be applied to find a global minimum. We examine a class of exclusion tests.

Set-Oriented Numerical Methods for Dynamical Systems

Michael Dellnitz

Department of Mathematics and Computer Science, University of Paderborn,
Germany
Email: dellnitz@uni-paderborn.de

Abstract Over the past few years so-called set-oriented numerical methods have been developed for the numerical study of dynamical systems. These methods do not just allow to compute *directly* – i.e. by avoiding long term simulations of the underlying system – invariant sets or invariant manifolds but they can also be used to approximate statistical quantities such as natural invariant measures. In this talk an overview about recent accomplishments in this area will be given. In particular, two concrete applications of these techniques will be presented: the approximation of so-called *almost invariant sets* and the construction of reliable global zero finding procedures.

What Can Numerical Linear Algebra Learn from Singular Point Computations?

Hubert Schwetlick

Institut für Numerische Mathematik
Technische Universität Dresden, D-01062 Dresden, Germany
E-Mail: schwetlick@math.tu-dresden.de
<http://www.math.tu-dresden.de/~schwetli/>

Computing the smallest q singular values and the corresponding right and left singular vectors or a specified group of eigenvalues – say, all negative and a few small positive ones – and the corresponding invariant subspaces of a matrix by rapidly convergent methods is an essential task of numerical linear algebra. Such problems arise, e.g., in path following methods for large parameter dependent nonlinear systems $F(x, \alpha) = 0$. Here small singular values of $\partial_x F$ signalize possible singularities, and the corresponding singular subspaces are needed in numerical Ljapunov-Schmidt reduction. Another source are large nonconvex optimization problems where invariant subspaces to negative eigenvalues are essential for determining directions of negative curvature or for treating the so-called *hard case* in trust region methods.

In the talk it will be shown how old and new techniques from nonlinear equations, in particular from singular point computations, lead to efficient algorithms of *shift and invert* type for the class considered above. These methods have the common property that they require to solve one or two linear systems per step with coefficient matrix

$$B_k = \begin{bmatrix} A - \mu_k I & Y_k \\ X_k^T & \Delta_k^T \end{bmatrix}$$

which is obtained from the original matrix A by bordering it in such a way that the bordered matrices have uniformly bounded inverses. The first approach goes back to JACOBI who, in the middle of the 19th century, after some preprocessing using his standard eigenvalue iteration, linearized the eigenvalue equation $Ax - \lambda x = 0$ and solved it by his Jacobi iteration for linear systems under the constraint $w^T x = 1$ as normalizing condition with $w = e_1$ as coordinate vector in order to obtain a final improvement, see the paper [12] by SLEIJPEN/VAN DER VORST and the historical remarks given there. This basic idea has been independently rediscovered in modern terminology by UNGER in [14], a ZAMM article in German from 1950 not recognized by the English speaking community, and by PETERS/WILKINSON in their famous paper [6]. Moreover, the now quite often cited and used improved Jacobi-Davidson method, see again SLEIJPEN/VAN DER VORST [12], can in different ways be considered as a special Newton method for an augmented or also a restricted eigenvalue system, see, e.g., SLEIJPEN/VAN DER VORST [13] and WU et al. [15], cf. also WU's PhD Thesis [16].

In the symmetric case, a block generalization has been introduced and analyzed by LÖSCHE/SCHWETLICK/TIMMERMANN in [4] where Newton's method

is applied to $AX - XM = 0$, $W^T X = I_q$ and then combined with the Rayleigh-Ritz process. Here the q columns of X span the invariant subspace searched for. This method converges even cubically as standard RQI to which it reduces in case $q = 1$, see [7]; in [4] only quadratic convergence is shown. Let us mention that this block RQI is equivalent to another block RQI [2] by FATTEBERT.

In the nonsymmetric case, the bordering delivered by Newton's method applied to $Ax - \lambda x = 0$, $w^T x = 1$ is, in general, geometrically not optimal. An optimal bordering, however, is automatically found when a new bifurcation point method developed by GRIEWANK/REDDIEN in [3] and modified and extended by ALLGOWER/SCHWETLICK in [1] is applied to the eigenvalue equation $Ax - \lambda x = 0$ alone without an additional normalizing condition. Note that $(0, \lambda)$ is a bifurcation point of this equation. This has been done with some useful modifications by SCHWETLICK/LÖSCHE [9]. The resulting method is a certain alternating RQI and related to a new RQI-type method of O'LEARY/STEWART [5].

The update formula of [9] for the left and right eigenvector approximation can, without a shift, also be used for approximating the left and right singular vectors of a matrix, see SCHWETLICK/SCHNABEL [10] for the case $q = 1$. This only linearly but globally convergent method has been extended to the block case $q > 1$ in [11]. Moreover, also block RQI type methods with superlinear convergence are possible, cf. SCHNABEL's Dissertation [8].

References

1. E. L. Allgower and H. Schwetlick. A general view of minimally extended systems for simple bifurcation points. *Z. Angew. Math. Mech.*, 77:83–97, 1997.
2. J.-L. Fattebert. A block Rayleigh quotient iteration with local quadratic convergence. *Electronic Transactions on Numer. Anal.*, 7:56–74, 1998.
3. A. Griewank and G. W. Reddien. Characterization and computation of generalized turning points. *SIAM J. Numer. Anal.*, 21:176–185, 1984.
4. R. Lösche, H. Schwetlick, and G. Timmermann. A modified block Newton iteration for approximating an invariant subspace of a symmetric matrix. *Linear Algebra Appl.*, 275/276:381–400, 1998.
5. D. P. O'Leary and G. W. Stewart. On the convergence of a new Rayleigh quotient method with applications to large eigenproblems. *Electronic Transactions on Numer. Anal.*, 7:182–189, 1998.
6. G. Peters and J. H. Wilkinson. Inverse iteration, ill-conditioned equations and Newton's method. *SIAM Rev.*, 21:339–360, 1979.
7. U. Schnabel and H. Schwetlick. The modified block Newton iteration for computing invariant subspaces (block Rayleigh quotient iteration) is cubically convergent. Manuscript, in preparation for publication, 2001.
8. Uwe Schnabel. *Berechnung singulärer Punkte nichtlinearer Gleichungssysteme*. Dissertation, Fakultät Mathematik u. Naturwissenschaften, Fachrichtung Mathematik, Techn. Univers. Dresden, Germany, 2000.
9. H. Schwetlick and R. Lösche. A generalized Rayleigh quotient iteration for computing simple eigenvalues of nonnormal matrices. *Z. Angew. Math. Mech.*, 80:9–25, 2000.

10. H. Schwetlick and U. Schnabel. Iterative computation of the smallest singular value and the corresponding singular vectors of a matrix. Preprint IOKOMO-06-97, Techn. Univ. Dresden, 1997.
11. H. Schwetlick and U. Schnabel. A generalized alternating inverse subspace iteration for approximating the smallest q singular values and the corresponding left and right singular subspaces of a matrix. Manuscript, in preparation for publication, 2001.
12. G. Sleijpen and H. van der Vorst. A generalized Jacobi-Davidson iteration method for linear eigenvalue problems. *SIAM J. Matrix Anal. Appl.*, 17:410–425, 1996.
13. G. L. G. Sleijpen and H. A. van der Vorst. The Jacobi-Davidson method for eigenvalue problems and its relation with accelerated inexact Newton schemes. In S. D. Margenov and P. S. Vassilevski, editors, *Iterative methods in Linear Algebra, II.*, volume 3 of *IMACS Series in Computational and Applied Mathematics*, pages 377–389. Proceedings of the Second IMACS International Symposium on Iterative Methods in Linear Algebra, June 17-20, 1995, Blagoevgrad, Bulgaria.
14. H. Unger. Nichtlineare Behandlung von Eigenwertaufgaben. *Z. Angew. Math. Mech.*, 30:281–282, 1950.
15. K. Wu, Y. Saad, and A. Stathopoulos. Inexact Newton preconditioning techniques for large symmetric eigenvalue problems. *Electron. Trans. Numer. Anal.*, 7:202–214, 1998.
16. Kesheng Wu. Preconditioned techniques for large eigenvalue problems. Tech. Report 97-038, University of Minnesota, Computer Science Dept., 1997.

A postprocessing procedure for symmetry-breaking bifurcation (a case study)

Dáša Janovská¹ and Vladimír Janovský²

Institute of Chemical Technology, Prague¹
Faculty of Mathematics and Physics, Charles University, Prague²

Abstract: Let us assume that a symmetry-breaking bifurcation point of higher codimension has already been computed. The aim is to study the imperfect bifurcation scenario. A numerical tool is proposed for this purpose. It consists in an approximation of the diffeomorphism which links the bifurcation equation with an unfolded normal form of the problem.

Keywords: steady states, bifurcation points, symmetry-breaking, imperfect bifurcation diagrams, qualitative analysis

1 Introduction

The current state-of-the-art of the numerical bifurcation analysis of steady states, see [7], could be briefly described as follows: Going Down the hierarchy of bifurcation points, find an *organizing center*. This is a bifurcation point with the highest *codimension* locally available.

Going Up the hierarchy starts with a *postprocessing* of the already found organizing center. It consists, for example, in finding tangents to the curves of codim-1 bifurcation points passing through the organizing center, see [7], Section 7.8.

In papers [9], [2] and [3] a much more complex postprocessing analysis is proposed: The aim is to supply analytical predictors to *all* bifurcation points in a neighborhood of the processed organizing center. The technique is based on

- generalized version of Liapunov-Schmidt reduction algorithm (see [7])
- numerical treatment of the relevant *bifurcation equation*

The idea is to compute differential of the diffeomorphism that links the particular bifurcation equation with an *unfolded normal form*, see [4], [5].

For another related topics namely computing parameter dependent center manifolds, see [13] and [8].

As far as the symmetry is concerned, computation of symmetry-breaking bifurcation points was proposed in [11] and [10]. Numerical treatment of higher codimension phenomena was suggested in [1]. In particular, the symmetry-breaking bifurcation points with nonlinear degeneracies were considered. A classification was also proposed. In fact, nonlinear degeneracies are characterized via a classification of a scalar bifurcation equation with \mathfrak{t} -symmetry or \mathbf{Z}_2 -symmetry, see [1].

The aim is to study imperfect bifurcation scenario of the bifurcation equation. The main idea of our approach is as follows: We will try to approximate the

diffeomorphism that links an unfolded normal form with the real bifurcation problem. We present a case study of a particular item of the classification list.

From the technical point of view, we assume that a symmetry-breaking bifurcation point was already detected. We also assume that leading terms of Taylor expansion of the bifurcation equation are available (for the relevant computational techniques, see [1]).

The outline of the paper is as follows: In Preliminaries (Section 2), we give a brief review of [1] (the notion of \mathbf{t} -symmetry, classification list). We review a list of universal unfoldings of normal forms with \mathbf{t} -symmetry. We prove (Proposition 1) a statement concerning an unfolding of the contact diffeomorphism with \mathbf{t} -symmetry. In Section 3, we consider a particular singularity as a case study. We formulate the main result namely, the algorithm for computing differential of the unfolded diffeomorphism.

2 Preliminaries

We consider a smooth parameter dependent mapping $F : \mathbb{R}^N \times \mathbb{R}^1 \times \mathbb{R}^k \rightarrow \mathbb{R}^N$. Let $F = F(u, \beta)$, $\beta = (\lambda, \alpha) \in \mathbb{R}^1 \times \mathbb{R}^k$. In the bifurcation context, see e.g. [5], u is the state variable, λ and α are the control and unfolding parameters.

Let $\mathbf{\Gamma}$ be a compact Lie group with a faithful representation in the state space \mathbb{R}^N , so that we can identify each group element $\gamma \in \mathbf{\Gamma}$ with its action on \mathbb{R}^N i.e., a linear transformation $\gamma \in \mathbf{GL}(N)$ on \mathbb{R}^N . We assume the mapping F to be $\mathbf{\Gamma}$ -equivariant i.e.,

$$F(\gamma u, \lambda, \alpha) = \gamma F(u, \lambda, \alpha) \quad (1)$$

for $(u, \lambda, \alpha) \in \mathbb{R}^N \times \mathbb{R}^1 \times \mathbb{R}^k$ and $\gamma \in \mathbf{\Gamma}$. The set $\text{Fix } \mathbf{\Gamma} \equiv \{u \in \mathbb{R}^N : \gamma u = u \text{ for all } \gamma \in \mathbf{\Gamma}\}$ of fixed points (of $\mathbf{\Gamma}$) is the set of all states $u \in \mathbb{R}^N$ that exhibit the symmetry of the given group $\mathbf{\Gamma}$.

Let $(u^*, \lambda^*, \alpha^*)$ be a $\mathbf{\Gamma}$ -symmetry breaking bifurcation point of F , see [6]. The solution set of $F(u, \lambda, \alpha) = 0$ is locally identified with the solution set of an equivariant *bifurcation equation* $g(x, t, z) = 0$, where $g : \mathbb{R}^m \times \mathbb{R}^1 \times \mathbb{R}^k \rightarrow \mathbb{R}^m$, $g = g(x, t, z)$, is the reduced version of F obtained via a symmetry-adapted *bordering technique*, see [1], [7]. Following the generic scenario, see [6], Proposition 3.2, p 82, m is the dimension of absolutely irreducible representation of $\mathbf{\Gamma}$. Note that the isomorphism between the solution sets of F and g relates the singular point $(u^*, \lambda^*, \alpha^*) \in \mathbb{R}^N \times \mathbb{R}^1 \times \mathbb{R}^k$ to the origin of $\mathbb{R}^m \times \mathbb{R}^1 \times \mathbb{R}^k$.

A further reduction due to Equivariant Branching Lemma, see [6], is generically possible. Namely, the germ g can be reduced just to 1-D state variable, i.e.,

$$g : \mathbb{R}^1 \times \mathbb{R}^1 \times \mathbb{R}^k \rightarrow \mathbb{R}^1. \quad (2)$$

Following [1], classification of higher codimension phenomena (namely those of nonlinear degeneracies) together with a numerical processing (the construction of *test functions*) can be reduced to 1-D.

Let us comment on the classification. In fact, we classify *perfect bifurcation scenario*, i.e. unfolding parameters are set to $z = 0$. We define $h(x, t)$ as

$$h(x, t) \equiv g(x, t, 0) \quad (3)$$

The classification consists in linking h with a suitable *normal form* h^* ; $h^* = h^*(x, t)$ is a smooth scalar function (a germ of mapping centred at the origin). For the list of normal forms, see [1]; these can be easily deduced from the list of \mathbf{Z}_2 -equivariant normal forms, see [5]. The particular link is either \mathbf{t} -equivalence or \mathbf{Z}_2 -equivalence. In symbols,

$$h \overset{\mathbf{t}}{\sim} h^*, \quad h \overset{\mathbf{Z}_2}{\sim} h^*,$$

see [1].

In this paper, we consider the former case only. To this end, we recall the former notion:

Definition 1. $h \overset{\mathbf{t}}{\sim} h^*$ provided that there exist smooth

$$M = M(x, t), \quad \Psi(x, t) = (\chi(x, t), \tau(t)), \quad \chi(x, t) = x \cdot \bar{\chi}(x, t) \quad (4)$$

satisfying

$$M(0, 0) > 0, \quad \bar{\chi}(0, 0) > 0, \quad \tau(0) = 0, \quad \tau_t(0) > 0, \quad (5)$$

so that

$$h = M \cdot h^* \circ \Psi \quad (6)$$

holds on a neighborhood of the origin.

Note that $\chi_x(0, 0) > 0$, $\chi_t(0, 0) = 0$. It is important to point out that M and Ψ are *not* defined uniquely (e.g., some scaling is possible).

We consider the list of \mathbf{t} -equivariant normal forms h^* with $\text{codim} \leq 3$, see [1]; codim stands for *codimension* of a particular singularity. To each item of the mentioned list, a *universal unfolding*

$$g^* = g^*(x, t, z), \quad g^* : \mathbb{R}^1 \times \mathbb{R}^1 \times \mathbb{R}^k \rightarrow \mathbb{R}^1$$

satisfying

$$g^*(x, t, 0) = h^*(x, t) \quad (7)$$

is available, see Table 1. Each g^* represents *all* qualitatively significant perturbations of the relevant h^* . Moreover, dimension k of the parameter-space is minimal namely, $k = \text{codim}$. Since g^* always factors as $g^* = x \cdot r^*(x, t, z)$, we just list the relevant r^* . Table 1 also includes an equivalent definition of the singularity (see [1]): g , see (2), belongs to a particular class (case) provided that $g = x \cdot r(x, t, z)$ and Defining equations / Nondegeneracy conditions are satisfied at the origin.

The following statement is concerned with an unfolding Φ of the contact diffeomorphism Ψ . It becomes crucial for the applications we have in mind.

Proposition 1. *Let us consider g and h , see (2) and (3). Let $h \stackrel{t}{\sim} h^*$, $k = \text{codim} \leq 3$. We choose M, Ψ to satisfy (4), (5) and (6). Let g^* be the particular universal unfolding of h^* , see Table 1.*

There exists a smooth $S : \mathbb{R}^{2+k} \rightarrow \mathbb{R}^1$, $S = S(x, t, z)$ and a smooth mapping

$$\Phi : \mathbb{R}^{2+k} \rightarrow \mathbb{R}^{2+k}, \quad \Phi(x, t, z) = (X(x, t, z), T(t, z), Z(z))$$

such that

$$X(x, t, z) = x \cdot \bar{X}(x, t, z), \quad (8)$$

$$\Phi(\cdot, \cdot, 0) = \Psi(\cdot, \cdot), \quad S(\cdot, \cdot, 0) = M(\cdot, \cdot), \quad (9)$$

and

$$g = S \cdot g^* \circ \Phi \quad (10)$$

in a neighborhood of the origin $0 \in \mathbb{R}^{2+k}$.

Proof Let us extend $\Psi : \mathbb{R}^2 \rightarrow \mathbb{R}^2$ as $\bar{\Psi} : \mathbb{R}^{2+k} \rightarrow \mathbb{R}^{2+k}$, setting $\bar{\Psi}(x, t, z) = (\chi(x, t), \tau(t), z) = (x\bar{\chi}(x, t), \tau(t), z)$. We define $f : \mathbb{R}^{2+k} \rightarrow \mathbb{R}^1$,

$$f(x, t, z) = (M \circ \Psi^{-1}(x, t))^{-1} \cdot g \circ \bar{\Psi}^{-1}(x, t, z).$$

Then, $f(x, t, 0) = (M \circ \Psi^{-1}(x, t))^{-1} \cdot h \circ \Psi^{-1}(x, t) = h^*(x, t)$, i.e., $f = f(x, t, z)$ is a k -parameter unfolding of $h^* = h^*(x, t)$, see [5], p. 120.

Since we assume $g^* = g^*(x, t, z)$ to be an universal unfolding of $h^* = h^*(x, t)$, then f factors through g^* ([5], p.120, Definition 1.2). Namely, there exist smooth $\tilde{S} : \mathbb{R}^{2+k} \rightarrow \mathbb{R}^1$ and $\tilde{\Phi} : \mathbb{R}^{2+k} \rightarrow \mathbb{R}^{2+k}$, $\tilde{\Phi}(x, t, z) = (x\tilde{X}(x, t, z), \tilde{T}(t, z), \tilde{Z}(z))$, satisfying the following conditions

$$\tilde{\Phi}(x, t, 0) = (x, t, 0), \quad \tilde{S}(x, t, 0) = 1, \quad f = \tilde{S} \cdot g^* \circ \tilde{\Phi}$$

in a neighborhood of $0 \in \mathbb{R}^{2+k}$.

case	$r^* = r^*(x, t, z)$	Defining equations / Nondegeneracy conditions
1.	$\varepsilon x + \delta t$	$r = 0$ $\text{sgn } r_x = \varepsilon, \text{sgn } r_t = \delta$
2 a.	$\varepsilon x^2 + \delta t + z_1 x$	$r = r_x = 0$ $\text{sgn } r_{xx} = \varepsilon, \text{sgn } r_t = \delta$
2 b.	$\varepsilon x^3 + \delta t + z_1 x + z_2 x^2$	$r = r_x = r_{xx} = 0$ $\text{sgn } r_{xxx} = \varepsilon, \text{sgn } r_t = \delta$
2 c.	$\varepsilon x^4 + \delta t + z_1 x + z_2 x^2 + z_3 x^3$	$r = r_x = r_{xx} = r_{xxx} = 0$ $\text{sgn } r_{xxxx} = \varepsilon, \text{sgn } r_t = \delta$
3 a.	$\varepsilon x + \delta t^2 + z_1$	$r = r_t = 0$ $\text{sgn } r_x = \varepsilon, \text{sgn } r_{tt} = \delta$
3 b.	$\varepsilon x + \delta t^3 + z_1 + z_2 t$	$r = r_t = r_{tt} = 0$ $\text{sgn } r_x = \varepsilon, \text{sgn } r_{ttt} = \delta$
3 c.	$\varepsilon x + \delta t^4 + z_1 + z_2 t + z_3 t^2$	$r = r_t = r_{tt} = r_{ttt} = 0$ $\text{sgn } r_x = \varepsilon, \text{sgn } r_{tttt} = \delta$
4.	$\varepsilon x^2 + 2mtx + \delta t^2 + z_1 + 2z_2 x$	$r = r_x = r_t = 0$ $\text{sgn } r_{xx} = \varepsilon, \text{sgn } r_{tt} = \delta,$ $D_2(r) \neq 0, m^2 \neq \varepsilon\delta$
5.	$\varepsilon x^2 + 2\delta tx + \phi t^3 +$ $+z_1 + z_2 t + z_3 t^2$	$r = r_x = r_t = r_{tt} = 0$ $\text{sgn } r_{xx} = \varepsilon, \text{sgn } r_{xt} = \delta,$ $\text{sgn } r_{ttt} = \phi$
6.	$\varepsilon x^3 + 2\delta tx + \phi t^2 +$ $+z_1 + z_2 x + z_3 x^2$	$r = r_x = r_{xx} = r_t = 0$ $\text{sgn } r_{xxx} = \varepsilon, \text{sgn } r_{xt} = \delta,$ $\text{sgn } r_{tt} = \phi$
7.	$\phi x^3 + \varepsilon x^2 + 2mtx + \varepsilon t^2 +$ $+z_1 + 2z_2 x$ $m \approx 1$	$r = r_x = r_t = D_2(r) = 0$ $\text{sgn } r_{xx} = \varepsilon, \text{sgn } r_{xt} = \delta,$ $-\text{sgn } (r_{xt} r_{tt} D_3(r)) = \phi$

Notation: $|\varepsilon| = |\delta| = |\phi| = 1$, $m \equiv r_{xt}/\sqrt{|r_{xx}r_{tt}|}$,
 $D_2(r) \equiv r_{xx}r_{tt} - r_{xt}r_{xt}$, $D_3(r) \equiv r_{xx}(D_2(r))_t - r_{xt}(D_2(r))_x$

Table 1: The list of unfolded normal forms $g^* = x \cdot r^*(x, t, z)$,

Then it is easy to verify that

$$S = M(x, t) \cdot \tilde{S} \circ \bar{\Psi}(x, t, z), \quad \Phi = \tilde{\Phi} \circ \bar{\Psi}$$

satisfy (9) and (10). ■

Remark 1. If g is an universal unfolding of h then, under the assumptions of Proposition 1, the mapping Φ is even a *diffeomorphism*. In Case Study, we give sufficient conditions for this situation to happen.

3 A case study

Let us consider a symmetry-breaking bifurcation point which corresponds to the degeneracy labelled as case 2a in Table 1. Let g and h be the germs (2) and (3), respectively.

First, we point out applications of Proposition 1 and Remark 1. Taking into account the particular g^* , we claim that

$$g(x, t, z) = S(x, t, z) \cdot X \cdot (\varepsilon X^2 + \delta T + ZX), \quad (11)$$

where

$$X = x \cdot \bar{X}(x, t, z), \quad T = T(t, z), \quad Z = Z(z). \quad (12)$$

The statement holds in the obvious local sense.

In particular,

$$g(x, t, z) = 0 \quad \text{if and only if} \quad g^*(X, T, Z) = 0.$$

It suggests the following solution of $g = 0$: Choose an imperfection $z \in \mathbb{R}^1$ and a control parameter $t \in \mathbb{R}^1$; map them as $z \mapsto Z(z)$, $(t, z) \mapsto T(t, z)$; solve $g^*(X, T(t, z), Z(z)) = 0$ for X , which amounts to finding roots of an quadratic equation; define $\Phi^{-1}(X, T(t, z), Z(z))$ as (x, t, z) . Then (x, t, z) solves $g = 0$.

The same applies to singular roots of g and g^* since Φ^{-1} provides a one-to-one link between stratified manifolds of singular points of g and those of g^* .

The diffeomorphism Φ is not available but we can compute $D\Phi(0)$ as the natural first order approximation of Φ . Then as the solution of $g = 0$ is concerned, the following approximation procedure is at hand:

- Choose $z \in \mathbb{R}^1$ and $t \in \mathbb{R}^1$;
- map them as $z \mapsto Z_z(0)z$ and $(t, z) \mapsto T_t(0, 0)t + T_z(0, 0)z$;
- solve the algebraic equation $g^*(X, T_t(0, 0)t + T_z(0, 0)z, Z_z(0)z) = 0$ for X ;
- then $(D\Phi(0))^{-1}(X, T_t(0, 0)t + T_z(0, 0)z, Z_x(0)z) \approx (x, t, z)$.

Similarly, all *singular* solutions of $g = 0$ in a neighborhood of the origin can be approximated by the singular solutions of $g^* = 0$.

We just concluded that the differential $D\Phi(0)$ yields a piece of "first order" information concerning imperfect bifurcation scenario.

Let us compute $D\Phi(0)$. Partial derivatives of g at the origin are considered as data. Then chain rule differentiation of (11) yields a list of conditions upon partial differentials of \bar{X} , T , Z , S evaluated at the origin.

In order to simplify notation, let us agree on the convention that all partials are evaluated at the origin (if it is not stated explicitly otherwise). For example, g_{xt} , \bar{X}_x and T_{tz} are $g_{xt}(0, 0, 0)$, $\bar{X}_x(0, 0, 0)$ and $T_{tz}(0, 0)$.

We already mentioned that M and Ψ in Definition 1 (and the more S and Φ in Proposition 1) are *not* uniquely defined. In fact, a scaling is possible. From this reason, we claim that $\bar{X} = 1$ without loss of generality.

Let S , Φ satisfy (8)-(10). Given $c \neq 0$, we define \tilde{S} , $\tilde{\Phi}$ as

$$\tilde{S} = \frac{1}{c^3}S, \quad \tilde{\Phi} = \tilde{\Phi}(xc\bar{X}, c^2T, cZ).$$

It is easy to check that

$$\tilde{S} \cdot g^* \circ \tilde{\Phi} = S \cdot g^* \circ \Phi.$$

In order to finish the argument, choose c such that $c\bar{X} = 1$.

Therefore, we may assume

$$D\Phi(0) = \begin{pmatrix} 1 & 0 & 0 \\ 0 & T_t & T_z \\ 0 & 0 & Z_z \end{pmatrix}. \quad (13)$$

The above mentioned chain rule differentiation of (11) yields the following identity:

$$\mathbf{B} = \mathbf{A} \cdot \mathbf{B}^* \cdot D\Phi(0), \quad (14)$$

where

$$\mathbf{B} = \begin{pmatrix} g_{xx} & g_{xt} & g_{xz} \\ g_{xxx} & g_{xxt} & g_{xxz} \end{pmatrix}, \quad (15)$$

$$\mathbf{B}^* = \begin{pmatrix} g_{xx}^* & g_{xt}^* & g_{xz}^* \\ g_{xxx}^* & g_{xxt}^* & g_{xxz}^* \end{pmatrix} = \begin{pmatrix} 0 & \delta & 0 \\ 6\varepsilon & 0 & 2 \end{pmatrix},$$

and

$$\mathbf{A} = \begin{pmatrix} S\bar{X} & 0 \\ 2(S_x\bar{X} + S\bar{X}_x) & S\bar{X}^2 \end{pmatrix} = \begin{pmatrix} S & 0 \\ 2(S_x + S\bar{X}_x) & S \end{pmatrix}.$$

Recall that the items of \mathbf{B} are considered as data. Note that $g_{xx} = 0$ and $g_{xxx} \neq 0$ due to the Defining conditions (see Table 1, case 2 a.: $r_x = 0$, $r_{xx} \neq 0$). Note also that the matrices \mathbf{B}^* , \mathbf{A} have full rank.

Remark 2. As the regularity of the differential $D\Phi(0)$ is concerned, it depends on the regularity of the data matrix \mathbf{B} . In case 2a:

$$\det \begin{pmatrix} g_{xt} & g_{xz} \\ g_{xxt} & g_{xxz} \end{pmatrix} \neq 0 \quad \text{if and only if} \quad \det \begin{pmatrix} T_t & T_z \\ 0 & Z_z \end{pmatrix} \neq 0. \quad (16)$$

This statement follows from identity (14).

Let us assume

$$\det \begin{pmatrix} g_{xt} & g_{xz} \\ g_{xxt} & g_{xxz} \end{pmatrix} \neq 0 \quad . \quad (17)$$

Therefore, the mapping Φ is a *local diffeomorphism*.

We can resume that the identity (14) represents 6 conditions for 6 unknowns T_t, T_z, Z_z, S, S_x and \bar{X}_x . Unfortunately, these are *not* independent. It is manifested by the fact that g_{xx} is forced to be zero due Defining conditions.

Proposition 2. *Consider a Liapunov-Schmidt reduction g of F at a singular point $(u^*, \lambda^*, \alpha^*)$. Let $h \equiv g(x, t, 0)$ be classified as a singular point case 2a from Table 1. Let (17) hold. Construct diffeomorphism Φ in Proposition 1.*

Then $D\Phi(0)$ is uniquely defined up to a scaling. Consider the particular scaling (13). The algorithm for computing items of the matrix $D\Phi(0)$ is resumed in Table 2. It requires $g_{xxx}, g_{xt}, g_{xz}, g_{xxt}, g_{xxz}$ as data.

Proof We consider the identity (14) again. Observe that it can be interpreted as the relationship between data (5 selected partial derivatives of g) and the following partials

- T_t, T_z and Z_z which are the entries of the scaled $D\Phi(0)$
- $S, S_x + S\bar{X}_x$ which come out from Chain Rule and represent a chunk.

Table 2 suggests canonical solution of the resulting system of 5 equations for $S, T_t, T_z, S_x + S\bar{X}_x$ and Z_z . ■

Data (derivatives evaluated at $0 \in \mathbb{R}^3$)	\Rightarrow
$g_{xxx} = 6\varepsilon S$	S
$g_{xt} = \delta S T_t$	T_t
$g_{xz} = \delta S T_z$	T_z
$g_{xxt} = 2\delta T_t (S_x + S\bar{X}_x)$	$S_x + S\bar{X}_x$
$g_{xxz} = 2\delta T_z (S_x + S\bar{X}_x) + 2S Z_z$	Z_z

Table 2: Computing $D\Phi(0)$, case 2a.

To complete the argument, we give a *constructive* proof of the existence of contact diffeomorphism in case 2a.

Lemma 1. *Let $h \overset{t}{\sim} h^*$, $h^* = x \cdot (\varepsilon x^2 + \delta t)$, $|\varepsilon| = |\delta| = 1$. Then there exist smooth $M = M(x, t)$, $\chi = \chi(x, t)$ and $\tau = \tau(t)$ such that (5), (6) hold. Moreover,*

$$\chi(x, t) = x \cdot \bar{\chi}(x, t), \quad \bar{\chi}(x, t) = \sqrt{\frac{\varphi(x)}{\varphi(0)}}, \quad (18)$$

$$\tau(t) = c \cdot t, \quad (19)$$

where $\varphi = \varphi(x)$ is a smooth function satisfying $\text{sgn } \varphi(0) = -\varepsilon\delta$ and $c > 0$ is a constant.

Proof Function h has to satisfy Defining equations / Nondegeneracy conditions, Table 1, case 2a. In particular, if $h(x, t) = xr(x, t, 0)$ then

$$r = r_x = 0, \quad \text{sgn } r_t = \delta, \quad \text{sgn } r_{xx} = \varepsilon. \quad (20)$$

Consider the solution set to $r(x, t, 0) = 0$. Due to Implicit Function Theorem, t is a function of x namely, there exists a smooth function $\varphi(x)$ such that

$$t = x^2 \cdot \varphi(x), \quad \text{sgn } \varphi(0) = -\varepsilon\delta.$$

Therefore, $r(x, t, 0)$ factors as

$$r(x, t, 0) = \widetilde{M}(x, t) \cdot (x^2\varphi(x) - t)$$

and

$$h(x, t) = \widetilde{M}(x, t) \cdot x \cdot (x^2\varphi(x) - t).$$

Note that $\text{sgn } \widetilde{M}(0, 0) = -\delta$.

Finally, we set

$$\begin{aligned} \chi(x, t) &= x \cdot \bar{\chi}(x, t), \quad \bar{\chi}(x, t) = \sqrt{\frac{\varphi(x)}{\varphi(0)}}, \\ \tau(t) &= c \cdot t, \quad c = -\frac{\varepsilon\delta}{\varphi(0)} \\ M(x, t) &= \frac{\varepsilon\varphi(0)\widetilde{M}(x, t)}{\bar{\chi}(x, t)}. \end{aligned}$$

The above functions $\chi = \chi(x, t)$, $\tau = \tau(t)$ and $M = M(x, t)$ have the required properties (5), (6), (18) and (19). ■

4 Conclusions

The objective is to study symmetry-breaking bifurcation points subject to parameter perturbations (*imperfect bifurcation analysis*). We have motivated that scalar problems with \mathbf{t} -symmetry are important as our aim is concerned.

We suggest a numerical tool for such analysis. The idea is to find a diffeomorphism Φ between the actual \mathbf{t} -symmetry breaking bifurcation problem and its unfolded normal form (Table 1). The key argument is that such diffeomorphism exists, Proposition 1 and Remark 1.

There is no chance to acquire Φ . But computation of its differential $D\Phi(0)$ can be a reasonable numerical task. We have given a simple example in Section 3. There is explained that $D\Phi(0)$ yields the first order predictors for imperfect bifurcation phenomena.

We admit that we have treated a very simple singularity as a Case Study. We have already considered generalizations:

The class of *cuspoïds* (case 2a, 2b, 2c) represents no problem. We may say that cases 2b and 2c can be treated similarly as case 2a. Let us remark that the class of cuspoïds represents singularities *without* a distinguished parameter (i.e., just due to the classical singularity theory).

The remaining cases in Table 1 stem from the classification suggested in [5]. One can encounter troubles even in the case 3a: We obtain an analogy of (14). It defines a nonlinear relationship between data (in this case $g_{xx}, g_{xz}, g_{xtt}, g_{xxt}, g_{xtz}$) and selected differentials of S, \bar{X}, T and Z . We observe that the number of unknowns exceeds the number of data. The way out is to find an auxiliary information concerning contact diffeomorphism $\bar{\Psi}$ (a statement which would be an analogy of Lemma 1). In this particular case, one can prove that the function \bar{X} is constant. It results in a reduction of unknowns.

References

1. K. BÖHMER, W. GOVAERTS AND V. JANOVSÝ, *Numerical detection of symmetry breaking bifurcation points with nonlinear degeneracies*, Mathematics of Computation, Vol.68, No.227. pp.1097-1108, 1999
2. K. BÖHMER, D. JANOVSÁ AND V. JANOVSÝ, *Computer aided analysis of the imperfect bifurcation diagrams*, East-West J.Numer.Math., Vol 6, No 3, pp 207-222, 1998
3. K. BÖHMER, D. JANOVSÁ AND V. JANOVSÝ, *Computing differential of an unfolded contact diffeomorphism*, Bericht Nr.69(2000), Fachbereich Mathematik und Informatik, Phillips Universität Marburg
4. M. GOLUBITSKY AND D. SCHAEFFER, *A theory for imperfect bifurcation via singularity theory*, Commun. Pure Appl. Math., 32 (1979), pp. 21–98
5. M. GOLUBITSKY AND D. SCHAEFFER, *Singularities and Groups in Bifurcation Theory, Vol. 1*, Springer Verlag, New York, 1985.
6. M. GOLUBITSKY, I. STEWART AND D. SCHAEFFER, *Singularities and Groups in Bifurcation Theory, Vol. 2*, Springer Verlag, New York, 1988.
7. W. GOVAERTS, *Numerical methods for bifurcations of dynamical equilibria*, SIAM, Philadelphia, 2000
8. M. IPSEN, F. HYNNE AND P. G. SORENSEN, *Systematic derivation of amplitude equations and normal forms for dynamical systems*, Chaos, Vol.8, No.4, 1998
9. V. JANOVSÝ AND P. PLECHÁČ, *Computer aided analysis of imperfect bifurcation diagrams I. Simple bifurcation point and isola formation centre*, SIAM J.Num.Anal., 21 (1992), pp. 498-512
10. V. JANOVSÝ AND P. PLECHÁČ, *Numerical application of equivariant reduction techniques*, in Bifurcation and Symmetry, M. Golubitsky, E. Allgower and K. Böhmer, eds., p. 203-213, Birkhauser Verlag, 1992
11. M. DELLNITZ AND B. WERNER, *Computational methods for bifurcation problems with symmetries - with special attention to steady state and Hopf bifurcation points*, J.Comput.Appl.Math., 26: 97-123, 1989.
12. M. KUBÍČEK AND M. MAREK, *Computational Methods in Bifurcation Theory and Dissipative Structures*, Springer-Verlag, New York, 1983

13. Y.A. KUZNETSOV, *Elements of Applied Bifurcation Theory*, Springer-Verlag, New York, 1995
14. M. MAREK AND I. SCHREIBER, *Chaotic Behavior of Deterministic Dissipative Systems*, Academia, Prague, 1991

Acknowledgments: The authors acknowledge with pleasure the support of the Grant Agency of the Czech Republic (grant # 201/98/0220, grant # 201/98/0528) and support of the grants VZ CEZ J19/98 : 223400007 and MSM 113200007.

Stability of Spatially Homogeneous Solutions in Lattice Dynamical Systems

Daniel Turzík, Alois Klíč, Miroslava Dubcová and Pavel Pokorný

Department of Mathematics
Institute of Chemical Technology, Prague

1 Introduction

Lattice dynamical systems arise for example as a result of a discretization in partial differential equations (PDE). Let us have PDE

$$u_t = u_{xx} + f(u), \quad (1)$$

where $u = u(t, x)$ is a solution of (1), $t \geq 0$, $x \in \mathbb{R}$.

Let Δt and Δx be a time and space step, respectively. We set

$$u_j(n) = u(n \Delta t, j \Delta x), \quad (2)$$

where $n \in \mathbb{N}_0$ and $j \in \mathbb{Z}$. In such a way we obtain the quantity (two-sided sequence of real numbers for fixed n)

$$\mathbf{u}(n) = \{u_j(n)\}_{j \in \mathbb{Z}}, \quad (3)$$

which can be interpreted as a state of the system at the time n . The time evolution of this system can be described as follows. If $\{S^t\}_{t \geq 0}$ is the corresponding **semiflow** of PDE (1) (see [4]), then the solution $u(t, x)$ can be written in the form

$$u(t, x) = S^t(g(x)), \quad (4)$$

where $g(x)$ is the initial condition for PDE (1).

From (2) and (4) we obtain

$$\begin{aligned} u_j(n+1) &= u((n+1)\Delta t, j\Delta x) = S^{(n+1)\Delta t}(g(j\Delta x)) = \\ &= S^{\Delta t}(S^{n\Delta t}(g(j\Delta x))) = S^{\Delta t}(u(n \Delta t, j \Delta x)) = S^{\Delta t}(u_j(n)), \end{aligned}$$

i.e. the time evolution of the quantity (3) is described by the relation

$$u_j(n+1) = S^{\Delta t}(u_j(n)). \quad (5)$$

Let us denote the mapping $S^{\Delta t}$ by the symbol \mathcal{F} . By making use of the left hand side of (3) we can rewrite the relation (5) in the form

$$\mathbf{u}(n+1) = \mathcal{F}(\mathbf{u}(n)).$$

Remark 1 This procedure can be generalized to the case when (1) is a system of PDE, i.e. $\mathbf{u}(t, x) \in \mathbb{E}^p$ and the spatial variable x is two-dimensional or three-dimensional. In this case we have $u_j(n) \in \mathbb{E}^p$ in (3), where $j \in \mathbb{Z}^d$, $j = (j_1, j_2, j_3)$ is the multiindex ($d = 3$), such that $\mathbf{x} = (j_1 \Delta x, j_2 \Delta x, j_3 \Delta x)$. The set \mathbb{Z}^d can be interpreted as the "integer lattice" in \mathbb{E}^d , i.e. the set of "points" in \mathbb{E}^d with integer coordinates.

The set \mathbb{Z}^d (the cartesian product of d copies of the set of integers \mathbb{Z}) is called the **lattice space** or d -dimensional integer lattice. Further let \mathbb{E}^p be a p -dimensional Euclidean space with the ordinary scalar product (\cdot, \cdot) and the norm $|\cdot| = \sqrt{(\cdot, \cdot)}$. The E^p can be called the **value space**.

Let us denote

$$\tilde{\mathbb{B}} = \{\mathbf{u} ; \mathbf{u} = \{u_j\}_{j \in \mathbb{Z}^d}, u_j \in E^p\}.$$

For $\mathbf{u} = \{u_j\} \in \tilde{\mathbb{B}}$, the symbol $(\mathbf{u})_j$ denotes u_j , i.e.

$$(\mathbf{u})_j = u_j, \forall j \in \mathbb{Z}^d.$$

Several norms can be introduced in $\tilde{\mathbb{B}}$, for example:

$$\begin{aligned} 1) \quad & \|\mathbf{u}\|_\infty = \sup_{j \in \mathbb{Z}^d} |u_j|, \\ 2) \quad & \|\mathbf{u}\|_q = \left(\sum_{j \in \mathbb{Z}^d} \frac{|u_j|^2}{q^{|j|}} \right)^{\frac{1}{2}}, \text{ where } q \geq 1, |j| = \max\{|j_1|, \dots, |j_d|\}. \end{aligned} \quad (6)$$

Convention: In this paper, the sup-norm (6) will be used only. We shall denote shortly $\|\cdot\|_\infty = \|\cdot\|$.

The set

$$\mathbb{B} = \{\mathbf{u} \in \tilde{\mathbb{B}}; \|\mathbf{u}\| < \infty\}$$

is the Banach space, which plays the role of the **phase space**.

For a fixed integer s and $\{u_j\} \in \mathbb{B}$ we denote

$$\{u_j\}^s = \{u_i ; |i - j| \leq s\}.$$

We define the mapping

$$\mathcal{F} : \mathbb{B} \rightarrow \mathbb{B}$$

by the relation

$$(\mathcal{F}\mathbf{u})_j = f(\{u_j\}^s), j \in \mathbb{Z}^d,$$

where

$$f : (E^p)^{(2s+1)^d} \rightarrow E^p$$

is a differentiable mapping of class C^2 .

Remark 2 In the case of 1-dimensional lattice space \mathbb{Z} , some authors (see e.g. [2]) use the following equivalent approach. For fixed nonnegative integers s_1, s_2 and $\mathbf{u} = \{u_j\}_{j \in \mathbb{Z}} \in \mathbb{B}$, set

$$\{u_j\}_{s_1}^{s_2} = (u_{j-s_1}, u_{j-s_1+1}, \dots, u_{j+s_2-1}, u_{j+s_2}).$$

and consider $f : (E^p)^{s_1+s_2+1} \rightarrow E^p$ instead of $f : (E^p)^{2s+1} \rightarrow E^p$.

Under some additional assumptions on the function f (Lipschitz condition) it is not difficult to show that

$$\mathcal{F}(\mathbb{B}) \subset \mathbb{B}.$$

Thus the discrete dynamical system

$$(\mathcal{F}^n, \mathbb{B})_{n \in \mathbb{Z}^+}$$

is correctly defined. This discrete dynamical system (DDS) is called a **lattice dynamical system** (LDS).

We shall write

$$\mathbf{u}(n+1) = \mathcal{F}(\mathbf{u}(n)) \quad \text{or} \quad u_j(n+1) = f(\{u_j(n)\}^s). \quad (7)$$

Definition 1 The fixed point \mathbf{u}^* of the mapping \mathcal{F} , i.e. the point satisfying

$$\mathcal{F}\mathbf{u}^* = \mathbf{u}^*,$$

is called the **steady-state solution** of the LDS.

The $\mathbf{u}^* = \{u_j^*\}_{j \in \mathbb{Z}^d}$ is fixed point of \mathcal{F} iff

$$u_j^* = f(\{u_j^*\}^s) \quad \forall j \in \mathbb{Z}^d.$$

Definition 2 Let $\mathbf{u}^* = \{u_j^*\}$ be a steady-state solution of LDS $(\mathcal{F}^n, \mathbb{B})_{n \in \mathbb{Z}^+}$. If

$$u_j^* = u^0 \quad \forall j \in \mathbb{Z}^d,$$

then \mathbf{u}^* is called **spatially homogeneous solution**. If there exists $j_0 \in \mathbb{Z}^d$, such that

$$u_{j+j_0}^* = u_j^* \quad \forall j \in \mathbb{Z}^d,$$

then \mathbf{u}^* is called **spatially periodic solution**.

In the following we derive the conditions for the stability of a spatially homogeneous solution of LDS given by (7). We will consider the case of 1-dimensional lattice space \mathbb{Z} and 1-dimensional value space $E^1 = E$ only.

2 Stability of spatially homogeneous solutions

For 1-dimensional lattice space \mathbb{Z} and one-dimensional value space E , the dynamical system (7) is given by $f : E^{2s+1} \rightarrow E$. We denote $\frac{\partial f}{\partial x_i}$ the partial derivative of f by the i -th variable, $i = 1, \dots, 2s+1$.

Let \mathbf{u}^* be a fixed point of \mathcal{F} . It is well known, that the stability of \mathbf{u}^* of \mathcal{F} is determined by the spectrum of the linear operator $d\mathcal{F}|_{\mathbf{u}^*}$, i.e. by

$$\sigma(d\mathcal{F}|_{\mathbf{u}^*}).$$

Let us denote

$$\mathcal{A} = d\mathcal{F}|_{\mathbf{u}^*}$$

and for $j \in \mathbb{Z}$ and $k = j-s, \dots, j+s$ let

$$a_k^j = \frac{\partial f(u_{j-s}^*, \dots, u_{j+s}^*)}{\partial x_{k-j+s+1}}. \quad (8)$$

Then

$$\mathcal{A} : \mathbb{B} \rightarrow \mathbb{B}$$

is a linear bounded operator, such that $\mathbf{u} = \{u_j\}_{j \in \mathbb{Z}} \in \mathbb{B}$ satisfies (with respect to the relation (8))

$$(\mathcal{A}\mathbf{u})_j = \sum_{k=j-s}^{j+s} a_k^j u_k = \sum_{k=-s}^s a_{j+k}^j u_{j+k}. \quad (9)$$

Remark 3 If we formally set $a_k^j = 0$ for $j \in \mathbb{Z}$ and $k \neq j-s, \dots, j+s$, then the numbers a_k^j form the biinfinite matrix \mathbf{A} (where a_k^j is the number in the j -th row and in the k -th column). \mathbf{A} represents the linear operator \mathcal{A} as

$$\mathbf{A}\mathbf{u} = \mathcal{A}\mathbf{u}.$$

All nonzero elements of \mathbf{A} lie on the main diagonal or on s diagonal strips below and s diagonal strips above the main diagonal of \mathbf{A} .

In the following we shall consider the case, when the steady-state solution \mathbf{u}^* is the spatially homogeneous solution, i.e.

$$u_j^* = u^0 \quad \forall j \in \mathbb{Z}.$$

In this case (8) gives

$$a_{k+1}^{j+1} = a_k^j \quad \text{for all } j \in \mathbb{Z} \text{ and } k = j-s, \dots, j+s$$

or equivalently

$$a_{l+k}^l = a_{j+k}^j \quad \text{for all } l, j \in \mathbb{Z} \text{ and } k = -s, \dots, +s,$$

i.e. all rows of the matrix \mathbf{A} are identical except for a shift.

Let us denote

$$a_k = a_{j+k}^j \quad \text{for } k = -s, \dots, s.$$

Then the relation (9) has the form

$$(\mathcal{A}\mathbf{u})_j = \sum_{k=-s}^s a_k u_{j+k}. \quad (10)$$

3 Spectrum of the operator \mathcal{A}

In this section we consider the complex Banach space

$$\mathbb{B} = \{\mathbf{u} = \{u_j\}_{j \in \mathbb{Z}}; u_j \in \mathbb{C}, \sup\{|u_j|; j \in \mathbb{Z}\} < \infty\}$$

with the sup-norm and a linear bounded operator $\mathcal{A} : \mathbb{B} \rightarrow \mathbb{B}$ given by

$$(\mathcal{A}\mathbf{u})_j = \sum_{k=-s}^s a_k u_{j+k}, \quad (11)$$

where a_{-s}, \dots, a_s are given numbers. We describe the spectrum $\sigma(\mathcal{A})$ of the operator \mathcal{A} and in some cases we give a simple formula for the spectral radius $r_\sigma(\mathcal{A})$ of \mathcal{A} . Let us recall that $r_\sigma(\mathcal{A}) = \sup\{|\lambda|; \lambda \in \sigma(\mathcal{A})\}$.

Theorem 1 *The spectrum of the operator \mathcal{A} is given by*

$$\sigma(\mathcal{A}) = \left\{ \sum_{k=-s}^s a_k e^{ik\varphi}; \varphi \in [0, 2\pi] \right\}.$$

Moreover, the whole spectrum $\sigma(\mathcal{A})$ is formed by eigenvalues of \mathcal{A} .

At first, we prove Theorem 1 for a particular case of the left-shift operator $\mathcal{S} : \mathbb{B} \rightarrow \mathbb{B}$,

$$(\mathcal{S}\mathbf{u})_j = u_{j+1},$$

i.e. the only nonzero number in (10) is $a_1 = 1$.

Lemma 1 *The spectrum of the operator \mathcal{S} is given by*

$$\sigma(\mathcal{S}) = \{e^{i\varphi}; \varphi \in [0, 2\pi]\}.$$

Proof :

a) Let $\lambda \in \mathbb{C}$ and $\mathbf{u} \in \mathbb{B}$, $\mathbf{u} \neq \mathbf{o}$ be an eigenvalue and a corresponding eigenvector of \mathcal{S} , i.e. $(\mathcal{S} - \lambda\mathcal{I})\mathbf{u} = \mathbf{o}$. This implies

$$u_{n+1} - \lambda u_n = 0 \quad \text{for } n \in \mathbb{Z} \quad (12)$$

or

$$u_n = \lambda^n u_0 \text{ for } n \in \mathbb{Z} .$$

As \mathbf{u} is bounded and $\mathbf{u} \neq \mathbf{o}$, λ has to be a complex unit, i.e. $\lambda = e^{i\varphi}$ for some $\varphi \in [0, 2\pi]$.

Conversely, let $\lambda = e^{i\varphi}$ for $\varphi \in [0, 2\pi]$. We set

$$u_n = e^{in\varphi} , \quad n \in \mathbb{Z} .$$

Then λ and $\mathbf{u} = \{u_n\}_{n \in \mathbb{Z}}$ satisfy (12). Thus λ is an eigenvalue of \mathcal{S} .

b) Let $\lambda \neq e^{i\varphi}$ for all $\varphi \in [0, 2\pi]$. We show that $(\mathcal{S} - \lambda\mathcal{I})$ is a one-to-one mapping and consequently $\lambda \notin \sigma(\mathcal{S})$. It follows from part a) of the proof that $(\mathcal{S} - \lambda\mathcal{I})$ is injective. For $\mathbf{y} \in \mathbb{B}$ we will construct $\mathbf{x} \in \mathbb{B}$ such that $\mathbf{y} = (\mathcal{S} - \lambda\mathcal{I})\mathbf{x}$, i.e.

$$y_n = x_{n+1} - \lambda x_n , \quad n \in \mathbb{Z} . \quad (13)$$

We distinguish 3 cases.

i. $\lambda = 0$.

Then clearly $x_{n+1} = y_n$, $n \in \mathbb{Z}$, satisfy (13).

ii. $0 < |\lambda| < 1$.

For $n \in \mathbb{Z}$ set $x_n = \sum_{j=0}^{\infty} \lambda^j y_{n-j-1}$. Then

$$\begin{aligned} x_{n+1} - \lambda x_n &= \sum_{j=0}^{\infty} \lambda^j y_{n-j} - \sum_{j=0}^{\infty} \lambda^{j+1} y_{n-j-1} \\ &= y_n + \sum_{j=1}^{\infty} \lambda^j y_{n-j} - \sum_{j=0}^{\infty} \lambda^{j+1} y_{n-j-1} = y_n . \end{aligned}$$

iii. $|\lambda| > 1$.

For $n \in \mathbb{Z}$ set $x_n = -\sum_{j=0}^{\infty} \left(\frac{1}{\lambda}\right)^{j+1} y_{n+j}$. Then

$$\begin{aligned} x_{n+1} - \lambda x_n &= -\sum_{j=0}^{\infty} \left(\frac{1}{\lambda}\right)^{j+1} y_{n+j+1} + \sum_{j=0}^{\infty} \left(\frac{1}{\lambda}\right)^j y_{n+j} = \\ &= -\sum_{j=0}^{\infty} \left(\frac{1}{\lambda}\right)^{j+1} y_{n+j+1} + \sum_{j=1}^{\infty} \left(\frac{1}{\lambda}\right)^j y_{n+j} + y_n = y_n . \end{aligned}$$

■

Proof of Theorem 1:

It is easy to see that

$$\mathcal{A} = \sum_{k=-s}^s a_k \mathcal{S}^k ,$$

where \mathcal{S}^{-1} is the inverse operator to \mathcal{S} . As the function $g(z) = \sum_{k=-s}^s a_k z^k$ is analytical on the set $\{z \in \mathbb{C} ; z \neq 0\}$, Theorem 1 follows immediately from the following Theorem (see [3, Chapter 7, Theorem 11]):
Let $\mathcal{T} : X \rightarrow X$ be a linear bounded operator on a Banach space X . Let g be an analytical function on a neighbourhood of $\sigma(\mathcal{S})$. Then $\sigma(g(\mathcal{T})) = \{g(\lambda); \lambda \in \sigma(\mathcal{T})\}$. ■

Remark 4 The proof of Theorem 1 can be also based on the following weaker Theorem (see [5, Chapter 5, Theorem 5.2-D]):

Let P be a polynomial and $\mathcal{T} : X \rightarrow X$ be a linear bounded operator on a Banach space X . Then $\sigma(P(\mathcal{T})) = \{P(\lambda); \lambda \in \sigma(\mathcal{T})\}$.

Using this Theorem and Lemma 1 we have

$$\begin{aligned}
\lambda \in \sigma(\mathcal{A}) &\Leftrightarrow \mathcal{A} - \lambda \mathcal{I} \text{ is not a one-to-one mapping} \\
&\Leftrightarrow (\mathcal{A} - \lambda \mathcal{I})\mathcal{S}^s \text{ is not a one-to-one mapping} \\
&\Leftrightarrow a_{-s}\mathcal{I} + a_{-s+1}\mathcal{S} + \dots + a_{-1}\mathcal{S}^{s-1} + (a_0 - \lambda)\mathcal{S}^s + \\
&\quad + a_1\mathcal{S}^{s+1} + \dots + a_s\mathcal{S}^{2s} \text{ is not a one-to-one mapping} \\
&\Leftrightarrow -a_{-s} \in \sigma(a_{-s+1}\mathcal{S} + \dots + a_{-1}\mathcal{S}^{s-1} + (a_0 - \lambda)\mathcal{S}^s + \\
&\quad + a_1\mathcal{S}^{s+1} + \dots + a_s\mathcal{S}^{2s}) \\
&\Leftrightarrow -a_{-s} = a_{-s+1}e^{i\varphi} + \dots + a_{-1}e^{i(s-1)\varphi} + (a_0 - \lambda)e^{is\varphi} + \\
&\quad + a_1e^{i(s+1)\varphi} + \dots + a_se^{i2s\varphi} \\
&\Leftrightarrow \lambda = \sum_{k=-s}^s a_k e^{ik\varphi} .
\end{aligned}$$

Theorem 2 Let $a_k, -s \leq k \leq s$, be real numbers satisfying one of the following four conditions

- a) $a_k \geq 0$ for $-s \leq k \leq s$,
- b) $a_k \leq 0$ for $-s \leq k \leq s$,
- c) $a_{-s+2k} \geq 0$ for $0 \leq k \leq s$ and $a_{-s+2k+1} \leq 0$ for $0 \leq k \leq s-1$,
- or
- d) $a_{-s+2k} \leq 0$ for $0 \leq k \leq s$ and $a_{-s+2k+1} \geq 0$ for $0 \leq k \leq s-1$.

$$\text{Then } r_\sigma(\mathcal{A}) = \sum_{k=-s}^s |a_k|.$$

Proof :

Clearly

$$\begin{aligned}
\|\mathcal{A}\| &= \sup_{\|\mathbf{x}\|=1} \|\mathcal{A}(\mathbf{x})\| = \sup_{\|\mathbf{x}\|=1} \left(\sup_{j \in \mathbb{Z}} |(\mathcal{A}(\mathbf{x}))_j| \right) \\
&= \sup_{\|\mathbf{x}\|=1} \left(\sup_{j \in \mathbb{Z}} \left| \sum_{k=-s}^s a_k x_{j+k} \right| \right) = \sum_{k=-s}^s |a_k| .
\end{aligned}$$

Hence $r_\sigma(\mathcal{A}) \leq \sum_{k=-s}^s |a_k|$. On the other hand, the conditions a) - d) in fact mean that all a_k have the same sign or their sign alternates. If we choose $\varphi = 0$ for

cases a), b) and $\varphi = \pi$ for cases c), d) and apply Theorem 1, we get an eigenvalue λ satisfying $|\lambda| = \sum_{k=-s}^s |a_k|$. ■

Corollary 1 *Under the conditions of Theorem 2 it holds*

$$\|\mathcal{A}^n\| = \|\mathcal{A}\|^n$$

for all $n \in \mathbb{N}$.

Proof :

Suppose that $\|\mathcal{A}^k\| < \|\mathcal{A}\|^k$ for some $k > 1$. As $r_\sigma(\mathcal{A}) = \lim_{n \rightarrow \infty} \sqrt[n]{\|\mathcal{A}^n\|}$ (see [5, Chapter 5, Theorem 5.2-E]), we have

$$\begin{aligned} r_\sigma(\mathcal{A}) &= \lim_{n \rightarrow \infty} \sqrt[n]{\|\mathcal{A}^n\|} = \lim_{n \rightarrow \infty} \sqrt[nk]{\|\mathcal{A}^{nk}\|} \leq \lim_{n \rightarrow \infty} \sqrt[nk]{\|\mathcal{A}^k\|^n} = \\ &= \sqrt[k]{\|\mathcal{A}^k\|} < \sqrt[k]{\|\mathcal{A}\|^k} = \|\mathcal{A}\| , \end{aligned}$$

a contradiction. ■

Remark 5 It is also possible to prove Corollary 1 directly (e.g. by induction) and thus immediately get the proof of Theorem 2.

4 Applications

In this section we apply the above results to the discrete model arising in the reaction diffusion equation:

$$u_j(n+1) = u_j(n) + d(u_{j+1}(n) - 2u_j(n) + u_{j-1}(n)) + \alpha F_j(u_n) + \beta , \quad (14)$$

where $j \in \mathbb{Z}$, $n \in \mathbb{Z}^+$, $u_j(n) \in \mathbb{R}$, constants α, β and a diffusion coefficient d satisfy $\alpha, \beta, d > 0$ and the function F is given by

$$F(u) = \begin{cases} -2u , & u < \frac{1}{2} \\ -2(u-1) , & u > \frac{1}{2} . \end{cases}$$

This model was considered e.g. in [1], where it is also shown that the stability of steady-state solutions of (14) leads to the investigation of the spectrum of the operator $\mathcal{A} : \mathbb{B} \rightarrow \mathbb{B}$ given by

$$(\mathcal{A}u)_j = du_{j-1} + bu_j + du_{j+1} , \quad (15)$$

where $b = 1 - 2d - 2\alpha$. It follows immediately from Theorem 2 that

$$r_\sigma(\mathcal{A}) < 1 \quad \text{if and only if} \quad 2|d| + |1 - 2d - 2\alpha| < 1 .$$

This is equivalent (under conditions $d, \alpha > 0$) to

$$2d + \alpha < 1 . \tag{16}$$

The whole spectrum $\sigma(\mathcal{A})$ of the linear operator (15) is obtained immediately from Theorem 1 as follows:

$$\begin{aligned} \sigma(\mathcal{A}) &= \{de^{-i\varphi} + b + de^{i\varphi} ; \varphi \in [0, 2\pi]\} = \{b + 2d \cos \varphi ; \varphi \in [0, 2\pi]\} = \\ &= [b - 2d, b + 2d] = [1 - 4d - 2\alpha, 1 - 2\alpha] , \end{aligned}$$

i.e.

$$\sigma(\mathcal{A}) = [1 - 4d - 2\alpha, 1 - 2\alpha] . \tag{17}$$

This confirms derived stability condition (16). This result was obtained also in [1], though the methods used there are not always correct.

Acknowledgment

This work is supported by the grants GAČR 201/98/0220 and VZ CEZ: J19/98:223400007.

References

1. Afraimovich, V. S., Nekorkin, V. I.: Stable stationary motions in a chain diffusively coupled maps (in Russian). Preprint No 267, Inst. of Appl. Phys., N. Novgorod, 1991.
2. Chow, S.-N., Shen, W.: Stability and bifurcation of travelling wave solutions in coupled map lattice. Preprint, CDSNS177, 1994.
3. Dunford, N., Schwartz, J. T.: Linear operators, Part I: General Theory. Interscience Publishers, New York, London 1958.
4. Henry D.: Geometric Theory of Semilinear Parabolic Equations, Lecture Notes in Math., 840, Springer-Verlag, Berlin (1981).
5. Taylor, A. E.: Introduction to functional analysis. John Wiley & Sons, Inc., New York 1967.

A Simple Example of Lattice Dynamical System with Spatial Chaos

Alois Klíč, Daniel Turzík, Miroslava Dubcová, and Pavel Pokorný

Department of Mathematics
Institute of Chemical Technology, Prague

1 Introduction

The diversity of a pattern generation in spatially-extended systems is investigated by means of **lattice dynamical systems** (LDS), which consist of local discrete-time dynamical systems coupled in a spatial lattice. LDS can be as well interpreted as a time and spatial discretisation of the parabolic PDE. The last years were characterized by an increasing interest in the dynamics of spatially extended systems, see for example [1], [2]. This paper deals with a simple example of LDS on which we will demonstrate some interesting features.

2 Preliminaries

Let \mathbb{Z} be the set of all integers, the so called **lattice space**, and \mathbb{R} be the standard 1-dimensional real space.

Let us consider the set

$$\tilde{\mathbb{B}} = \{\mathbf{u}; \mathbf{u} = \{u_j\}, j \in \mathbb{Z}\}, \quad (1)$$

where $u_j \in \mathbb{R}$ for all $j \in \mathbb{Z}$, i.e. $\tilde{\mathbb{B}}$ is the set of all two-sided sequences of real numbers.

For

$$\mathbf{u} = \{u_j\}_{j \in \mathbb{Z}}$$

we denote

$$(\mathbf{u})_j = u_j.$$

Several norms can be defined on $\tilde{\mathbb{B}}$. In this paper we shall use the sup-norm

$$\|\mathbf{u}\|_\infty = \|\mathbf{u}\| = \sup_{j \in \mathbb{Z}} |u_j|. \quad (2)$$

The space

$$\mathbb{B} = \{\mathbf{u} \in \tilde{\mathbb{B}}; \|\mathbf{u}\| < \infty\} \quad (3)$$

is the Banach space, which plays the role of a **phase space**.

For a fixed integer s and $\{u_j\}_{j \in \mathbb{Z}} \in \mathbb{B}$ we denote

$$\{u_j\}^s = (u_{j-s}, \dots, u_j, \dots, u_{j+s}) \in \mathbb{R}^{2s+1}. \quad (4)$$

We define the mapping

$$\mathcal{F} : \mathbb{B} \rightarrow \mathbb{B} \quad (5)$$

by the relation

$$(\mathcal{F}\mathbf{u})_j = f(\{u_j\}^s), \quad j \in \mathbb{Z}, \quad (6)$$

where

$$f : \mathbb{R}^{2s+1} \rightarrow \mathbb{R} \quad (7)$$

is a differentiable mapping of class C^2 . Under some additional assumptions on the function f (Lipschitz condition) it is not difficult to show, that

$$\mathcal{F}(\mathbb{B}) \subset \mathbb{B}.$$

Thus the **discrete dynamical system** (DDS)

$$(\mathcal{F}^n, \mathbb{B})_{n \in \mathbb{Z}^+} \quad (8)$$

is correctly defined. This DDS is called the **lattice dynamical system** (LDS).

Remark 1 A more general definition of LDS can be found for example in [2].

Definition 1 The fixed point \mathbf{u}^* of the mapping \mathcal{F} , i.e.

$$\mathcal{F}\mathbf{u}^* = \mathbf{u}^*, \quad (9)$$

is called a **steady-state solution** of the LDS (8).

Remark 2 The $\mathbf{u}^* = \{u_j^*\}_{j \in \mathbb{Z}}$ is fixed point of \mathcal{F} iff the following relation holds

$$u_j^* = f(\{u_j^*\}^s) \quad (10)$$

for all $j \in \mathbb{Z}$.

Definition 2 Let $\mathbf{u}^* = \{u_j^*\}_{j \in \mathbb{Z}}$ be a steady-state solution of LDS $(\mathcal{F}^n, \mathbb{B})_{n \in \mathbb{Z}^+}$. If there exists $p \geq 1$ such that

$$u_{j+p}^* = u_j^* \quad \text{for all } j \in \mathbb{Z}, \quad (11)$$

then \mathbf{u}^* will be called the **spatially periodic solution**. If $p = 1$, then the \mathbf{u}^* is called the **spatially homogeneous solution**.

Remark 3 The spatially homogeneous solution $\mathbf{u}^* = \{u_j^*\}_{j \in \mathbb{Z}}$ satisfies

$$u_j^* = u_0, \quad \text{for all } j \in \mathbb{Z}. \quad (12)$$

On the space \mathbb{B} **another** dynamical system can be defined as follows: Let us fix $j_0 \in \mathbb{Z}$ and define the mapping

$$\mathcal{S}_{j_0} : \mathbb{B} \rightarrow \mathbb{B}$$

by the relation

$$(\mathcal{S}_{j_0}\mathbf{u})_j = u_{j+j_0}, \quad \text{for all } j \in \mathbb{Z}. \quad (13)$$

Definition 3 *The mapping \mathcal{S}_{j_0} , $j_0 \in \mathbb{Z}$ defines the DDS $(\mathcal{S}_{j_0}^n, \mathbb{B})$, which is called the **translation dynamical system** (TDS).*

Remark 4 Clearly, each map \mathcal{S}_{j_0} is a linear bounded operator, which commutes with the evolution operator \mathcal{F} , i.e.

$$\mathcal{F} \circ \mathcal{S}_{j_0} = \mathcal{S}_{j_0} \circ \mathcal{F}. \quad (14)$$

Moreover, if \mathbf{u}^* is a spatially p -periodic solution, then

$$\mathcal{S}_p \mathbf{u}^* = \mathbf{u}^*.$$

The relation (14) yields the following simple but important result. If \mathbf{u}^* is a steady-state solution of LDS, then for every $j_0 \in \mathbb{Z}$ the $\mathcal{S}_{j_0} \mathbf{u}^*$ is **also** a steady-state solution, because with respect to the relation (14) we have

$$\mathcal{F}(\mathcal{S}_{j_0} \mathbf{u}^*) = \mathcal{S}_{j_0}(\mathcal{F} \mathbf{u}^*) = \mathcal{S}_{j_0} \mathbf{u}^*.$$

3 An example

In this section we set $s = 1$, hence the relation (4) has the form

$$\{u_j\}^{s=1} = (u_{j-1}, u_j, u_{j+1}).$$

In (7) we shall consider the function f of the form

$$f(u_{j-1}, u_j, u_{j+1}) = u_j + u_{j-1}^2 + u_j^2 + u_{j+1}^2 - 1. \quad (15)$$

3.1 Steady-state solutions

We are interesting in steady-state solutions of the corresponding LDS. The equation (10) for these ones has the form (without asterisks)

$$u_j = u_j + u_{j-1}^2 + u_j^2 + u_{j+1}^2 - 1, \quad (16)$$

i.e.

$$u_{j-1}^2 + u_j^2 + u_{j+1}^2 - 1 = 0. \quad (17)$$

The equation (17) defines the following four functions:

$$u_{j+1} = \sqrt{1 - u_{j-1}^2 - u_j^2}, \quad (18)$$

$$u_{j+1} = -\sqrt{1 - u_{j-1}^2 - u_j^2}, \quad (19)$$

$$u_{j-1} = \sqrt{1 - u_j^2 - u_{j+1}^2}, \quad (20)$$

$$u_{j-1} = -\sqrt{1 - u_j^2 - u_{j+1}^2}. \quad (21)$$

All these functions are defined on the closed unit disk

$$\mathbb{D} = \{(x, y) \in \mathbb{R}^2; x^2 + y^2 \leq 1\}.$$

We will use the relations (18) - (21) for the creation of the steady-state solutions of our LDS. The procedure is as follows: We choose

$$u_0 = x, u_1 = y, (x, y) \in \mathbb{D}$$

and all u_j for $j \geq 2$ are determined by the relations (18) resp. (19). Further, all u_j for $j \leq -1$ are determined by the relations (20) resp. (21).

At the same time, we can **alternate** the using of the relations (18), (19) resp. (20), (21) in an arbitrary described order.

We shall use the notation from **symbolic dynamics**, i.e.

$$\Sigma_2 = \{0, 1\}^{\mathbb{Z}} = \{\boldsymbol{\omega} = (\dots, \omega_{-1}, \omega_0, \omega_1, \dots); \omega_j \in \{0, 1\}, \text{ for all } j \in \mathbb{Z}\}.$$

The shift map

$$\sigma : \Sigma_2 \rightarrow \Sigma_2$$

is defined by

$$(\sigma(\boldsymbol{\omega}))_j = \omega_{j+1} \quad (22)$$

for all $j \in \mathbb{Z}$ (see [3] for more details).

Remark 5 To every $(x, y) \in \mathbb{D}$ and $\boldsymbol{\omega} \in \Sigma_2$ there corresponds one steady-state solution

$$\mathbf{u}^* = \mathbf{u}^*(x, y, \boldsymbol{\omega}) \quad (23)$$

of the LDS defined by the function (15) as follows: Let $\boldsymbol{\omega} = \{\omega_n\}_{n \in \mathbb{Z}} \in \Sigma_2$ and $u_0^* = (-1)^{\omega_0} x$, $u_1^* = (-1)^{\omega_1} y$. Then for the calculation of u_2^* we shall use the relation (18) for $\omega_2 = 0$, the relation (19) for $\omega_2 = 1$ and so on. Similarly we shall calculate u_{-1}^* using (20) for $\omega_{-1} = 0$, using (21) for $\omega_{-1} = 1$ and so on.

More precisely, for every $(x, y) \in \mathbb{D}$ and $\boldsymbol{\omega} \in \Sigma_2$ we can construct inductively a steady-state solution $U(x, y, \boldsymbol{\omega}) = \{u_j\}_{j \in \mathbb{Z}}$ as follows:

- a. Set $u_0 = (-1)^{\omega_0} x$ and $u_1 = (-1)^{\omega_1} y$.
- b. For $j = 2, 3, \dots$ set $u_j = (-1)^{\omega_j} \sqrt{1 - u_{j-1}^2 - u_{j-2}^2}$.
- c. For $j = -1, -2, \dots$ set $u_j = (-1)^{\omega_j} \sqrt{1 - u_{j+1}^2 - u_{j+2}^2}$.

Clearly $\mathbf{u} = \{u_j\}_{j \in \mathbb{Z}}$ satisfies (17) for every $j \in \mathbb{Z}$, which means that \mathbf{u} is a steady-state solution of our LDS.

Conversely, it is not difficult to see that every steady-state solution of our LDS arises by that way. Really, if $\mathbf{u} = \{u_j\}_{j \in \mathbb{Z}}$ is a steady-state solution, we set

$$x = |u_0|, y = |u_1| \text{ and } \omega_j = \begin{cases} 1 & \text{if } u_j < 0 \\ 0 & \text{if } u_j \geq 0 \end{cases} \text{ for } j \in \mathbb{Z}. \quad (24)$$

Then $\mathbf{u} = U(x, y, \boldsymbol{\omega})$. Thus we defined the mapping

$$U : \mathcal{A} \rightarrow \mathbb{B}, \quad \text{where } \mathcal{A} = \mathbb{D} \times \Sigma_2, \quad (25)$$

which to each element $(x, y, \boldsymbol{\omega}) \in \mathcal{A}$ assigns a steady-state solution of our LDS, i.e. satisfies

$$\mathcal{F}(U(x, y, \boldsymbol{\omega})) = U(x, y, \boldsymbol{\omega}) \quad (26)$$

for every $(x, y, \boldsymbol{\omega}) \in \mathcal{A}$.

Let us fix $\boldsymbol{\omega} \in \Sigma_2$. Then we obtain the mapping

$$U^{\boldsymbol{\omega}} : \mathbb{D} \rightarrow \mathbb{B}, \quad U^{\boldsymbol{\omega}}(x, y) = U(x, y, \boldsymbol{\omega}). \quad (27)$$

For example, if $\boldsymbol{\omega}_0 = \{\omega_n\}_{n \in \mathbb{Z}}$, where $\omega_n = 0$ for all $n \in \mathbb{Z}$ and $x \geq 0, y \geq 0, (x, y) \in \mathbb{D}$, the corresponding steady-state solution has the following form :

$$\{\dots, x, y, \sqrt{1 - x^2 - y^2}, u_0 = x, u_1 = y, \sqrt{1 - x^2 - y^2}, x, y, \dots\}. \quad (28)$$

This steady-state solution is spatially 3-periodic with respect to the following relations:

$$\begin{aligned} u_0 = x, \quad u_1 = y, \quad u_2 = \sqrt{1 - x^2 - y^2}, \\ u_3 = \sqrt{1 - u_1^2 - u_2^2} = x, \quad u_4 = \sqrt{1 - u_2^2 - u_3^2} = y. \end{aligned}$$

Similarly for u_{-1}, u_{-2}, \dots

It is easy to see, that the general steady-state solution for an arbitrary $\boldsymbol{\omega} \in \Sigma_2$ has the form

$$\begin{aligned} U(x, y, \boldsymbol{\omega}) = \{ \dots, (-1)^{\omega_{-1}} \sqrt{1 - x^2 - y^2}, u_0 = (-1)^{\omega_0} x, \\ u_1 = (-1)^{\omega_1} y, (-1)^{\omega_2} \sqrt{1 - x^2 - y^2}, (-1)^{\omega_3} x, (-1)^{\omega_4} y, \dots \}. \end{aligned} \quad (29)$$

Proposition 1 *Let \mathbb{D}_0 denote the interior of the set \mathbb{D} , i.e.*

$$\mathbb{D}_0 = \{(x, y) ; x^2 + y^2 < 1\} .$$

Then the map $U^{\boldsymbol{\omega}} : \mathbb{D}_0 \rightarrow \mathbb{B}$ is differentiable on \mathbb{D}_0 .

Taking into account the relation (29) and the norm (2) the proof is evident.

For fixed $\boldsymbol{\omega} \in \Sigma_2$, the relation (26) has the form

$$\mathcal{F}(U^{\boldsymbol{\omega}}(x, y)) = U^{\boldsymbol{\omega}}(x, y). \quad (30)$$

By differentiation of this equality by x and y , respectively we obtain

$$\begin{aligned} d\mathcal{F}|_{U^{\boldsymbol{\omega}}(x, y)} U_x^{\boldsymbol{\omega}}(x, y) &= U_x^{\boldsymbol{\omega}}(x, y), \\ d\mathcal{F}|_{U^{\boldsymbol{\omega}}(x, y)} U_y^{\boldsymbol{\omega}}(x, y) &= U_y^{\boldsymbol{\omega}}(x, y), \end{aligned} \quad (31)$$

where $U_x^\omega(x, y) = \frac{\partial}{\partial x} U^\omega(x, y)$ and $d\mathcal{F}|_{U^\omega(x, y)}$ is a linear operator - the linearization of the mapping \mathcal{F} at the steady-state solution $U^\omega(x, y)$.

Conclusion: The relations (31) show, that the linear operator $d\mathcal{F}|_{U^\omega(x, y)}$ has (at least) **double** eigenvalue 1 and the corresponding two-dimensional eigenspace is generated by two eigenvectors $U_x^\omega(x, y)$ and $U_y^\omega(x, y)$. For example, for the steady-state solution (28) we have the corresponding eigenvectors

$$U_x^{\omega_0}(x, y) = \left\{ \dots, 1, 0, \frac{-x}{\sqrt{1-x^2-y^2}}, 1, 0, \frac{-x}{\sqrt{1-x^2-y^2}}, \dots \right\},$$

$$U_y^{\omega_0}(x, y) = \left\{ \dots, 0, 1, \frac{-y}{\sqrt{1-x^2-y^2}}, 0, 1, \frac{-y}{\sqrt{1-x^2-y^2}}, \dots \right\}.$$

Remark 6 The conclusion yields that all steady-state solutions $U(x, y, \omega)$ are not linearly asymptotically stable with respect to the system $(\mathcal{F}^n, \mathbb{B})$ determined by the function (15).

Remark 7 The whole spectrum of $d\mathcal{F}|_{\mathbf{u}^*}$, where $\mathbf{u}^* = U^{\omega_0}(\frac{1}{2}, \frac{1}{2})$, consists of two intervals on the real axis:

$$\sigma(d\mathcal{F}|_{\mathbf{u}^*}) = \left[\frac{2 + \sqrt{2} - \sqrt{2 + 8\sqrt{2}}}{2}, 3 \right] \cup \left[\frac{2 + \sqrt{2} + \sqrt{2 + 8\sqrt{2}}}{2}, 3 + \sqrt{2} \right],$$

see [4].

Remark 8 Every steady-state solution

$$U(x_0, y_0, \omega) = \{u_j^*\}_{j \in \mathbb{Z}}$$

determines a mapping S on \mathbb{D}_0 by the following relation:

$$S(u_0^*, u_1^*) = (u_1^*, u_2^*).$$

The action of the translation operator \mathcal{S}_1 on the steady-state solution $U(x_0, y_0, \omega)$ can be expressed by the relation

$$\mathcal{S}_1 U(x_0, y_0, \omega) = U(S(x_0, y_0), \sigma(\omega)).$$

3.2 Spatial chaos

Let us fix $(x_0, y_0) \in \mathbb{D}_0$, $x_0 > 0$, $y_0 > 0$. We denote

$$\tilde{\Lambda} = \tilde{\Lambda}(x_0, y_0) = \{U(x_0, y_0, \omega) ; \omega \in \Sigma_2\}.$$

Let us consider the TDS $(\mathcal{S}_1^n, \mathbb{B})$ (see Definition 3) and set

$$\Lambda = \bigcup_{n \in \mathbb{Z}} \mathcal{S}_1^n \tilde{\Lambda}. \tag{32}$$

Clearly, the set A consists entirely of steady-state solutions and it is a closed invariant set of the TDS $(\mathcal{S}_1^n, \mathbb{B})$. We shall show, that the $\mathcal{S}_1|_A$ behaves stochastically, that means the $\mathcal{S}_1|_A$ has a **positive topological entropy**. To this aim we will apply some results from the theory of the topological Markov chains (TMC), see e.g. [3] and [5].

Let us denote

$$z_0 = \sqrt{1 - x_0^2 - y_0^2}.$$

Then every element $\mathbf{u}^* \in A$, $\mathbf{u}^* = \{u_j^*\}_{j \in \mathbb{Z}}$, is two-sided sequence of **six** elements (or symbols)

$$x_0, y_0, z_0, -x_0, -y_0, -z_0,$$

numbered by turn 1, 2, 3, 4, 5, 6.

All admissible transitions between these symbols are determined by the following **transition matrix**:

$$\mathbf{A} = \begin{bmatrix} 0 & 1 & 0 & 0 & 1 & 0 \\ 0 & 0 & 1 & 0 & 0 & 1 \\ 1 & 0 & 0 & 1 & 0 & 0 \\ 0 & 1 & 0 & 0 & 1 & 0 \\ 0 & 0 & 1 & 0 & 0 & 1 \\ 1 & 0 & 0 & 1 & 0 & 0 \end{bmatrix} \quad (33)$$

We remark that $\mathcal{S}_1|_A = \sigma_A$ - **the subshift of finite type**. The matrix \mathbf{A} in (33) has the following **eigenvalues**:

$$\lambda_{1,2,3} = 0; \lambda_4 = 2, \lambda_{5,6} = -1 \pm i\sqrt{3}. \quad (34)$$

Since the **greatest positive** eigenvalue $\lambda(\mathbf{A})$ of the matrix \mathbf{A} is equal to 2, the topological entropy of the mapping $\mathcal{S}_1|_A$ is (see [5])

$$h(\mathcal{S}_1|_A) = \ln \lambda(\mathbf{A}) = \ln 2 > 0. \quad (35)$$

It is easy to see that the matrix \mathbf{A} (or corresponding TMC) is **indecomposable**, because

$$a_{12} \cdot a_{23} \cdot a_{34} \cdot a_{45} \cdot a_{56} \cdot a_{61} > 0.$$

Further, because $|\lambda_{5,6}| = 2$, there are **three** eigenvalues of the matrix \mathbf{A} lying on the circle $|z| = \lambda(\mathbf{A})$. Thus according to the Frobenius-Perron Theorem, the matrix \mathbf{A} splits on 3 primitive matrix and the cyclicity index of the matrix \mathbf{A} is equal to 3.

Conclusion: We have shown, that the translation mapping \mathcal{S}_1 behaves on the set of the steady-state solutions A by the same way as the subshift of the finite type σ_A on the set Σ_A of all admissible sequences of six symbols. In our case, the topological entropy of the mapping $\mathcal{S}_1|_A$ is **positive**, hence the **spatial chaos** in our LDS is realized, see [2]

Acknowledgment

This work is supported by the grants GAČR 201/98/0220 and VZ CEZ: J19/98:223400007.

References

1. V. S. Afraimovitch, L. A. Bunimovich: Density of defects and spatial entropy in extended systems. *Physica D80 (1995) pp. 277-288.*
2. V. S. Afraimovitch, S.-N. Chow: Topological Spatial Chaos and Homoclinic Points of \mathbb{Z}^d in Lattice Dynamical Systems. *Japan Journal of Industrial and Appl. Math., Vol. 12, No. 3, (1995) pp.367-383.*
3. A. Katok, B. Hasselblatt: Introduction to the Modern Theory of Dynamical Systems. *Encyclopedia of Mathematics and its Applications, CAMBRIDGE University Press., 1995*
4. P. Pokorný, D. Turzík, A. Klíč, M. Dubcová: Stability of Spatially periodic Steady - State Solutions of LDS (in preparation).
5. V. M. Aleksejev, M. V. Jakobson: Symbolic Dynamics and Hyperbolic Dynamical Systems. Appendix in: R. Bowen, *Methods of Symbolic Dynamics, (in Russian) Mir, Moskva 1979.*

On Spectra of Certain Class of Linear Operators

P. Pokorný, D. Turzík, M. Dubcová, A. Klíe

Department of Mathematics,
Institute of Chemical Technology, Prague

Abstract Certain class of linear operators arising in the study of the stability of solution of lattice dynamical systems is investigated. Fourier transform and the theory of distributions are used to show that the spectrum consists of the point spectrum only and its explicit form is found. Several examples are presented.

1 Introduction

Lattice dynamical systems, besides being an interesting mathematical problem of its own, present a useful simplification for the investigation of partial differential equations describing e.g. reaction diffusion dynamical systems, see [1].

In finite dimensional discrete dynamical systems, the stability of a solution is given by the spectrum of the linearization matrix evaluated at the solution. For an infinite dimensional discrete dynamical system the stability of a solution is again given by the spectrum of the linearized operator, see [3]. We will consider a linear operator $\mathcal{A} : \mathbb{B} \rightarrow \mathbb{B}$, where \mathbb{B} is a Banach space, which arises in the study of stability of the spatially homogeneous steady state solutions of a certain lattice dynamical system [2], [6].

The spectrum $\sigma(\mathcal{A})$ of a general operator $\mathcal{A} : \mathbb{B} \rightarrow \mathbb{B}$ consists of three parts (see [5]):

(i) the point spectrum $\sigma_p(\mathcal{A})$ formed by the eigenvalues λ satisfying

$$\mathcal{A}\mathbf{x} = \lambda\mathbf{x} , \tag{1}$$

(ii) the residual spectrum $\sigma_r(\mathcal{A})$ formed by all the complex values λ for which the range of the operator $\mathcal{A} - \lambda I$ is not dense in \mathbb{B} (here I denotes the identity operator), and

(iii) the continuous spectrum $\sigma_c(\mathcal{A})$ formed by all the complex values λ for which the operator $\mathcal{A} - \lambda I$ has not a bounded inverse and the range of $\mathcal{A} - \lambda I$ is dense in \mathbb{B} .

The complement of the spectrum in the complex plane is the resolvent set $\rho(\mathcal{A})$.

In section 2 we state the main result and indicate the idea of its proof despite the fact that the derivation is not correct. In section 3 the theory of distributions is used for the rigorous proof of the main statement about the spectrum of the operator.

2 The main result

Consider a linear operator $\mathcal{A} : \mathbb{B} \rightarrow \mathbb{B}$ acting on a Banach space \mathbb{B} of bounded two-sided sequences \mathbf{x} of complex numbers x_n with the supremum norm

$$\|\mathbf{x}\| = \sup_{n \in \mathbb{Z}} |x_n|. \quad (2)$$

We consider a certain class of operators that are given by

$$(\mathcal{A}\mathbf{x})_j = \sum_{n \in \mathbb{Z}} a_n x_{j-n} \quad (3)$$

where a_n are complex numbers satisfying

$$\lim_{n \rightarrow \pm\infty} n^p a_n = 0 \quad (4)$$

for any positive integer p , i.e. a_n tend to zero for $|n| \rightarrow \infty$ faster than any power of $1/|n|$.

We prove the following:

Theorem *The spectrum $\rho(\mathcal{A})$ of \mathcal{A} consists of the point spectrum only and it is*

$$\sigma(\mathcal{A}) = \left\{ \sum_{n \in \mathbb{Z}} a_n e^{-i2\pi\nu n}; \nu \in \mathbb{R} \right\}, \quad (5)$$

where $i = \sqrt{-1}$, i.e. it is a closed finite length curve in the complex plane.

Now we informally describe the main ideas used in the next section for the proof of the Theorem.

The action of the operator \mathcal{A} on the sequence \mathbf{x} is actually a convolution between the sequence $\mathbf{a} = \{a_n\}_{n \in \mathbb{Z}}$ and the sequence $\mathbf{x} = \{x_n\}_{n \in \mathbb{Z}}$

$$(\mathbf{a} * \mathbf{x})_j = \sum_{n \in \mathbb{Z}} a_n x_{j-n}. \quad (6)$$

The Fourier type transform

$$\widehat{\mathbf{x}}(\nu) = \sum_{n \in \mathbb{Z}} x_n e^{-i2\pi\nu n} \quad (7)$$

converts the sequence of complex numbers into a complex function of a real argument.

The Fourier image of a convolution of two sequences is the product of the Fourier images of the two sequences:

$$\begin{aligned} \widehat{\mathbf{a} * \mathbf{x}}(\nu) &= \sum_{j \in \mathbb{Z}} (\mathbf{a} * \mathbf{x})_j e^{-i2\pi\nu j} = \sum_{j \in \mathbb{Z}} \sum_{n \in \mathbb{Z}} a_n x_{j-n} e^{-i2\pi\nu j} = \\ &= \sum_{n \in \mathbb{Z}} a_n \sum_{j \in \mathbb{Z}} x_{j-n} e^{-i2\pi\nu j} = \sum_{n \in \mathbb{Z}} a_n e^{-i2\pi\nu n} \sum_{j \in \mathbb{Z}} x_{j-n} e^{-i2\pi\nu(j-n)} = \end{aligned}$$

$$= \left(\sum_{n \in Z} a_n e^{-i2\pi\nu n} \right) \left(\sum_{j \in Z} x_j e^{-i2\pi\nu j} \right) = \widehat{\mathbf{a}}(\nu) \widehat{\mathbf{x}}(\nu).$$

Then (1) with respect to (3) can be written as

$$\mathbf{a} * \mathbf{x} = \lambda \mathbf{x}. \quad (8)$$

Applying the Fourier transform on both sides gives

$$\begin{aligned} \widehat{\mathbf{a} * \mathbf{x}} &= \widehat{\lambda \mathbf{x}}. \\ \widehat{\mathbf{a}}(\nu) \widehat{\mathbf{x}}(\nu) &= \lambda \widehat{\mathbf{x}}(\nu) \\ (\widehat{\mathbf{a}}(\nu) - \lambda) \widehat{\mathbf{x}}(\nu) &= 0. \end{aligned} \quad (9)$$

Now depending on λ we distinguish two cases.

(a) If $\lambda \neq \widehat{\mathbf{a}}(\nu)$ for all $\nu \in \mathbb{R}$, then (9) implies $\widehat{\mathbf{x}}(\nu) = 0$ for all $\nu \in \mathbb{R}$ and thus $x_n = 0$ for all $n \in Z$.

As the function

$$\frac{1}{\widehat{\mathbf{a}}(\nu) - \lambda}$$

is bounded, the equation

$$(\mathcal{A} - \lambda I) \mathbf{x} = \mathbf{b}$$

which is equivalent to

$$(\widehat{\mathbf{a}}(\nu) - \lambda) \widehat{\mathbf{x}}(\nu) = \widehat{\mathbf{b}}(\nu)$$

has a unique solution $\mathbf{x} \in \mathbb{B}$ for any $\mathbf{b} \in \mathbb{B}$ satisfying

$$\widehat{\mathbf{x}}(\nu) = \frac{\widehat{\mathbf{b}}(\nu)}{\widehat{\mathbf{a}}(\nu) - \lambda}.$$

Thus if $\lambda \neq \widehat{\mathbf{a}}(\nu)$ for all $\nu \in \mathbb{R}$, then λ belongs to the resolvent set $\varrho(\mathcal{A})$.

(b) If there exists a real value $\nu_0 \in \mathbb{R}$ such that $\lambda = \widehat{\mathbf{a}}(\nu_0)$ then the operator $\mathcal{A} - \lambda I$ is no longer invertible and λ is an eigenvalue of \mathcal{A} . The corresponding eigenvector \mathbf{x} can be found from (9)

$$\widehat{\mathbf{x}}(\nu) = \delta_{\nu_0}(\nu),$$

where $\delta_{\nu_0}(\nu)$ is the Dirac delta distribution in the point ν_0 .

Remark Some authors use the term Fourier transform for a transformation of a function of a continuous argument into a function of a continuous argument only. We use the term Fourier transform in a more general sense, to denote both the transform of a function (10) and that of a sequence (7). The full justification of our approach will be clear in the next section, where we use the theory of distributions. The reason is that a function φ (a sequence \mathbf{x} resp.) generates a distribution T_φ ($T\mathbf{x}$ resp.) and the Fourier transform of the resulting distribution is equal to the distribution generated by the Fourier transform of the given function (the sequence resp.) if they exist.

3 Proof of the Theorem

To prove the Theorem we have to show the following:

- I.** If $\lambda = \widehat{\mathbf{a}}(\nu_0) = \sum_{n \in \mathbb{Z}} a_n e^{-i2\pi\nu_0 n}$ for some $\nu_0 \in \mathbb{R}$, then λ is the eigenvalue of the operator \mathcal{A} .
- II.** If $\lambda \neq \widehat{\mathbf{a}}(\nu)$ for every $\nu \in \mathbb{R}$, then
 - (a) the operator $\mathcal{A} - \lambda I$ is injective,
 - (b) the equation $(\mathcal{A} - \lambda I)\mathbf{x} = \mathbf{b}$ has a solution for any $\mathbf{b} \in \mathbb{B}$.

The proof of **I.** is easy. For $\lambda = \widehat{\mathbf{a}}(\nu_0)$ set

$$x_n = e^{i2\pi\nu_0 n} .$$

Then

$$\begin{aligned} ((\mathcal{A} - \lambda I)\mathbf{x})_j &= (\mathcal{A}\mathbf{x})_j - \lambda x_j = \sum_{n \in \mathbb{Z}} a_n x_{j-n} - \lambda x_j = \\ &= \sum_{n \in \mathbb{Z}} a_n e^{i2\pi\nu_0(j-n)} - \sum_{n \in \mathbb{Z}} a_n e^{-i2\pi\nu_0 n} e^{i2\pi\nu_0 j} = 0 , \end{aligned}$$

which means that λ is the eigenvalue and \mathbf{x} is the corresponding eigenvector of the operator \mathcal{A} .

The proof of **II.** is more complicated.

The conditions of convergence of infinite series were ignored in the previous section. The convolution (6) is convergent due to the condition (4) on a_n and due to the assumption of the finite supremum norm (2) of \mathbf{x} . The necessary condition for the Fourier transform (7) to converge,

$$\lim_{n \rightarrow \infty} |x_n| = 0 ,$$

may not be satisfied for $\mathbf{x} \in \mathbb{B}$. The legal way out of this conflict is to use the theory of distributions, see [4].

The main idea is like this: instead of considering the values x_n of a given sequence \mathbf{x} (and its sum over all integers) we consider rather the “projection”

$$\langle T\mathbf{x}, \varphi \rangle = \sum_{n \in \mathbb{Z}} x_n \varphi(n)$$

of the sequence \mathbf{x} into various functions $\varphi \in \mathcal{S}$. Here \mathcal{S} is the space of all infinitely differentiable complex functions of a real variable x for which the absolute value of the function and the absolute value of all its derivatives tends for $|x| \rightarrow \infty$ to zero faster than any power of $1/|x|$.

The Fourier image $\widehat{\varphi}$ of $\varphi \in \mathcal{S}$ is defined as

$$\widehat{\varphi}(\nu) = \int_{-\infty}^{\infty} \varphi(t) e^{-i2\pi\nu t} dt \tag{10}$$

and the inverse Fourier image $\check{\varphi}$ of $\varphi \in \mathcal{S}$ is defined as

$$\check{\varphi}(\nu) = \int_{-\infty}^{\infty} \varphi(t) e^{i2\pi\nu t} dt. \quad (11)$$

We will apply the result of the theory of Fourier transform that

$$\check{\check{\varphi}} = \widehat{\widehat{\varphi}} = \varphi$$

for any $\varphi \in \mathcal{S}$ (see [4]).

Given a sequence

$$\mathbf{x} = \{x_n\}_{n \in \mathbb{Z}} \in \mathbb{B}$$

we construct a continuous linear functional, a distribution, $T_{\mathbf{x}} : \mathcal{S} \rightarrow \mathbb{C}$,

$$\langle T_{\mathbf{x}}, \varphi \rangle = \sum_{n \in \mathbb{Z}} x_n \varphi(n) \quad (12)$$

for any $\varphi \in \mathcal{S}$. Since x_n is bounded this series converges.

We will use the obvious fact that for any $\mathbf{x}, \mathbf{y} \in \mathbb{B}$

$$\langle T_{\mathbf{x}}, \varphi \rangle = \langle T_{\mathbf{y}}, \varphi \rangle \text{ for every } \varphi \in \mathcal{S} \text{ if and only if } \mathbf{x} = \mathbf{y} .$$

Further we use the fact that the function

$$\widehat{\alpha}(\nu) = \frac{1}{\widehat{\mathbf{a}}(\nu) - \lambda} \quad (13)$$

is smooth, bounded and periodic (as $\widehat{\mathbf{a}}(\nu)$ is so) and we can write $\widehat{\alpha}$ as a Fourier series

$$\widehat{\alpha}(\nu) = \sum_{k \in \mathbb{Z}} \alpha_k e^{-i2\pi\nu k} \quad (14)$$

where $\alpha_k \in \mathbb{C}$ and moreover satisfy (4)

The proof of **II.** is based on the following Lemma

Lemma

$$(\mathcal{A} - \lambda I)\mathbf{x} = \mathbf{b} \text{ if and only if } \langle T_{\mathbf{x}}, \varphi \rangle = \langle T_{\mathbf{b}}, \widehat{\alpha\widehat{\varphi}} \rangle \text{ for every } \varphi \in \mathcal{S} .$$

Proof :

Clearly, $(\mathcal{A} - \lambda I)\mathbf{x} = \mathbf{b}$ if and only if $\langle T_{(\mathcal{A} - \lambda I)\mathbf{x}}, \widehat{\varphi} \rangle = \langle T_{\mathbf{b}}, \widehat{\varphi} \rangle$ for every $\varphi \in \mathcal{S}$, i. e.

$$\sum_{n \in \mathbb{Z}} \left(\sum_{k \in \mathbb{Z}} a_k x_{n-k} \right) \widehat{\varphi}(n) - \sum_{n \in \mathbb{Z}} \lambda x_n \widehat{\varphi}(n) = \sum_{n \in \mathbb{Z}} b_n \widehat{\varphi}(n). \quad (15)$$

Let us manipulate the left hand side

$$L = \sum_{n \in \mathbb{Z}} \left(\sum_{k \in \mathbb{Z}} a_k x_{n-k} \right) \widehat{\varphi}(n) - \sum_{n \in \mathbb{Z}} \lambda x_n \widehat{\varphi}(n).$$

We change the order of the summation

$$L = \sum_{k \in \mathbb{Z}} a_k \sum_{n \in \mathbb{Z}} x_{n-k} \widehat{\varphi}(n) - \sum_{n \in \mathbb{Z}} \lambda x_n \widehat{\varphi}(n)$$

and we shift n by k by summing over $n_{new} = n - k$ in the inner sum (we drop the index *new*)

$$L = \sum_{k \in \mathbb{Z}} a_k \left(\sum_{n \in \mathbb{Z}} x_n \right) \widehat{\varphi}(n+k) - \sum_{n \in \mathbb{Z}} \lambda x_n \widehat{\varphi}(n).$$

Now we change back the order of the summation

$$\begin{aligned} L &= \sum_{n \in \mathbb{Z}} x_n \sum_{k \in \mathbb{Z}} a_k \widehat{\varphi}(n+k) - \sum_{n \in \mathbb{Z}} \lambda x_n \widehat{\varphi}(n) = \\ &= \sum_{n \in \mathbb{Z}} x_n \left(\sum_{k \in \mathbb{Z}} a_k \widehat{\varphi}(n+k) - \lambda \widehat{\varphi}(n) \right). \end{aligned}$$

Let us elaborate separately

$$\begin{aligned} w_n &= \sum_{k \in \mathbb{Z}} a_k \widehat{\varphi}(n+k) = \sum_{k \in \mathbb{Z}} a_k \int_{-\infty}^{\infty} \varphi(t) e^{-i2\pi(n+k)t} dt = \\ &= \int_{-\infty}^{\infty} \varphi(t) \left(\sum_{k \in \mathbb{Z}} a_k e^{-i2\pi kt} \right) e^{-i2\pi nt} dt. \end{aligned}$$

Denoting

$$\widehat{\mathbf{a}}(t) = \sum_{k \in \mathbb{Z}} a_k e^{-i2\pi kt}$$

we get

$$w_n = \int_{-\infty}^{\infty} \varphi(t) \widehat{\mathbf{a}}(t) e^{-i2\pi nt} dt = \widehat{\varphi \widehat{\mathbf{a}}}(n)$$

and thus

$$L = \sum_{n \in \mathbb{Z}} x_n (\widehat{\varphi \widehat{\mathbf{a}}}(n) - \lambda \widehat{\varphi}(n)) = \sum_{n \in \mathbb{Z}} x_n \widehat{(\widehat{\mathbf{a}} - \lambda) \varphi}(n) = \langle T_{\mathbf{x}}, \widehat{(\widehat{\mathbf{a}} - \lambda) \varphi} \rangle.$$

Recalling (15) this is

$$\langle T_{\mathbf{x}}, \widehat{(\widehat{\mathbf{a}} - \lambda) \varphi} \rangle = \langle T_{\mathbf{b}}, \widehat{\varphi} \rangle. \quad (16)$$

Replacing φ by ψ in (16) and using (13) we have

$$\langle T_{\mathbf{x}}, \widehat{\frac{1}{\alpha} \psi} \rangle = \langle T_{\mathbf{b}}, \widehat{\psi} \rangle. \quad (17)$$

Calling

$$\varphi(t) = \widehat{\frac{1}{\alpha}}\psi(t)$$

we have

$$\begin{aligned}\check{\varphi} &= \frac{1}{\widehat{\alpha}}\psi \\ \psi &= \widehat{\alpha}\check{\varphi} \\ \widehat{\psi} &= \widehat{\widehat{\alpha}\check{\varphi}}\end{aligned}\tag{18}$$

and since there is a unique $\varphi \in \mathcal{S}$ satisfying (18) to any $\psi \in \mathcal{S}$ and vice versa, (17) gives the action of the wanted distribution $T_{\mathbf{x}}$ on any $\varphi \in \mathcal{S}$:

$$\langle T_{\mathbf{x}}, \varphi \rangle = \langle T_{\mathbf{b}}, \widehat{\alpha}\check{\varphi} \rangle .$$

Using Lemma we immediately have **II.(a)** because $(\mathcal{A} - \lambda I)\mathbf{x} = \mathbf{0}$ implies ■

$$\langle T_{\mathbf{x}}, \varphi \rangle = \langle T_{\mathbf{0}}, \widehat{\alpha}\check{\varphi} \rangle = 0$$

for every $\varphi \in \mathcal{S}$, which implies $\mathbf{x} = \mathbf{0}$.

To complete the proof of the Theorem we have to prove **II.(b)**, i.e. we have to find a solution \mathbf{x} of $(\mathcal{A} - \lambda I)\mathbf{x} = \mathbf{b}$ for every $\mathbf{b} \in \mathbb{B}$.

We show that \mathbf{x} defined by

$$x_j = \sum_{k \in Z} \alpha_k b_{j-k}\tag{19}$$

is the solution. Recall that α_k are the Fourier coefficients of $\widehat{\alpha}$ introduced in (14) and thus \mathbf{x} is well defined and bounded.

For $k \in Z$ and $\varphi \in \mathcal{S}$ we denote by φ_k the function defined as

$$\varphi_k(\nu) = \varphi(\nu + k) .$$

Then we have

$$\begin{aligned}\check{\varphi}_k(\nu) &= \int_{-\infty}^{\infty} \varphi(t+k) e^{i2\pi\nu t} dt = \int_{-\infty}^{\infty} \varphi(t) e^{i2\pi\nu(t-k)} dt = \\ &= e^{-i2\pi\nu k} \int_{-\infty}^{\infty} \varphi(t) e^{i2\pi\nu t} dt = e^{-i2\pi\nu k} \check{\varphi}(\nu)\end{aligned}$$

and thus

$$\sum_{k \in Z} \widehat{\alpha_k} \varphi_k(\nu) = \sum_{k \in Z} \alpha_k \check{\varphi}_k(\nu) = \sum_{k \in Z} \alpha_k e^{-i2\pi\nu k} \check{\varphi}(\nu) = \widehat{\alpha}(\nu) \check{\varphi}(\nu) ,$$

i.e.

$$\sum_{k \in \mathbb{Z}} \alpha_k \varphi_k = \widehat{\alpha \tilde{\varphi}}.$$

Now

$$\begin{aligned} \langle T\mathbf{x}, \varphi \rangle &= \sum_{j \in \mathbb{Z}} \left(\sum_{k \in \mathbb{Z}} \alpha_k b_{j-k} \right) \varphi(j) = \sum_{k \in \mathbb{Z}} \alpha_k \left(\sum_{j \in \mathbb{Z}} b_j \varphi(j+k) \right) = \\ &= \sum_{j \in \mathbb{Z}} b_j \left(\sum_{k \in \mathbb{Z}} \alpha_k \varphi(j+k) \right) = \langle T\mathbf{b}, \sum_{k \in \mathbb{Z}} \alpha_k \varphi_k \rangle = \langle T\mathbf{b}, \widehat{\alpha \tilde{\varphi}} \rangle. \end{aligned}$$

Thus by the Lemma $(\mathcal{A} - \lambda I)\mathbf{x} = \mathbf{b}$ and the proof is finished.

4 Examples

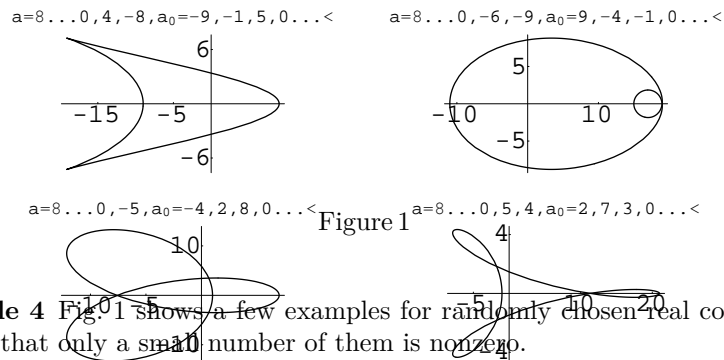
Example 1 If $a_n = a_{-n} \in \mathbb{R}$ for all $n \in \mathbb{N}$ then the spectrum is an interval of real numbers.

Example 2 If $a_n \in \mathbb{R}$ for all $n \in \mathbb{Z}$ then the spectrum is symmetric with respect to the real axis in the complex plane.

Example 3 For the shift, i.e. $a_1 = 1$ and $a_n = 0$ for $n \neq 1$ the spectrum is a unit circle

$$\{\widehat{\mathbf{a}}(\nu) = e^{-i2\pi\nu} : \nu \in \mathbb{R}\}$$

in the complex plane.



Example 4 Fig. 1 shows a few examples for randomly chosen real coefficients a_n such that only a small number of them is nonzero.

5 Concluding remarks

The obtained result generalizes the result of [6], where the case of the operator \mathcal{A} with only a finite number of nonzero a_k was considered. On the other hand the methods used in [6] can be applied to derive the Theorem, too. The advantage of the use of the Fourier transform is that it can be generalized to the case of two-sided sequences of vectors from \mathbb{R}^p (or \mathbb{C}^p), when coefficients a_k of the operator \mathcal{A} are the matrices. This enables us to investigate the stability of spatially periodical steady state solutions of lattice dynamical systems. This result will be published elsewhere.

Acknowledgement

This work is supported by the grants GACR 201/98/0220, VZ CEZ:J19/98:223400007, VZ CEZ:J19/98:223400008.

References

1. V.S. Afraimovich, V.I. Nekorkin: Stable stationary motions in a chain diffusively coupled maps (in Russian). Preprint No 267, Inst. of Appl. Phys., N. Novgorod, 1991.
2. S.-N. Chow, W. Shen: Stability and bifurcation of travelling wave solutions in coupled map lattice. Preprint, CDSNS177, 1994.
3. G. Ioos: Bifurcation of Maps and Applications, North-Holland Publishing Company, Amsterdam 1979.
4. L. Schwartz: Méthodes mathématiques pur les sciences physiques. Paris, Hermann (1961).
5. A.E. Taylor: Introduction to functional analysis. John Wiley & Sons, Inc., New York 1967.
6. D. Turzík, A. Klíe, M. Dubcová, P. Pokorný: Stability of Spatially Homogeneous Solutions in Lattice Dynamical Systems. 3rd Int. Coll. Math. Dept., Inst. Chem. Technol., Prague (2001).

Threshold Sets and Nonlinear Dynamics in Excitable Systems Subject to Periodic Stimuli

V. Nevoral, M. Voslař, I. Schreiber

Department of Chemical Engineering &
Center for Nonlinear Dynamics of Chemical and Biological Systems,
Institute of Chemical Technology, Prague,
Technická 5, 166 28 Prague 6, Czech Republic,
e-mail: schrig@vscht.cz

Abstract Excitable properties of dynamical systems are examined in terms of a threshold set which is then used to characterize dynamics in one compartment subject to external periodic stimuli and to describe spreading of signals to a second diffusion-coupled compartment. A method of calculating a threshold set and a criterion for its disappearance are formulated. Two kinds of excitability distinguished by either direct or indirect initiation of the activatory process are discussed. The response of the one- and two-compartment systems to periodic perturbations is studied via bifurcation diagrams. Transitions from periodicity to quasiperiodicity to chaos are observed.

1 Introduction

A distinct feature of excitable systems is their sensitivity to perturbations. Of particular interest in this paper are excitable chemical and biochemical processes. There are many examples of excitable systems in chemistry and biology [1], ranging from the Belousov-Zhabotinsky chemical reaction [2] to calcium spiking in many types of cells [3] to action potentials in specialized neural cells [4]. A typical excitatory event follows a superthreshold stimulus applied to the system at rest which triggers an autocatalytic increase of some intermediate(s) until an inhibitory decay dominates, leading eventually to the original rest state. Stimulus may be repeated periodically, either by externally controlled conditions (such as drug administration) or by some internal oscillatory process in the neighborhood of the cell transduced inside or an oscillatory subsystem within the cell. Periodic forcing induces repeated firings which may or may not catch up with the pace of stimuli depending on the strength and period of the stimulus. The dynamics may become complex when the cell is unable to respond by an excitation to each external stimulus [5], [6], [7], [8]. Apart from neurons, intercellular signalling is known to occur in various cell systems [9], [10].

In the first section of the paper we examine the threshold dynamics, identify threshold set, formulate a boundary value problem to find it in two-variable systems and provide an example of calcium dynamics in cytosol. In the second section, dynamical response to pulsed external perturbations in one and two such cells is studied.

2 Excitability

Following Ref. [11] we consider a threshold set as locally separating the phase space into a set of trajectories amplifying initial perturbations and a set of trajectories decaying to the steady state soon after the perturbation. However, this definition is only qualitative and it is the purpose of this section to give a precise meaning to the threshold set in the presence of a unique steady state and formulate an iterative procedure for numerically accurate location of the threshold. This in turn allows us to understand how excitability vanishes and how it is interlinked with nontransient dynamical phenomena, such as bistability and oscillations.

2.1 Theory for threshold sets

Let us assume a dynamical system described by ordinary differential equations:

$$\frac{d\mathbf{x}}{dt} = \mathbf{v}(\mathbf{x}), \quad \mathbf{x} \in R^n. \quad (1)$$

Although not explicitly stated, the vector field \mathbf{v} is assumed to depend on external parameters. In general, the threshold set \mathcal{T} should be a smooth codimension one semi-open surface which is bounded from one side by a codimension two surface providing an axis about which trajectories of (1) corresponding to excitations wind (for example, a semi-curve in R^2 bounded by a point, a semi-sheet in R^3 bounded by a curve etc.). Accordingly, it is convenient to assume that \mathcal{T} is invariant under the flow $\varphi(\mathbf{x}, t)$ of Eq. (1) in negative time direction, i.e., $\varphi(\mathcal{T}, t) \subseteq \mathcal{T}$ for all $t \leq 0$ where $\varphi(\mathcal{T}, t = 0)$ is the “end” of \mathcal{T} . Therefore the threshold set must be a (negatively directed) semiorbit in a two-variable system, a smooth one-parameter family of semiorbits in a three-variable system, etc.

For simplicity, we will assume that the system has two dynamical variables, $n = 2$, extension to more than two variables is possible. Let \mathbf{x}_S be the steady state point. To locate the threshold, we formulate a boundary value problem for a finite segment of the threshold orbit beginning at a point \mathbf{x}_L and terminating at another point \mathbf{x}_R . The point \mathbf{x}_L is specified by applying a perturbation shifting the initial steady state \mathbf{x}_S to \mathbf{x}_L so that

$$f_L = \mathbf{v}(\mathbf{x}_L) \cdot (\mathbf{x}_L - \mathbf{x}_S) = 0. \quad (2)$$

Since we assume that the response to this perturbation is amplified, the orbit passing through x_L is locally at a minimum distance P from the steady state which provides the size (or amplitude) of the pulse:

$$P = \| \mathbf{x}_L - \mathbf{x}_S \| . \quad (3)$$

Thus P is a minimal perturbation amplitude for the given orbit to cause an excitation. The system (1) responds to the perturbation by a motion along the orbit based at \mathbf{x}_L , the perturbation becomes amplified, eventually reaching a point \mathbf{x}_R such that

$$f_R = \mathbf{v}(\mathbf{x}_R) \cdot (\mathbf{x}_R - \mathbf{x}_S) = 0. \quad (4)$$

The response amplitude R ,

$$R = \|\mathbf{x}_R - \mathbf{x}_S\|, \quad (5)$$

at that point is, by virtue of (4), at its maximum, see Fig. 1.

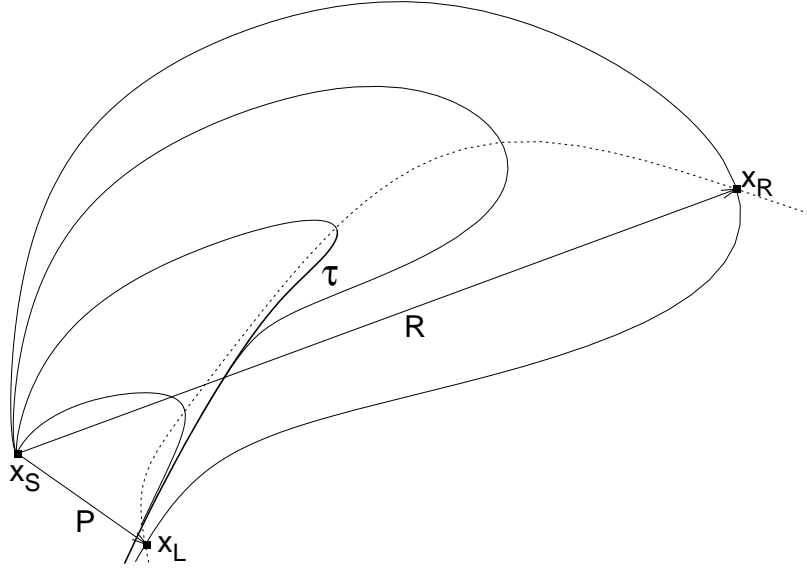


Figure 1: Phase portrait of an excitable system (schematically) showing the perturbation (P) and response (R) amplitudes used to find the threshold \mathcal{T} (shown as thick line) via Eqs.(6) and (9).

Eqs. (2) and (4) are in fact identical but each of them defines a separate part of the same curve in the state space of (1); the two parts meet at a point where the perturbation and response amplitudes are equal. Given P , the point \mathbf{x}_L is found by solving Eqs.(2) and (3) hence \mathbf{x}_L depends on P implicitly. The point \mathbf{x}_R depends on \mathbf{x}_L via the flow $\varphi(\mathbf{x}_L, \tau)$ where τ is a time necessary to reach \mathbf{x}_R from \mathbf{x}_L . Therefore R ultimately depends on P .

Let us define a relative amplification as the increase in amplitude from \mathbf{x}_L to \mathbf{x}_R relative to the amplitude of perturbation:

$$r = \frac{R(\mathbf{x}_L(P)) - P}{P}. \quad (6)$$

The first derivative of r with respect to P is, after some algebraic manipulation

$$\frac{dr}{dP} = \frac{\partial r}{\partial \mathbf{x}_L} \frac{d\mathbf{x}_L}{dP} + \frac{\partial r}{\partial P} = \frac{\text{grad } r \cdot \mathbf{d}^0}{\text{grad } P \cdot \mathbf{d}^0} - \frac{r+1}{P}, \quad (7)$$

where \mathbf{d}^0 is an arbitrarily normalized vector tangent to the curve defined by Eq. (2) at \mathbf{x}_L :

$$\text{grad } f_L \cdot \mathbf{d}^0 = 0, \quad \|\mathbf{d}^0\| = 1. \quad (8)$$

The derivative in Eq. (7) captures the sensitivity of the response to variations in perturbation amplitude and allows for a characterization of the threshold because r is expected to grow most significantly with P just on the orbit segment lying on \mathcal{T} . We use this property to single out the orbit segment from \mathbf{x}_L to \mathbf{x}_R so that the sensitivity coefficient dr/dP is at maximum:

$$\frac{dr}{dP} \stackrel{!}{=} \text{max}. \quad (9)$$

The threshold set \mathcal{T} is then defined as the negative semiorbit starting at \mathbf{x}_R – the endpoint of \mathcal{T} – and passing through \mathbf{x}_L further extending to arbitrary negative times. As an interesting byproduct, the constraint (9) is complemented by a condition for an orbit with smallest possible dr/dP . The associated orbit, in a sense, represents a typical excitatory response and therefore we refer to it as a *characteristic excitation*. Between the threshold and the characteristic excitation is an orbit with a maximal relative amplification r . Since the Euclidean distance depends on the scaling we need to assume that the variables in Eq.(1) are given in their natural scale. However, the results do not change significantly upon rescaling, unless it is very poor, so (9) may still be conveniently used as an operational definition of the threshold.

In summary, we have a boundary value problem for an orbit segment, satisfying the boundary conditions (2) and (4) and the steady state condition

$$\mathbf{v}(\mathbf{x}_S) = \mathbf{0}; \quad (10)$$

the unknowns are \mathbf{x}_S , \mathbf{x}_L and τ . For $n = 2$, there is one more unknown than the equations therefore one unknown may be taken as a free parameter and this problem is solved by combining shooting and continuation methods [13], [14]. The continuation provides a one-parameter family of orbit segments. The separation rate (7) is calculated at each point along this curve and searched for maximum and minimum values, indicating the threshold set and the characteristic excitation, respectively. When repeated continuations with sequentially varying external parameters are made, the threshold set and the characteristic excitation can meet and the minimum and maximum value of dr/dP plotted against P merge and disappear. If that happens, the excitability vanishes. Since the threshold trajectory is strongly unstable, a multiple shooting method with nonequidistant time subintervals is used in practical calculations rather than the simple shooting approach outlined above.

2.2 An example – biochemical excitable system

As an example of excitable system we use a model of intracellular calcium dynamics according to the one-pool variant of the CICR mechanism [12]. Dynamics of calcium in cells is ubiquitous in animal cells and displays both oscillatory and excitatory modes. According to the CICR (Calcium-Induced Calcium Release) model, the key species are the inositol 1,4,5-triphosphate (IP_3), the cytosolic Ca^{2+} (Ca_i) and the calcium ions sequestered in an intracellular store (Ca_s). From a mechanistic viewpoint, Ca_i has a positive self-feedback loop mediating the release of calcium into cytosol from internal stores; Ca_s plays a regulatory role involving a negative feedback mediating the sequestration of Ca_i into the store. IP_3 is assumed to have a constant concentration controlling thus the system as a constraint.

In the absence of a mass transport within the cell the dynamics is governed by the mass balance equations

$$\frac{dx}{dt} = f(x, y) = V_{in} - V_2 + V_3 + k_f y - kx, \quad (11)$$

$$\frac{dy}{dt} = g(x, y) = V_2 - V_3 - k_f y, \quad (12)$$

where

$$V_{in} = v_0 + v_1 \beta, \quad V_2 = V_{M2} \frac{x^n}{(K_2^n + x^n)},$$

$$V_3 = \beta V_{M3} \frac{y^m}{(K_R^m + y^m)} \frac{x^p}{(K_A^p + x^p)},$$

and x is the concentration of Ca_i , y is the concentration of Ca_s , V_{in} is total constant entry of Ca^{2+} into the cytosol consisting of v_0 , the constant influx and $v_1 \beta$, the IP_3 -stimulated influx from extracellular medium, V_2 is the rate of pumping into the internal store, V_3 is the rate of release from the store, k_f is the coefficient of the passive efflux from the store, k is the rate coefficient of the passive efflux from the cytosol. The saturation parameter β represents the regulatory role of IP_3 . In all the calculations we use the values as follows: $k_f = 1.0 \text{ min}^{-1}$, $k = 10.0 \text{ min}^{-1}$, $v_1 = 1.7 \text{ } \mu\text{M min}^{-1}$, $V_{M2} = 50.0 \text{ } \mu\text{M min}^{-1}$, $V_{M3} = 325.0 \text{ } \mu\text{M min}^{-1}$, $K_2 = 0.5 \text{ } \mu\text{M}$, $K_R = 1.0 \text{ } \mu\text{M}$, $K_A = 0.45 \text{ } \mu\text{M}$, $n = 2$, $m = 4$, $p = 4$. In order to find excitable conditions we treat v_0 and β as adjustable parameters to set appropriate dynamics.

By using continuation we construct a bifurcation diagram including the boundaries along which excitability vanishes as shown in Fig. 2. The region of periodic oscillations is marked by the Hopf bifurcation curve. In fact, this bifurcation is mostly subcritical and thus the oscillations occur also outside this region. However, the additional region of hysteresis is negligibly narrow. As indicated in Fig. 2 we find two different kinds of excitability in this system. The first one, which we call the *activatory excitability*, is associated with a low- x -high- y steady state. Addition of x or y triggers the ordinary excitatory event beginning with the activatory (or autocatalytic) phase which increases x and

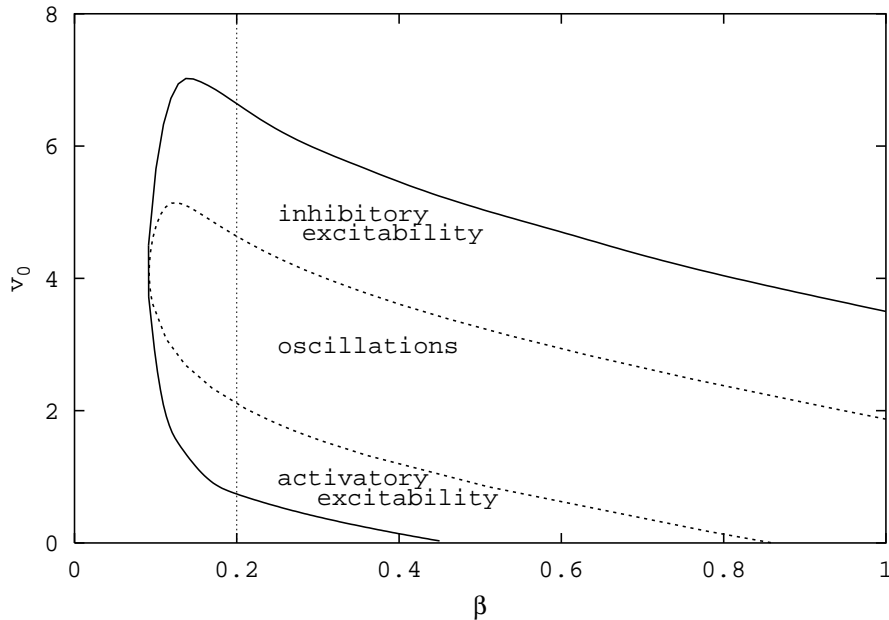


Figure 2: Bifurcation diagram in the parameters v_0 and β , dashed line – Hopf bifurcation, full line – vanishing excitability

depletes y until the inhibitory phase sets in to consume x and replete y . The other, somewhat counterintuitive type – *inhibitory excitability* – is associated with a high- x -low- y steady state. The excitation elicited by removing x or y begins with the inhibitory process which removes x even more and simultaneously repletes y , and terminates by the autocatalysis. Another classification of excitable systems distinguishes between multiple steady state (type I) and single steady state (type II) phase portraits [15]; in the present case we have a unique steady state and therefore the type II excitability.

The threshold set for both activatory and inhibitory excitability near the oscillatory region in Fig. 2 is shown in Fig. 3. As the parameters v_0 and β approach the outer boundary, the perturbation amplitude increases, the threshold set shrinks and its separation properties weaken. The excitability of the system may vanish in two ways, either the amplification drops below the limiting value of $r = 1$, or the maximum of dr/dP disappears by colliding with a minimum. Which one is the case depends on the model – the former is the actual mechanism for the CICR model. Of course, there is no qualitative change of the phase portrait in the sense of a bifurcation when crossing the boundary of vanishing excitability, the change is continuous but quite sudden and this is what the amplification ratio and its derivative reflect. Similar quantities as r may be defined but all give very similar results.

3 Dynamics in periodically pulsed cell systems

3.1 Periodic forcing of one cell

Here we examine how the presence of a threshold set influences the dynamics of a periodically perturbed cell and what changes to dynamics appear when the excitability vanishes. We assume that the concentration of Ca_i can be changed suddenly as a consequence of a periodically repeated external perturbation. This can be modelled as a periodic series of delta pulses shifting immediately the value of x and Eqs. (11),(12) now become

$$\frac{dx}{dt} = f(x, y) + h(x) \sum \delta(t - kT), \quad k = 1, \dots, \quad (13)$$

$$\frac{dy}{dt} = g(x, y), \quad (14)$$

where k counts the number of pulses, T is the period of pulse deliveries and $h(x)$ is the change in x due to the pulse. When addition of Ca_i is considered, this function is chosen to be simply a constant, $h(x) = A$. However, removal of Ca_i modelled in this way might shift x to negative values and thus we choose $h(x) = -x(1 - e^{-A})$. In both cases we call A the forcing amplitude.

We examine the system (13),(14) numerically by using continuation method to find variations of periodic solutions with A and/or T , their stability and bifurcations. In addition, we also solve Eqs. (13),(14) directly and characterize the complexity of dynamics by Poincare maps and Lyapunov exponents. Moreover, the excitatory dynamics is well characterized by introducing excitation (or firing) number ν ,

$$\nu = \frac{\text{number of excitatory responses}}{\text{number of pulses}} \quad (15)$$

in the limit of large number of pulses k . Thus ν is an average number of excitations per one pulse.

Here we can conveniently use the notion of the threshold set introduced earlier to distinguish between excitatory and nonexcitatory responses. A response is considered as excitatory if the pulse penetrates the threshold set or, equivalently, if the trajectory loops around the endpoint of the threshold set. Periodic orbits have $\nu = p/q$ where p, q are integers and qT is the period. For further calculations we fix β at 0.2 and examine the dynamics of the forced system at various values of v_0 within the two regions of excitability (cf. Fig. 2).

By performing the continuation with respect to A or T we observe that periodic orbits may pass through the threshold set. For example, a family of one-periodic orbits (i.e., $q = 1$) at $v_0 = 1.2$ (activatory excitability) and $v_0 = 5.0$ (inhibitory excitability) obtained by continuation with respect to A is represented in Fig. 3. The curves (a) and (c) show that the response amplitude (difference between maximum and minimum of x) changes rapidly within a narrow structure of fold bifurcations and the sets of orbits representing the (continuous) family

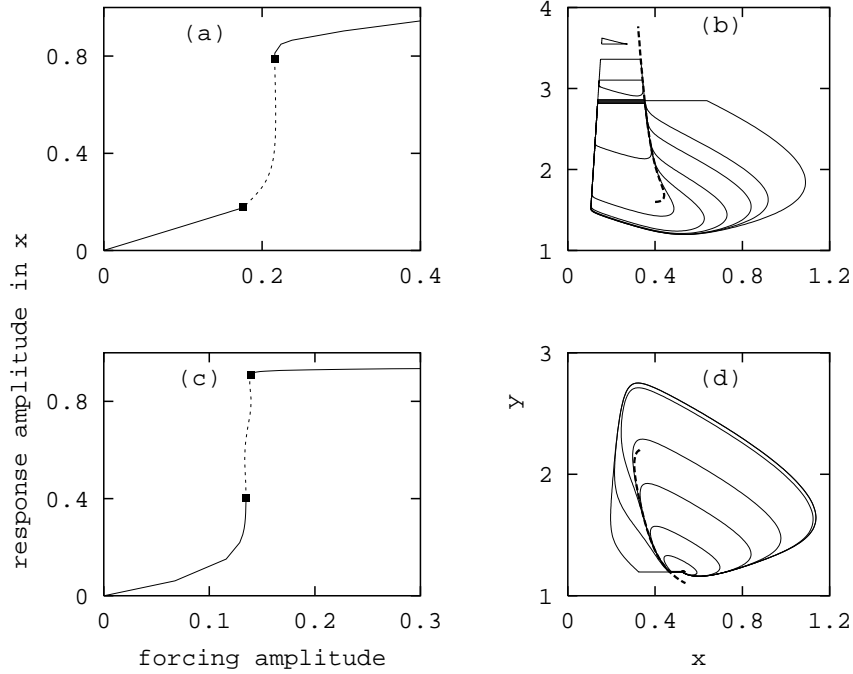


Figure 3: (a),(c) – variation of the response amplitude in x with the forcing amplitude A ; (b),(d) – sequence of phase portraits of period one orbits along the branches in (a),(c), the threshold set is shown as dashed line; parameter values: (a),(b) – $v_0 = 1.2$, $T = 1.5$, (c),(d) – $v_0 = 5.0$, $T = 1.0$

in (b) and (d) show how the originally small amplitude oscillations for A small grow and extend along the threshold set to become large amplitude oscillations. Therefore there is an intermediate value of A such that a whole segment of the threshold set is contained in the period one orbit. At that point the orbit originally with $\nu = 0/1$ “sneaks through” and becomes one with $\nu = 1/1$ because the pulse now penetrates the threshold orbit. This principle applies equally to both kind of excitabilities, and likewise to q -periodic orbits with $q > 1$. As the threshold orbit by itself is at a maximum of instability, periodic orbits near the passage through it are typically extremely unstable except for rare cases when the stable part of orbit that closes the loop compensates for the instability.

Fig. 4a,b shows the A - T bifurcation diagrams of the period one orbit at $v_0 = 1.2$ and $v_0 = 5.0$. There are additional instabilities apart from the fold bifurcation due to period doubling and torus bifurcations. The corresponding unstable regions suggest where the dynamics will likely become complex. Also, the threshold perturbation amplitude for the period one orbit to become unstable

is nearly constant for large T as one might expect but decreases rapidly when T becomes smaller. Let us remark that analogous calculations for v_0 below the boundary for activatory excitability and above the boundary for the inhibitory excitability show that these bifurcation structures shrink and disintegrate almost completely and thus suggest that the criteria (6),(7) used for constructing the boundary have significant predictive power.

Next we shall examine dynamics with fixed A as indicated in Fig. 5 at sequentially selected values of T through the region of instability. Fig. 5 shows the excitation number ν and the maximal Lyapunov exponent λ_1 with varying T for the case of the activatory excitability. The excitation number is at the first glance a nondecreasing step-wise function of T (panel (a)) reflecting the gradually larger time for the system to recover before next pulse is delivered and hence more frequent excitations. Every p/q regime corresponds to a plateau. The

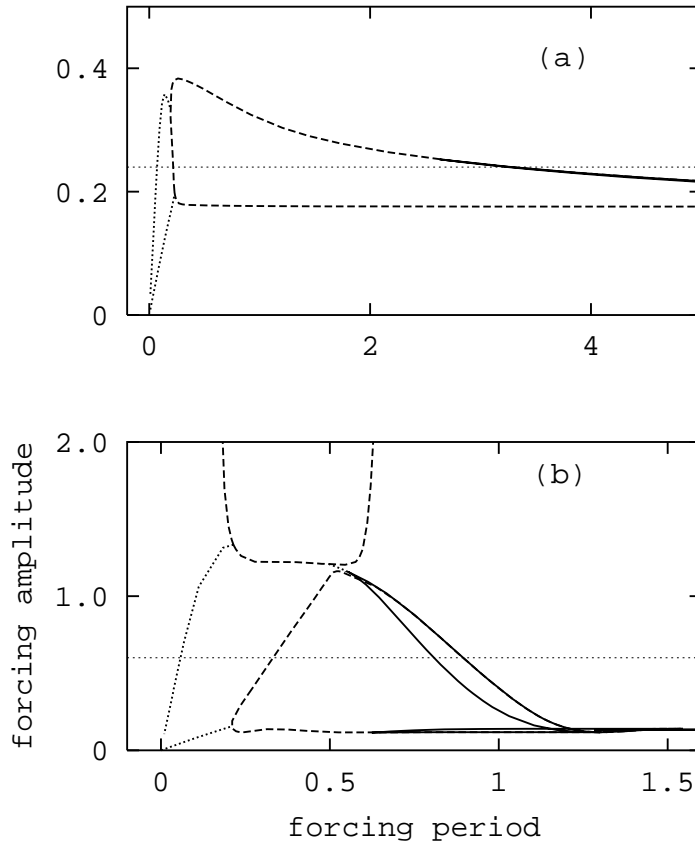


Figure 4: Bifurcation diagrams for period one orbit in the parameters T and A ; (a) $v_0 = 1.2$, (b) $v_0 = 5.0$; full line – fold bifurcation, dashed line – period doubling, dotted line – torus bifurcation

blow-up in panel (b) shows that even a very narrow step between $1/3$ and $1/2$ resonances reveals fine step-wise structure but it also indicates that the value of ν drops occasionally. More information provides the plot of λ_1 . First of all, there are positive exponents (and hence chaotic dynamics) at some of the steps and second, these chaotic dynamical regimes occur predominantly where ν drops. A similar picture emerges when the inhibitory excitable system is periodically perturbed, see Fig. 6. The staircase dependence of ν on T displays drops where the chaos is observed. Only here the relaxation time indicated by the value of T when $\nu = 1$ is reached is much shorter than in the earlier case. This is due to much longer inhibitory phase in the activatory case.

The nature of chaotic attractors appearing in many windows is indicated in Fig. 7 showing phase portraits and Poincare sections taken successively at $t=kT$. The first case corresponds to the activatory excitability. The phase portrait (a) indicates the separating role played by the threshold set. Clearly, an additional feature is the extreme instability of the threshold set, contributing to the positive Lyapunov exponent. On the other hand, the Poincare map (b) is extremely simple, suggesting that a 1D map is operating here. The second example is from the region of inhibitory excitability. Likewise here the organizing role of the threshold set is well observable (panel (c)). The Poincare map (d) is, however, indicating that a fractalization of a torus leads to this attractor. The rather small

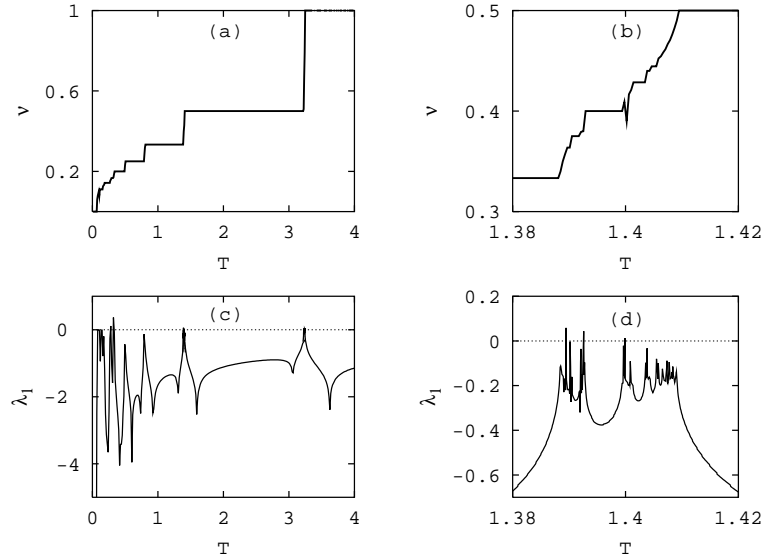


Figure 5: Excitation number ν and maximal Lyapunov exponent λ_1 against forcing period T , $v_0 = 1.2$, $A = 0.24$; (b) and (d) are enlarged portions of (a) and (c)

forcing period relates to the region of torus bifurcation in Fig. 4b, whereby the torus originates. The last example is showing an attractor with a well pronounced fractal structure which occurs when v_0 is selected closer to the boundary of vanishing inhibitory excitability.

3.2 Periodic forcing of two cells

Diffusion-coupled array of cells is the basic model for describing communication between cells via gap junctions. In advanced organisms with specialized cells the cell-cell interaction may be much more complex, such as synaptical junctions in neural tissue. Nevertheless, the simple diffusion driven interaction takes place whenever suitable conditions as provided by gap junctions occur. In the case of calcium dynamics, the interaction can be mediated by cytosolic calcium Ca_i since the transport of sequestered calcium Ca_s is hindered. Taking the simplest possible array – two coupled cells – the Eqs. (11),(12) extend to

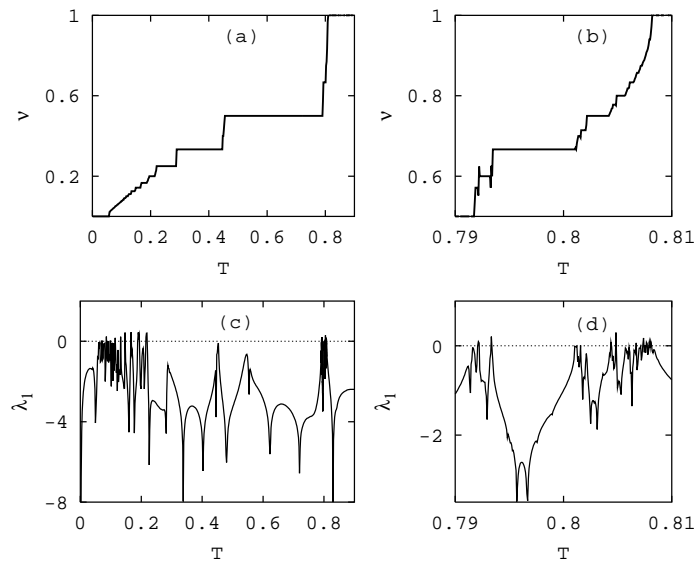


Figure 6: Excitation number ν and maximal Lyapunov exponent λ_1 against forcing period T , $v_0 = 5.0$, $A = 0.6$; (b) and (d) are enlarged portions of (a) and (c)

$$\frac{dx_1}{dt} = f(x_1, y_1) + d(x_2 - x_1), \quad (16)$$

$$\frac{dy_1}{dt} = g(x_1, y_1), \quad (17)$$

$$\frac{dx_2}{dt} = f(x_2, y_2) + d(x_1 - x_2), \quad (18)$$

$$\frac{dy_2}{dt} = g(x_2, y_2), \quad (19)$$

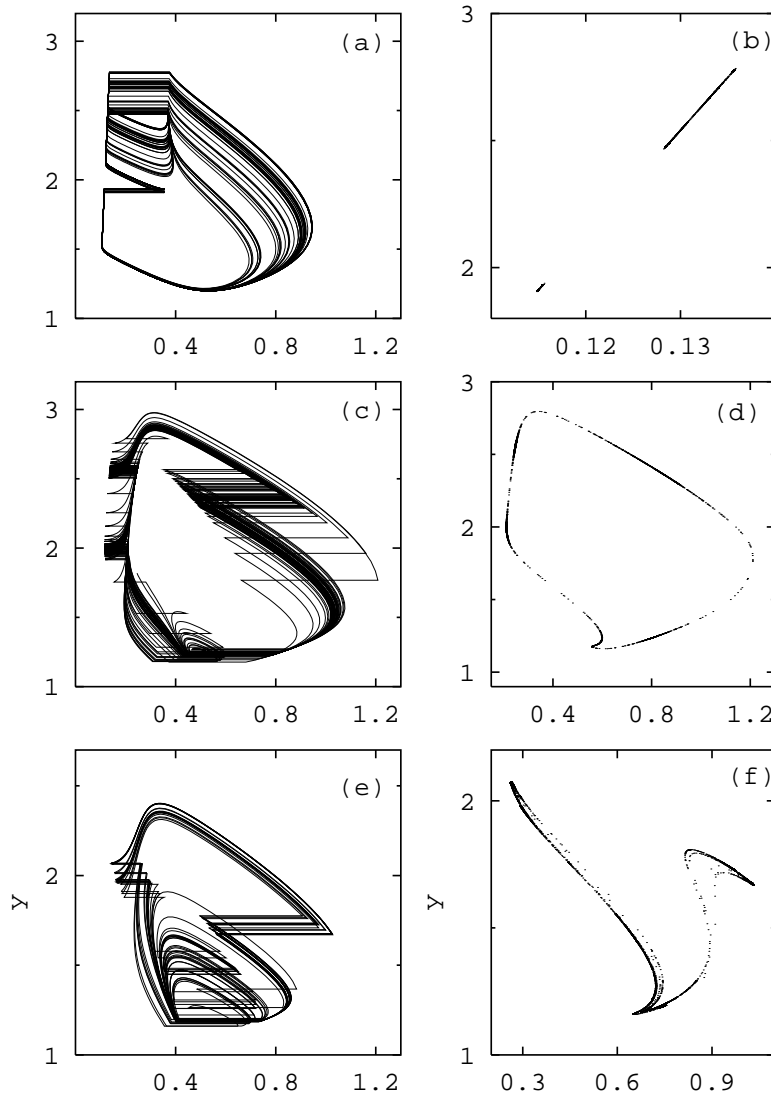


Figure 7: Phase portraits \vec{x} (a),(c),(e) and Poincaré plots \vec{x} (b),(d),(f) for three chaotic attractors; parameter values: (a),(b) $v_0 = 1.2$, $A = 0.24$, $T = 1.38945$, (c),(d) $v_0 = 5.0$, $A = 0.6$, $T = 0.2153$, (e),(f) $v_0 = 6.0$, $A = 0.6$, $T = 0.219$

where d is the transport coefficient.

We assume that cell 1 is periodically pulsed as before and examine how the excitation signal gets transferred to the second cell. The conditions in both cells are set to activatory excitability ($v_0 = 1.2$) and inhibitory excitability ($v_0 = 5.0$). The coupling strength has two obvious limits, when d is too small, no signal is propagated; when d is large enough, the cells fire synchronously. Depending on circumstances, the actual coupling strength may operate between the two limiting cases, in fact, this situation allows for a controlled way of signal transduction. The coupling is expected to alter the threshold set to some extent. Since the system has a four-dimensional phase space the calculation of the threshold set would not be a simple matter. Instead we assume that the threshold for one cell applies for each of the coupled cells. This is supported by numerical calculations showing that particularly the end part of the threshold set is not significantly altered which in turn implies that the excitation numbers ν_1, ν_2 can be defined by counting the number of loops about the endpoint of the threshold set in each cell separately.

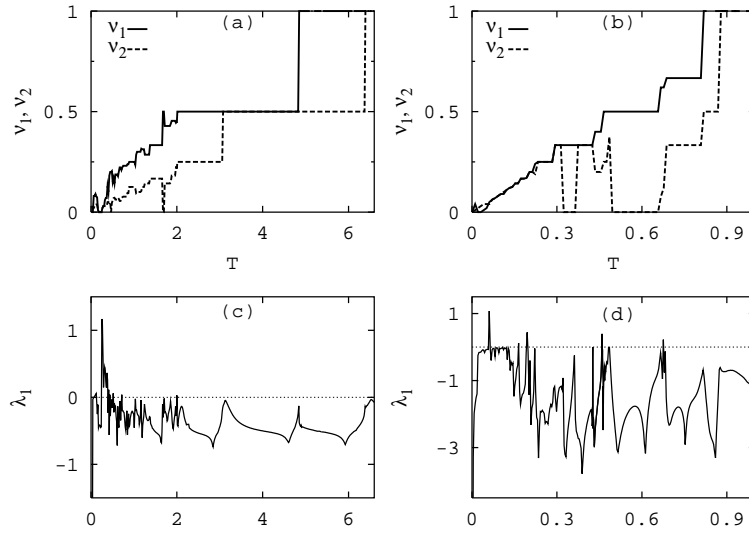


Figure 8: Excitation numbers ν_1, ν_2 and maximal Lyapunov exponent λ_1 against forcing period T for two coupled cells; parameter values: (a),(c) $v_0 = 1.2, A = 0.24$, (b),(d) $v_0 = 5.0, A = 0.6$

Adjusting the transport coefficient properly, complex dynamics is revealed by plotting ν_1, ν_2 and the maximal Lyapunov exponent λ_1 against T , see Fig. 8. The cases (a) and (c) correspond to the activatory excitability with d set to 6.0 and the cases (b) and (d) represent the dynamics of the inhibitory excitable system with d adjusted to 1.6; the forcing amplitude A is the same as for the corresponding one-cell systems. Excitation numbers in (a) show a complex pattern with mostly a partial propagation of the excitation to the second cell. The dominating pattern is 1:2 locking between the cells, only occasionally there is

no propagation or complete propagation. Frequent drops of the staircase suggest possible chaotic dynamics which correspond well with positive λ_1 in (c). Panels (b) and (d) show essentially a similar pattern of alternating periodic and chaotic dynamics. However, there are some differences in the degree of synchronized firings – while for small T the two cells fire synchronously, for larger values the pattern alternates between no propagation and complete synchrony. This pattern cannot be made similar to that in (a) by adjusting d . This seems to reflect the difference between the activatory and inhibitory excitability. Notice also, that the transport coefficient for the former to achieve a complex firing patterns is much larger than that for the latter. This points to a more subtle nature of the inhibitory excitability.

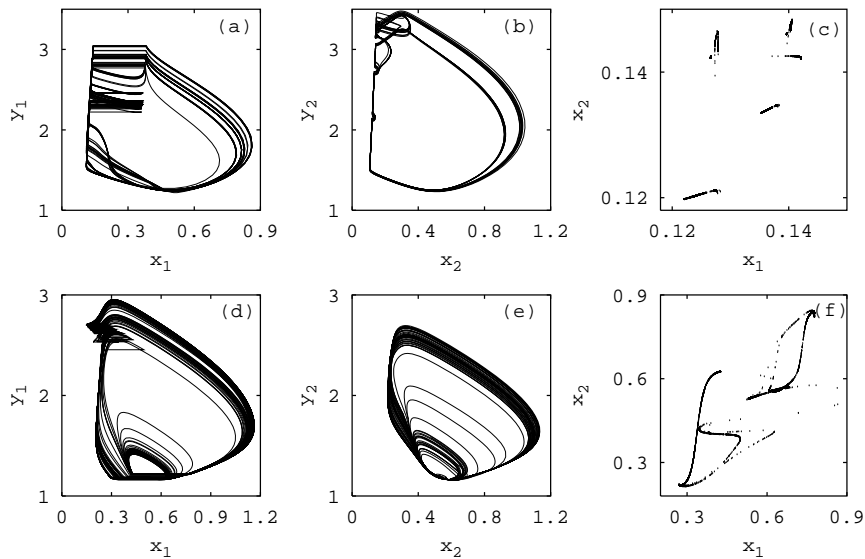


Figure 9: Phase portraits in x_1 - y_1 plane (a),(d), in x_2 - y_2 plane (b),(e) and x_1 - x_2 Poincaré plots (c),(f) for chaotic attractors in two coupled cells; parameter values: (a),(b),(c) $v_0 = 1.2$, $A = 0.24$, $T = 2.0$, $d = 6.0$ (c),(d),(e) $v_0 = 5.0$, $A = 0.6$, $T = 0.459$, $d = 1.6$

The chaotic dynamics is represented by phase portraits in both cells and Poincaré plots showing x in both cells taken at $t = kT$ in Fig. 9. The activatory case (a)-(c) reveals a less structured Poincaré plot than the inhibitory one (d)-(f). Both attractors are roughly comparable as to their firing pattern since they are taken from a window between $1/3$ and $1/2$ resonance in the first cell. Oscillations in the first cell ((a) and (d)) show a clear separation between excitatory and nonexcitatory responses caused by the presence of the threshold set. The oscillations in the second cell ((b) and (e)) indicate the diffusion driven transition across the threshold. While the separation of the orbits is very distinct in (b),

it is not as clear in (e) and this is why the Poincare plot has a richer structure in (f). Again, this observation relates to a much weaker separation power of the threshold set for the inhibitory excitability.

4 Conclusions

A quantitative criterion for existence of a threshold set in excitable systems has been defined and a boundary value problem for calculating the threshold has been formulated and solved for an example biochemical system. This enables us to clearly define an excitation number which characterizes dynamics of periodically pulsed systems.

We find that the degree of dynamic complexity in pulsed excitable systems depends on the type of excitability and on the strength of the excitatory event. It is shown that complex dynamic patterns occur even in the simplest case of one periodically pulsed excitable cell and they are associated with localized drops of the staircase-like dependence of excitation number on forcing period.

Diffusion-like coupling of two cells increases further the complexity of the pattern if the coupling strength is appropriately adjusted. Spatio-temporal structures of partially propagated pulses occur for intermediate coupling strengths and chaotic regimes are again associated with drops of the excitation number when the forcing period is increased.

Acknowledgments: The authors thank to the Grant Agency of Czech Republic (Grant GACR 203/98/1304) and to the Ministry of Education of Czech Republic (Grant MSM223400007) for financial support of this project.

References

1. HOLDEN, A. V., MARKUS, M. and OTHMER, M. G., eds. (1990) *Nonlinear Wave Processes in Excitable Media*, Plenum Press, New York.
2. FIELD, R. J. and BURGER, M., eds. (1990) *Oscillations and Travelling Waves in Chemical Systems*, Wiley, New York.
3. GOLDBETER, A. (1996) *Biochemical oscillations and cellular rhythms*, Cambridge University Press, Cambridge.
4. HODGKIN A. L. and HUXLEY, A. F. (1954) *A quantitative description of membrane current and application to conduction and excitation in nerve*, J. Physiol., **117**, 500-544.
5. VOTRUBOVÁ, V., HASAL, P., SCHREIBEROVÁ, L. and MAREK, M. (1998) *Dynamical Patterns in Arrays of Coupled Chemical Oscillators and Excitators*, J. Phys. Chem. A, **102**, 1318-1328.
6. HASAL, P., NEVORAL, V., SCHREIBER, I., ŠEVČÍKOVÁ, H., ŠNITA, D. and MAREK, M. (1996) *Waves in ionic reaction-diffusion-migration systems*. In: *Nonlinear Dynamics, Chaotic and Complex Systems*, E. Infeld *et al.*-Eds., (Cambridge Univ.Press, Cambridge).
7. SCHREIBER, I., HASAL, P. and MAREK, M. (1999) *Chaotic patterns in a coupled oscillator–excitator biochemical cell system*, CHAOS, **9**, 43-54.

8. NEVORAL V., VOSLAŘ M., SCHREIBER, I., HASAL, P. and MAREK, M. (2000) *Complex dynamical response of chemical and biochemical excitable systems to periodic stimuli* FORMA, **15**, 291-308.
9. COOPER, M.S. (1995) *Intercellular signaling in neuronal-glia cells*, BioSystems **34**, 65-85.
10. BOITANO, S., DIRKSEN, E.R. and SANDERSON, M.J. (1992) *Intercellular propagation of calcium waves mediated by inositol trisphosphate*, Science **258**, 292-295.
11. ALEXANDER, J. C., DOEDEL, E. J. and OTHMER, H. G. (1990) *On the resonance structure in a forced excitable system*, SIAM J. Appl. Math. **50**, 1373-1418.
12. DUPONT, G. and GOLDBETER, A. (1993) *One-Pool Model for Ca^{2+} Oscillations Involving Ca^{2+} and inositol 1,4,5-Trisphosphate as Co-Agonists for Ca^{2+} Release*, Cell Calcium **14**, 311-322.
13. KUBÍČEK, M. and MAREK, M. (1983) *Computational Methods in Bifurcation Theory and Dissipative Structures*, Springer, New York.
14. MAREK, M. and SCHREIBER, I. (1995) *Chaotic Behaviour of Deterministic Dissipative Systems*, Cambridge University Press, Cambridge.
15. MAREK, M., FINKEOVÁ, J. and SCHREIBER, I. (1989), *Devil's staircase in chemical excitable systems*, in Workshop "Irreversible Processes and Selforganization", ed. W. Ebeling, Teubner Verlag, Leipzig, pp. 76-79.

Continuation methods for homo/heteroclinic orbits and their applications for nonlinear chemical problems

M. Kohout^{1,3}, I. Schreiber^{1,3} and M. Kubíček^{2,3}

Department of Chemical Engineering¹, Department of Mathematics²,
Center for Nonlinear Dynamics of Chemical and Biological Systems³
Institute of Chemical Technology, Prague
Technická 5, 166 28 Prague 6, Czech Republic.
email: kohoutm@tiger.vscht.cz

Abstract A method for numerical continuation of trajectories connecting two different stationary points (heteroclinic orbit) or doubly asymptotic to a single stationary point (homoclinic orbit) is introduced. This method is used to study travelling front and pulse waves in reaction-transport systems, such as tubular reactors with nonlinear internal dynamics coupled with transport. A computer implementation of this method included in a continuation program CONT is applied to two systems: the first one - reaction-diffusion system with cubic auto-catalysis (Gray-Scott model) and the second one - biochemical reaction-diffusion system describing the dynamics of intracellular calcium (CICR model). In these systems we study front waves, pulse waves, wave trains and their iterations.

1 Introduction

Waves in spatially distributed media occur due to a nonlinear internal dynamics such as chemical reaction [1], [7], [11] coupled with transport (usually linear). Solitary fronts or pulses are the simplest cases. The former are associated with couple of steady states while the latter occur under conditions of excitability. The waves can be standing or travelling and for fronts mediate a transition from one type of steady dynamics to another one. In this contribution we present numerical methods of finding front and pulse waves that enable us to perform parametric studies using the method of continuation [5], [6].

2 Methods of computing pulse and front waves

Travelling waves occur typically in reaction-diffusion-convection systems described by the following system of PDEs:

$$\frac{\partial y}{\partial t} = D \frac{\partial^2 y}{\partial z^2} + V \frac{\partial y}{\partial z} + g(y), \quad (1)$$

where y is a vector valued function of time t and one-dimensional spatial coordinate z ; D and V are (diagonal) matrices of diffusion coefficients and convective velocities (or mobilities), respectively. It is assumed that one or more spatially homogeneous steady states $y(z, t) = y^S$ exist. A solitary pulse wave on an infinite space domain $-\infty < z < \infty$ is a transient dynamical state that can be represented by a trajectory doubly asymptotic to a single steady state y^S . Analogously, a front wave can be seen as a dynamical transient connecting two different steady states y^{S1} , y^{S2} .

2.1 Transformation to a Boundary Value Problem for ODEs

Assuming that u is the velocity of the wave we can introduce a moving frame coordinate $\zeta = z - ut$ so that the system (1) converts to a system of second order ODEs ($y(z, t) \mapsto y(\zeta)$),

$$D \frac{d^2 y}{d\zeta^2} + V \frac{dy}{d\zeta} + u \frac{dy}{d\zeta} + g(y) = 0, \quad (2)$$

which, upon denoting $x_1 = y$ and $x_2 = \frac{dy}{d\zeta}$, can be rewritten as a first order system

$$\frac{dx_1}{d\zeta} = x_2, \quad \frac{dx_2}{d\zeta} = -D^{-1}(Vx_2 + ux_2 + g(x_1)) \quad (3)$$

or in a compact form

$$\frac{dx}{d\zeta} = f(x; \alpha, \beta), \quad x \in \mathbb{R}^n, \quad (4)$$

where $x = (x_1, x_2)$, $f(x_1, x_2, \alpha, \beta) = (x_2, -D^{-1}(Vx_2 + ux_2 + g(x_1)))$ and α, β are selected parameters. We shall use $\psi(\zeta, x)$ to denote the flow (4).

A homoclinic orbit represents a special solution of this system ODE's which is in positive and negative direction of time asymptotic to a steady state

$$\lim_{\zeta \rightarrow \pm\infty} x(\zeta) = x^S = (y^S, 0). \quad (5)$$

Similarly, boundary conditions for a heteroclinic orbit are

$$\lim_{\zeta \rightarrow -\infty} x(\zeta) = x^{S1} = (y^{S1}, 0), \quad \lim_{\zeta \rightarrow +\infty} x(\zeta) = x^{S2} = (y^{S2}, 0). \quad (6)$$

2.2 Method for continuation of 'nonoscillatory' homoclinic orbits

The boundary conditions (5), (6) must be reformulated for a numerical solution of Eqs. (4) because of the infinite extent of the independent variable ζ (in the vicinity of x^S the velocity of phase point goes to zero). Rather, we have to truncate the infinite time domain to a finite interval by introducing two points x^1 and x^N in ε_1 and ε_2 distance from x^S (for the case of *homoclinic orbit*) - $\varepsilon_1, \varepsilon_2$ are sufficiently small. Points x^1 and x^N are connected by boundary condition

using vectors $-f(x^1)$ and $f(x^N)$. For finding a trajectory going from x^1 to x^N we use multiple shooting method (we introduce points x^2, x^3, \dots, x^{N-1} with possibly nonequidistant nodes ζ_i). The formulation of a continuation problem assumes introducing two bifurcation parameters, say α and β , a hot candidate for one of them is the wave velocity u . The equations may be then written as follows:

$$x^1 - x^N = \varepsilon_2 \frac{f(x^N; \alpha, \beta)}{\|f(x^N; \alpha, \beta)\|} + \varepsilon_1 \frac{f(x^1; \alpha, \beta)}{\|f(x^1; \alpha, \beta)\|}, \quad (7)$$

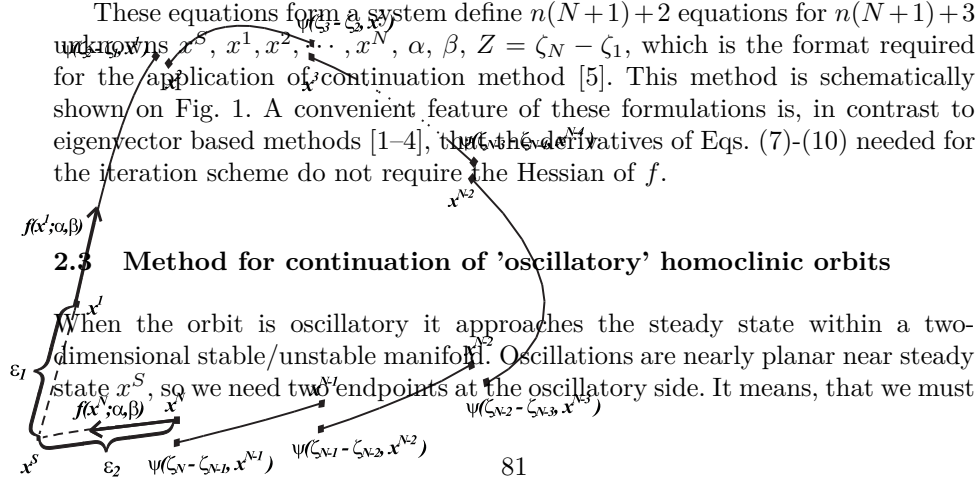
$$\psi(\zeta_{i+1} - \zeta_i, x^i) - x^{i+1} = 0, \quad i = 1, \dots, N-1, \quad (8)$$

$$f(x^S; \alpha, \beta) = 0, \quad (9)$$

$$\|x^1 - x^S\| = \varepsilon_1, \quad \|x^S - x^N\| = \varepsilon_2. \quad (10)$$

Figure 1: Method for computing of a homoclinic orbit with nonoscillatory approach to steady state - schematically

These equations form a system define $n(N+1)+2$ equations for $n(N+1)+3$ unknowns $x^S, x^1, x^2, \dots, x^N, \alpha, \beta, Z = \zeta_N - \zeta_1$, which is the format required for the application of continuation method [5]. This method is schematically shown on Fig. 1. A convenient feature of these formulations is, in contrast to eigenvector based methods [1-4], that the derivatives of Eqs. (7)-(10) needed for the iteration scheme do not require the Hessian of f .



modify boundary condition (Eqs. (7)) to a 'oscillatory form'.

$$x^1 - x^N = \varepsilon_2 \frac{f(x^N; \alpha, \beta)}{\|f(x^N; \alpha, \beta)\|} + \varepsilon_1 \left(c_1 \frac{f(x^1; \alpha, \beta)}{\|f(x^1; \alpha, \beta)\|} + c_2 \frac{f(x^0; \alpha, \beta)}{\|f(x^0; \alpha, \beta)\|} \right), \quad (11)$$

$$\psi(\zeta_{i+1} - \zeta_i, x^i) - x^{i+1} = 0, \quad i = 1, \dots, N-1, \quad (12)$$

$$f(x^S; \alpha, \beta) = 0, \quad (13)$$

$$\|x^1 - x^S\| = \varepsilon_1, \quad \|x^S - x^N\| = \varepsilon_2, \quad (14)$$

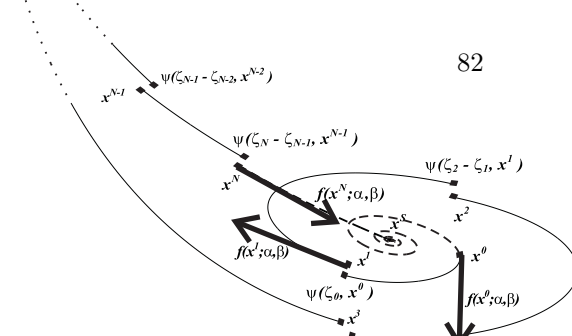
$$\psi(\zeta_0, x^0) - x^1 = 0, \quad \|x^0 - x^S\| = \frac{1}{2}\varepsilon_1, \quad (15)$$

$$G^T G \begin{pmatrix} c_1 \\ c_2 \end{pmatrix} = G^T \begin{pmatrix} \frac{x_1^1 - x_1^S}{\|x^1 - x^S\|} \\ \vdots \\ \frac{x_n^1 - x_n^S}{\|x^1 - x^S\|} \end{pmatrix}, \quad G = \begin{pmatrix} \frac{f_1(x^1; \alpha, \beta)}{\|f(x^1; \alpha, \beta)\|} & \frac{f_1(x^0; \alpha, \beta)}{\|f(x^0; \alpha, \beta)\|} \\ \vdots & \vdots \\ \frac{f_n(x^1; \alpha, \beta)}{\|f(x^1; \alpha, \beta)\|} & \frac{f_n(x^0; \alpha, \beta)}{\|f(x^0; \alpha, \beta)\|} \end{pmatrix}. \quad (16)$$

Here Eq. (11) represents the boundary conditions. The approach to x^S is assumed oscillatory and thus an auxiliary point x^0 at distance $\varepsilon_1/2$ is introduced so that x^1 is reached in time ζ_0 from x^0 , see Eqs. (15). The vectors $f(x^1)$ and $f(x^0)$ provide approximately a basis of a plane of oscillations and a linear combination of the two vectors is sought so that points x^S and x^1 are connected by the vector $x^S - x^1$. At the endpoint x^N of the orbit a nonoscillatory approach to x^S is assumed in the direction of $f(x^N)$. Eqs. (12) define the multiple shooting procedure and Eq. (13) defines the steady state (the same equations as in homoclinic orbit with nonoscillatory approach. Finally, Eq. (16) represents a Gauss-Newton procedure for finding best fit of the linear overdetermined problem for the oscillatory plane.

Figure 2: Method for computing of a homoclinic orbit with oscillatory approach to steady state - schematically.

An analogous method for continuation of *heteroclinic orbits* can be formulated by considering two equations determining the two steady states x^{S1}, x^{S2}



rather than Eq. (9) or Eq. (13) and locating the points x^1, x^N at the ε_1 and ε_2 distances from x^{S1}, x^{S2} respectively.

Both methods have been incorporated into a numerical package for continuation and stability analysis CONT [6].

3 Example 1 – Gray-Scott Model (2-variable Autocatalator)

We examine a two-variable reaction-diffusion system with cubic autocatalysis in an open unstirred tubular reactor with equal diffusion coefficients of both species. Mass balance equations for this model can be written in the following dimensionless form [7]:

$$\frac{\partial y_1}{\partial t} = \frac{\partial^2 y_1}{\partial z^2} + 1 - y_1 - \mu y_1 y_2^2, \quad (17)$$

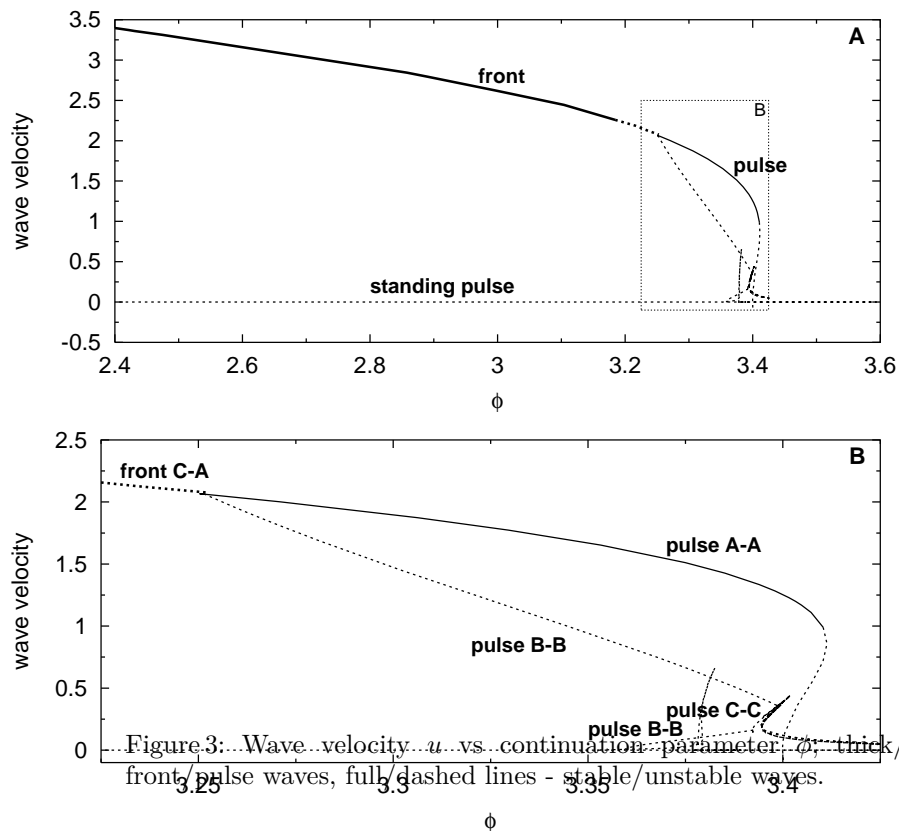
$$\frac{\partial y_2}{\partial t} = \frac{\partial^2 y_2}{\partial z^2} + \mu y_1 y_2^2 - \phi y_2, \quad (18)$$

where y_1, y_2 are the dimensionless concentrations of the reactant and autocatalyst, respectively; μ and ϕ are free parameters. The transformation to Eq. (4) is straightforward. We choose a fixed value of $\mu = 47.0$ and use ϕ as a variable parameter. The results of continuation are shown in Figs. 3 and 4. One branch of heteroclinic orbits - front waves - and three branches of homoclinic orbits - two kinds of pulse waves: travelling and standing - are presented. The heteroclinic orbits on the branch corresponding to front waves undergo a transition to oscillatory approach to the steady state x^{S1} (see curve **c** in panel **A**, Fig. 4). The branches of travelling pulse waves emerge from the branch of standing pulse by a symmetry breaking bifurcation and terminate at the bifurcation point where a second steady state becomes involved and causes the pulse wave to split into two front waves (a codimension two bifurcation point [8]). There are points of stability change on the travelling pulse wave and the front wave curves. The standing pulse waves are always unstable. Two branches of homoclinic and heteroclinic orbits extend from the point of heteroclinic cycle (see panel **B**, Fig. 3).

The travelling waves can be both stable and unstable, while the standing wave is always unstable. The stability has been determined by direct numerical integration of (17), (18) on a sufficiently large interval of z . Selected profiles of waves belonging to all four branches are presented in Fig. 4. Remarkably, the loss of stability of front waves is associated with emergence of chaotic behaviour [9,10] filling the gap between stable fronts and stable pulses.

4 Example 2 – CICR Model (intracellular calcium)

This model describes biochemical reaction-diffusion system with the dynamics of intracellular calcium (CICR means Calcium-Induced Calcium Release model).



The key species are the inositol 1,4,5-triphosphate (IP_3), the cytosolic Ca^{2+} (Ca_i) and the calcium ions sequestered in an intracellular store (Ca_s).

$$\frac{\partial y_1}{\partial t} = D_1 \frac{\partial^2 y_1}{\partial z^2} + V_{in} - V_2 + V_3 + k_f y_2 - k y_1, \quad (19)$$

$$\frac{\partial y_2}{\partial t} = D_2 \frac{\partial^2 y_2}{\partial z^2} + V_2 - V_3 - k_f y_2, \quad (20)$$

where

$$V_{in} = v_0 + v_1 \beta, V_2 = V_{M2} \frac{y_1^n}{K_2^n + y_1^n}, V_3 = \beta V_{M3} \frac{y_2^m}{K_R^m + y_2^m} \frac{y_1^p}{K_A^p + y_1^p}, \quad (21)$$

and y_1 , y_2 are the concentrations of Ca_i and Ca_s , V_{in} is total constant entry of Ca^{2+} into the cytosol consisting of v_0 (the constant influx) and $v_1 \beta$ (the IP_3 -stimulated influx from extracellular medium), V_2 is the rate of pumping into the internal store, V_3 is the rate of release from the store, k_f is the coefficient

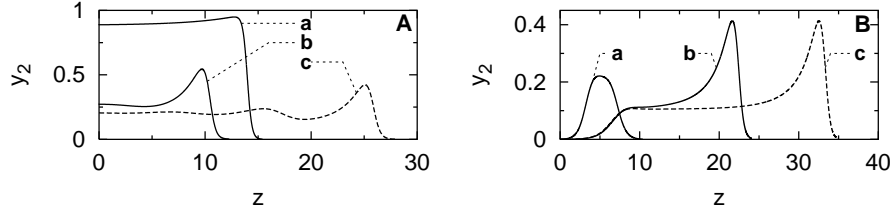


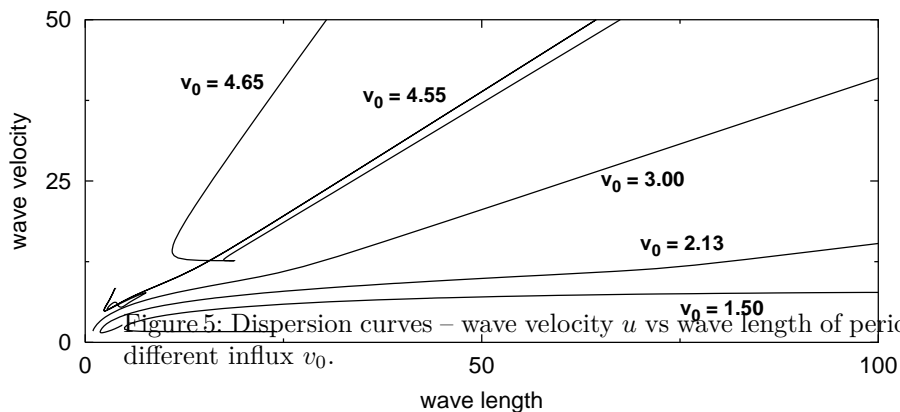
Figure 4: Selected profiles of waves: **panel A – front waves:** a) $\phi = 1.1$, $u = 4.46622$, b) $\phi = 2.51284$, $u = 3.30791$, c) $\phi = 3.23431$, $u = 2.12762$; **panel B – pulses A–A:** a) $\phi = 3.40017$, $u = -0.1$, b) $\phi = 3.25169$, $u = 2.06143$, c) $\phi = 3.25171$, $u = 2.06108$; **panel C – standing pulses:** a) $\phi = 2.86227$, $u = 0$, b) $\phi = 3.38758$, $u = 0$; **panel D – pulses B–B:** a) $\phi = 3.25139$, $u = 2.06578$, b) $\phi = 3.28749$, $u = 1.61192$, c) $\phi = 3.39849$, $u = 0.35531$.

of the passive efflux from the cytosol. The saturation parameter β represents regulatory role of IP_3 .

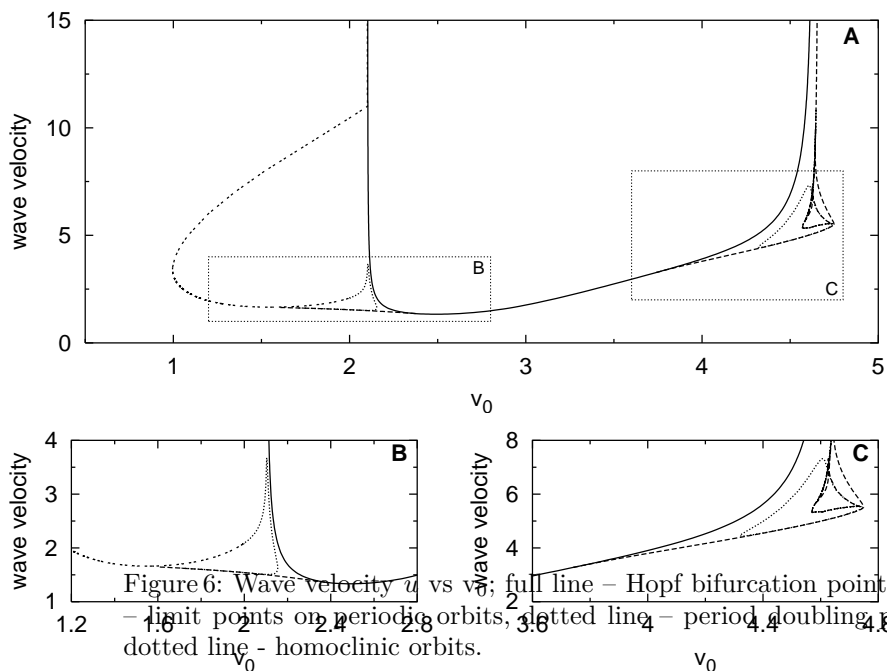
Values of parameters are shown in the following table:

par.	value	par.	value	par.	value
$K_2 =$	$0.5\mu\text{M}$	$k =$	10.0 min^{-1}	$n =$	2.0
$K_R =$	$1.0\mu\text{M}$	$k_f =$	1.0 min^{-1}	$m =$	2.0
$K_A =$	$0.45\mu\text{M}$	$V_{M2} =$	$50.0\mu\text{M min}^{-1}$	$p =$	4.0
$v_1 =$	$1.7\mu\text{M min}^{-1}$	$V_{M3} =$	$325.0\mu\text{M min}^{-1}$	$\beta =$	0.2

As continuation parameters we use influx v_0 and wave velocity u . Results of continuation are shown in Figs. 5 and 6. Using one-parameter continuation of periodic orbits (see Fig. 5) we can calculate dependence of the wave velocity on the wave length (dispersion curve). For $v_0=1.50$ wave length in both directions of continuation curve goes to infinity. It means that the curve of periodic orbits in both directions approaches a homoclinic orbit (pulse wave). For values of v_0 equal to 2.13 and 4.55 the continuation curve passes through limit and period doubling bifurcation points and ends in a subcritical Hopf bifurcation point. For $v_0=3.00$ the continuation curve ends in a supercritical Hopf bifurcation point



and for $v_0=4.65$ we can see very complex structure with many limit points and points of period doubling bifurcation.



Results of two-parameter continuation (bifurcation diagram) are shown in Fig. 6. Very complex dynamics is found for intervals of values of parameter v_0 approximately equal (1.2, 2.8) and (3.6,4.8) (see panels **B** and **C** in Fig. 6). We assume that curve of homoclinic orbits is closed and two curves of limit points split off this curve. The region delimited by curves of homoclinic orbit and Hopf bifurcation points on the left and by curve of limit points on the right is region where periodic orbits (wave trains) exist.

5 Conclusions

Numerical algorithms for continuation of homoclinic and heteroclinic orbits with both nonoscillatory and oscillatory approach to the steady state(s) presented here provides a practical tool for investigation of travelling waves in reaction-diffusion-convection-systems.

The two studied systems differ substantially in their bifurcation behaviour of the waves. This is mainly due to the presence of three steady states in Example 1 and a unique steady state in Example 2. Further research is needed for a system near a cusp point to find out how the two different bifurcation structures are interlinked.

Acknowledgments: This work has been supported by the project No. VS96073 and fund MSM 223400007 of the Czech Ministry of Education and grants No. 201/98/0220 and 203/98/1304 of the Czech Grant Agency.

References

1. Kuznetsov, Y. A. (1995) Elements of Applied Bifurcation Theory. Springer Verlag, New York
2. Champneys, A. R., Kuznetsov, Y. A. (1994) Numerical detection and continuation of codimension-two homoclinic bifurcations. Int. Journal of Bif. and Chaos **4**(4), 785–822
3. Champneys, A. R., Kuznetsov, Y. A., Sandstede, B. (1996) A numerical toolbox for homoclinic bifurcation analysis. Int. Journal of Bif. And Chaos **6**, 867–887
4. Beyn, W. J. (1990) The numerical computation of connecting orbits in dynamical systems. IMA J. Numer. Anal. **10**, 379–405
5. Kubíček, M., Marek, M. (1983) Computational Methods in Bifurcation Theory and Dissipative Structures. Springer Verlag, New York
6. Marek, M., Schreiber, I. (1995) Chaotic Behaviour of Deterministic Dissipative Systems. Cambridge University Press
7. Gray, P., Scott S. K. (1990) Chemical Oscillations and Instabilities. Clarendon Press, Oxford
8. Zimmermann, M. G., Firth, S. O., Natiello, M. A., Hildebrand, M., Eiswirth, M., Bär, M., Bangia, A. K., Kevrekidis, I. G. (1997) Pulse bifurcation and transition to spatiotemporal chaos in an excitable reaction-diffusion model. Physica D **110**, 290–299
9. Merkin, J. H., Petrov, V., Scott, S. K., Showalter, K. (1996) Wave-induced chemical chaos. Phys. Rev. Lett. **76**, 546–549

10. Merkin, J. H., Sadiq, M. A. (1996) The propagation of travelling waves in an open cubic autocatalytic chemical system. *IMA J. Appl. Math.* **57**, 273
11. Goldbeter A. (1996) *Biochemical oscillations and cellular rhythms*, Cambridge University Press, Cambridge

Projected version of the Recursive Projection Method algorithm

Vladimír Janovský, Ondřej Liberda

Faculty of Mathematics and Physics, Charles University, Prague

Abstract: A modified version of the Recursive Projection Method called Projected RPM is proposed. Both the original and the Projected RPM are compared. The latter underlines the stabilization effect. Both methods suffer from the same drawback, namely a poor update of the unstable invariant subspace.

Keywords: steady states, pathfollowing, stability exchange, unstable invariant subspace

1 Introduction

In the following we consider a parameter dependent dynamical system

$$\dot{u} = G(u, \lambda) \tag{1}$$

We assume that $G : \mathbb{R}^n \times \mathbb{R} \rightarrow \mathbb{R}^n$ is sufficiently smooth vector field.

In this paper, we shall concentrate on two issues:

1. Continuation of steady states; we have in mind large dynamical systems especially those arising from a discretisation of PDEs.
2. An indication of stability exchange in the course of pathfollowing.

As far as the first problem is concerned, the pathfollowing techniques are well known, see e.g. [14], [12], [1]. For the latest development, see [7]: Mixed block elimination techniques could exploit black box iterative solvers for very large matrices, [18].

The second problem is quite hard. There were some prospective ideas in this direction: The "global" test function for Hopf bifurcation points (based on the bialternate-product of matrices), see e.g. [9] or [7], would indicate the stability exchange. Unfortunately, this kind of test function could be reasonably computed for small scaled problems. Alternative techniques monitoring the "traffic" through the imaginary axis, see e.g. [8], suffer from the same shortcoming.

Continuation of the rightmost eigenvalue, see [17], can answer the posed question. This computational technique is based on properties of Cayley transform, see [6]. Direct continuation of an invariant subspace, [5] and [2] might be an expensive but a promising technique.

The Recursive Projection Method (RPM), [13], is designed to perform both of the above assigned jobs. The idea is to compute the steady states $G(u, \lambda) = 0$ as parameter dependent fixed points of a mapping F namely,

$$u = F(u, \lambda). \tag{2}$$

At each continuation step, the state space \mathbb{R}^n is splitted as

$$\mathbb{R}^n = \mathbb{P} \oplus \mathbb{Q}, \quad \mathbb{Q} = \mathbb{P}^\perp$$

where \mathbb{P} is the invariant subspace of $F_u(u, \lambda)$ containing all unstable modes. Denoting by P and Q the orthogonal projectors on \mathbb{P} and \mathbb{Q} respectively, the problem (2) can be reformulated as follows: Find $p \in \mathbb{P}$ and $q \in \mathbb{Q}$ such that

$$p = PF(p + q, \lambda) \tag{3}$$

$$q = QF(p + q, \lambda), \tag{4}$$

In [13] there is shown that QF is contractive. Therefore, fixed points of (4) can be computed via Picard iterations. In order to find p , Newton-like methods are suggested. Note that the choice of F also includes the possibility to use any black-box ODE solver in the Picard iteration step, see [13]. This step can be interpreted as a dynamical simulation.

Just to resume, the iteration step consists in *dynamical simulation* applied to (4) and a low-dimensional Newton's correction applied on (3).

The preconditioned version of RPM, [4], tries to fight the inevitable stiffness of ODE's. The technique is justified for semilinear PDE. The version of RPM designed for continuation of limit cycles, [16], has been very successful.

An attempt to improve RPM was made in [3]. Numerical tests reported failure, [15]. The present paper is another attempt to reformulate RPM in the spirit of [3]. The resulting algorithm is called *Projected RPM*.

The outline of this paper is as follows: In the section 2.1 the Projected RPM algorithm is formulated. Theorem justifying the convergence is quoted. For details see [11]. In the section 2.2 a pseudocode of the algorithm is given. Section 3 contains results of the numerical test. The last section are the conclusions.

2 Projected RPM

In this section we will outline the key idea behind the Projected RPM. Let us consider an autonomous system of ODEs (1). In practical computations G is often a spatial discretization of a differential operator. Let $\Gamma \subset \mathbb{R}^n \times \mathbb{R}$ be the path of steady states of (1), i.e. the solution set to

$$G(u, \lambda) = 0. \tag{5}$$

2.1 Coupled iterations

Let $(u^*, \lambda^*) \in \Gamma$ be a steady state of (1). We will keep this point fixed in the whole section. Let us denote

$$\mu_k = \rho_k + i\tau_k, \quad k = 1 \dots, n \tag{6}$$

the eigenvalues of the Jacobian $A \equiv G_u(u^*, \lambda^*)$ and arrange them so that

$$\rho_1 \geq \dots \geq \rho_m > 0 > \rho_{m-1} \geq \dots \geq \rho_n.$$

Generally $m \ll n$, i.e. only a few modes cause the instability. Let \mathbb{P} denote the maximal invariant subspace of A corresponding to the eigenvalues μ_1, \dots, μ_m . That means $A(\mathbb{P}) \subset \mathbb{P}$, $\sigma(A|_{\mathbb{P}}) = \{\mu_1, \dots, \mu_m\}$ and \mathbb{P} is maximal subspace with the above properties. Moreover let us define

$$\mathbb{Q} = \mathbb{P}^\perp.$$

Clearly $\mathbb{R}^n = \mathbb{P} \oplus \mathbb{Q}$. The above decomposition defines orthogonal projectors

$$P : \mathbb{R}^n \rightarrow \mathbb{P}, \quad \text{with } Ker(P) = \mathbb{Q} \quad (7)$$

$$Q : \mathbb{R}^n \rightarrow \mathbb{Q}, \quad \text{with } Ker(Q) = \mathbb{P}. \quad (8)$$

From the definition it is evident that

$$I = P + Q,$$

where I denotes the identity operator. Now the solution to (5) is equivalent to the solution of the coupled system

$$G^P(p, q, \lambda) \equiv PG(p + q, \lambda) = 0 \quad (9)$$

$$G^Q(p, q, \lambda) \equiv QG(p + q, \lambda) = 0, \quad (10)$$

where

$$G^P : \mathbb{P} \times \mathbb{Q} \times \mathbb{R} \rightarrow \mathbb{P} \quad \text{and} \quad G^Q : \mathbb{P} \times \mathbb{Q} \times \mathbb{R} \rightarrow \mathbb{Q}.$$

Let

$$p^* = Pu^*, \quad q^* = Qu^*$$

be the projections of the steady state u^* on \mathbb{P} and \mathbb{Q} , resp. Let us investigate equation (10). Partial differential $D_q G^Q(p^* + q^*, \lambda^*)$ is a linear mapping

$$QA : \mathbb{Q} \rightarrow \mathbb{Q}. \quad (11)$$

An analogy to the Lemma 2.10 from [13] can be proved:

Lemma: *The $n - m$ eigenvalues of the linear mapping (11) are exactly the stable modes μ_{m+1}, \dots, μ_n of A .*

The Lemma above gives us a possibility to solve the system (10) by dynamical simulation. Let us consider a dynamical system

$$\dot{q}(t) = G^Q(p, q(t), \lambda) \quad (12)$$

$$q(0) = q \in \mathbb{Q}. \quad (13)$$

We will denote its flow by

$$\psi(t, q; p, \lambda).$$

Here p and λ are parameters while q is a state variable and t denotes time. Let us take a fixed time step $\Delta t > 0$ and define a mapping

$$F^Q : \mathbb{P} \times \mathbb{Q} \times \mathbb{R} \rightarrow \mathbb{Q} \quad (14)$$

$$F^Q(p, q, \lambda) = \psi(\Delta t, q; p, \lambda). \quad (15)$$

An important consequence of the Lemma is a local convergence of Picard iterations via mapping F^Q in a neighborhood of (u^*, λ^*) for sufficiently large Δt . It is stated in the following theorem:

Theorem: Let $G \in \mathcal{C}^1(U_{\delta_1}(u^*, \lambda^*))$ where $\delta_1 > 0$, $U_{\delta_1}(u^*, \lambda^*)$ is a δ_1 -neighborhood of (u^*, λ^*) and F^Q be defined as above. Then there exist positive numbers γ , K , α and δ with

$$K\gamma < \alpha, \quad \delta < \delta_1$$

such that

$$\|F^Q(p^*, q, \lambda) - q^*\| \leq K\|q - q^*\|e^{-(\alpha - K\gamma)\Delta t}$$

whenever

$$\|q - q^*\| < \delta.$$

Moreover the sequence

$$q^{(k+1)} = F^Q(p^*, q^{(k)}, \lambda)$$

converges to the fixed point $q^* = F^Q(p^*, q^*)$.

The system (9) on the unstable subspace \mathbb{P} cannot be solved in the same manner as the system (10): the eigenvalues μ_1, \dots, μ_m of the linearization of G^P are to the right of the imaginary axis. Therefore we use Newton's method on \mathbb{P} . One Newton's step can be written in the form

$$p^{(k+1)} = F^P(p^{(k)}, q, \lambda)$$

with $F^P : \mathbb{P} \times \mathbb{Q} \times \mathbb{R} \rightarrow \mathbb{P}$,

$$F^P(p, q, \lambda) = p - \left(\frac{\partial G^P(p, q, \lambda)}{\partial p} \right)^{-1} G^P(p, q, \lambda). \quad (16)$$

Combining the two types of iterations on subspaces \mathbb{P} and \mathbb{Q} together we obtain the following iteration scheme:

$$p^{(k+1)} = F^P(p^{(k)}, q^{(k)}, \lambda) \quad (17)$$

$$q^{(k+1)} = F^Q(p^{(k)}, q^{(k)}, \lambda) \quad (18)$$

It can be shown that the above scheme is locally convergent. For details see [11]. We would like to emphasize that the analysis of local convergence is made under the assumptions that the decomposition $\mathbb{R}^n = \mathbb{P} \oplus \mathbb{Q}$ is known and the exact values of the flow ψ are available.

One step of the Projected RPM is sketched in the Fig.1. For comparison we introduce also a sketch of one iteration step of the original RPM method starting from the same point $u^{(k)}$, see Fig.2. Let us comment the differences between the two schemes. For simplicity we dropped the dependence on the bifurcation parameter λ .

In order to understand Fig.2 we introduce the flow $\varphi(t, u^{(k)})$ of the dynamical system

$$\dot{u} = G(u) \quad (19)$$

$$u(0) = u^{(k)}. \quad (20)$$

Figure 1: One step of the Projected RPM

In the original RPM, the dynamical simulation is applied to compute the flow $\varphi(\Delta t, u^{(k)})$. Then $q^{(k+1)}$ is the \mathbb{Q} -coordinate of $\varphi(\Delta t, u^{(k)})$, while $p^{(k+1)}$ is the \mathbb{P} -coordinate of $\varphi(\Delta t, u^{(k)})$ corrected by one Newton step.

On the other hand, see Fig.1, in the projected RPM $q^{(k+1)}$ is obtained by solving *projected* dynamical system (12), (13) and $p^{(k+1)}$ is computed by Newton's step.

2.2 Numerical implementation of the Projected RPM

In this section we provide a code of the Projected RPM. We drop details about the predictor and concentrate on the corrector routine.

Let us assume that a point (u_0, λ_0) lies on the solution curve Γ within the prescribed tolerance. A starting point $(u^{(0)}, \lambda^{(0)})$ is obtained via standard predictor (we used secant method in the computations). Afterwards coupled iterations (17), (18) are applied until a new point on Γ is reached. In order to benefit from the fact that Newton's method is necessary only in low-dimensional space \mathbb{P} we introduce new coordinate system which is represented by an orthonormal basis $Z \in \mathbb{R}^{n \times m}$. New coordinate $z \in \mathbb{R}^m$ is then defined by

$$z \equiv Z^T p = Z^T u.$$

Conversely

$$u = q + Zz.$$

Furthermore let

$$H(u, \lambda) \equiv Z^T G_u(u, \lambda) Z$$

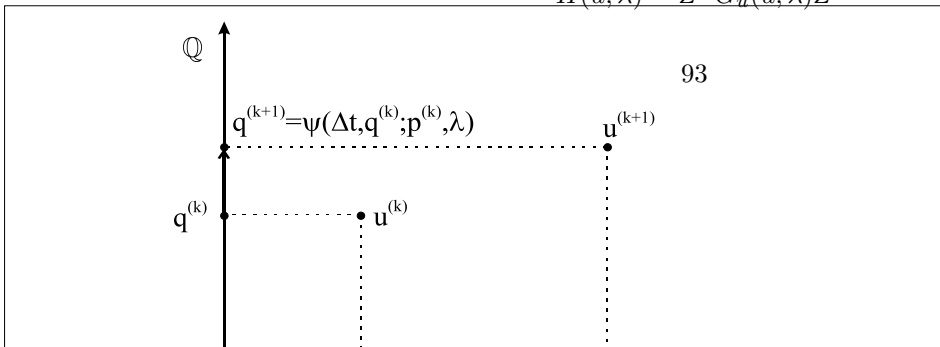


Figure 2: One step of the original RPM

denote $m \times m$ matrix which is the restriction of Jacobian $G_u(u, \lambda)$ on the subspace \mathbb{P} . To make the continuation past turning points possible we use one-dimensional bordering of the system (9). An augmented Newton's step in new coordinates has the form

$$\begin{pmatrix} H & Z^T G_\lambda \\ \dot{z} & \dot{\lambda} \end{pmatrix} \begin{pmatrix} z^{(k+1)} - z^{(k)} \\ \lambda^{(k+1)} - \lambda^{(k)} \end{pmatrix} = - \begin{pmatrix} Z^T G \\ 0 \end{pmatrix} \quad (21)$$

where $\dot{z}, \dot{\lambda}$ are approximations of the tangent vectors to the solution path in the "old" point (u_0, λ_0) projected on (\mathbb{P}, λ) plane. In the actual computation we have to approximate values of the flow ψ . We employed a standard Runge–Kutta integrator with automatic step control:

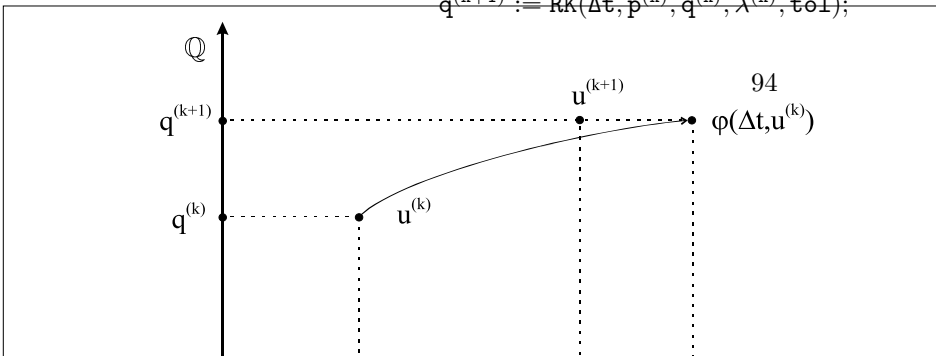
$$\psi(\Delta t, q; p, \lambda) \approx RK(\Delta t, p, q, \lambda, tol).$$

The last parameter sent to the Runge–Kutta procedure is the local discretization error tolerance tol . The Projected RPM corrector routine in terms of pseudocode looks as follows:

```

procedure ProjectedRPM ( $\mathbf{u}^{(0)}, \lambda^{(0)}$ )
   $\mathbf{G} := \mathbf{G}(\mathbf{u}^{(0)}, \lambda^{(0)});$ 
   $\mathbf{z}^{(0)} := \mathbf{Z}^T \mathbf{u}^{(0)}; \quad \mathbf{q}^{(0)} := \mathbf{u}^{(0)} - \mathbf{Z}\mathbf{z}^{(0)};$ 
   $\mathbf{H} := \mathbf{Z}^T \mathbf{G}_u(\mathbf{z}^{(0)}, \lambda^{(0)})\mathbf{Z};$ 
   $\mathbf{k} := 0;$ 
  while ( $\|\mathbf{G}\| > tolRes$ ) do
     $\mathbf{q}^{(k+1)} := RK(\Delta t, \mathbf{p}^{(k)}, \mathbf{q}^{(k)}, \lambda^{(k)}, tol);$ 

```



```


$$\begin{pmatrix} z^{(k+1)} \\ \lambda^{(k+1)} \end{pmatrix} := \begin{pmatrix} z^{(k)} \\ \lambda^{(k)} \end{pmatrix} - \begin{pmatrix} H & Z^T G_\lambda \\ \dot{z} & \dot{\lambda} \end{pmatrix}^{-1} \begin{pmatrix} Z^T G \\ 0 \end{pmatrix};$$

if ( $k > \text{iterMax}$ ) then IncreaseBasisSize();
 $\mathbf{u}^{(k+1)} := \mathbf{Z}\mathbf{z}^{(k+1)} + \mathbf{q}^{(k+1)}$ ;
 $\mathbf{G} := \mathbf{G}(\mathbf{u}^{(k+1)}, \lambda^{(k+1)})$ ;
 $k := k + 1$ ;
endwhile;
SubspaceIteration(Z);
end

```

In the algorithm above two procedure calls `IncreaseBasisSize` and `SubspaceIteration` are involved. The former is called in order to augment basis Z whenever coupled iterations fail to converge. The latter controls the accuracy of the invariant subspace \mathbb{P} . Both procedures are essentially based on the routines `increase_basis_size` and `power_iteration_step` described in sections 4.1 and 4.2 in [13].

The following table lists parameters used in the above algorithm together with values we used in the computations:

<code>tolRes</code>	$= 10^{-5}$	— used as a stopping criterion in the Projected RPM corrector.
<code>Δt</code>	$= 0.1$	— time step in the dynamical simulation
<code>iterMax</code>	$= 15$	— number of iterations after which the procedure <i>IncreaseBasisSize</i> is involved

3 Model problems

We compared performance of the Projected RPM with original RPM on two model problems. We provide three types of outputs:

- CPU times and number of function calls
- solution curves
- eigenvalue movies concerning unstable modes (paths of complex conjugate pairs are depicted in bold)

All computations were made on PC with processor Celeron on 433MHz and 384MB RAM under OS Linux. All methods were coded in C++ language and compiled by GNU gcc compiler.

3.1 Nonsymmetric system in dimension 1-D

We consider a nonsymmetric system of PDEs:

$$\begin{aligned} \frac{\partial v}{\partial t} &= \frac{1}{5} \frac{\partial^2 v}{\partial x^2} + \lambda(v - w) + \frac{1}{5} \lambda^2 e^v \\ \frac{\partial w}{\partial t} &= \frac{1}{5} \frac{\partial^2 w}{\partial x^2} + \lambda(v + w) + \frac{1}{5} \lambda^2 e^w \end{aligned}$$

with

$$v(0) = v(a) = 0, \quad w(0) = w(a) = 0.$$

In all computations we set $a = 1$. The above system is discretized by finite differences. A number of mesh points is denoted by nx . Table 1 shows CPU times and number of evaluation of the right-hand side G (nGCall) for problems with $nx = 30$ and $nx = 100$. Notice that the dimension of the resulting problem

	Original RPM		Projected RPM	
	$nx = 30$	$nx = 100$	$nx = 30$	$nx = 100$
CPU time [s]	400	1689	120	901
nGCall	6 499 101	8 803 972	1 705 799	3 677 995

Table 1: CPU times for nonsymmetric system in 1-D

is 60 or 200. Fig. 3 depicts the solution curve computed by Projected RPM for $nx = 100$. Fig. 4 shows the dependence of real parts of the eigenvalues μ_1, \dots, μ_m on the number of continuation steps cs . For comparison we computed the whole spectrum by Newton's method (QR method applied on Jacobian). Fig. 5 depicts the actual eigenvalue movie of the unstable modes. We observed that Hopf bifurcation point H2 was not detected by the Projected RPM.

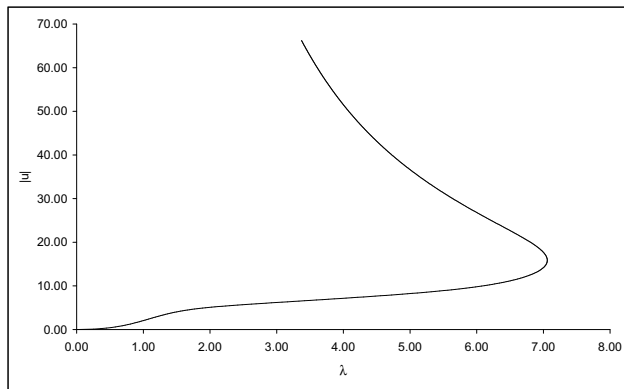


Figure 3: Solution path of nonsymmetric system in 1D for $nx=100$ computed by the Projected RPM

3.2 Nonsymmetric system in 2-D

Let us consider nonsymmetric system described in section 3.1 on a rectangle

$$(0, a) \times (0, b) \subset \mathbb{R}^2,$$

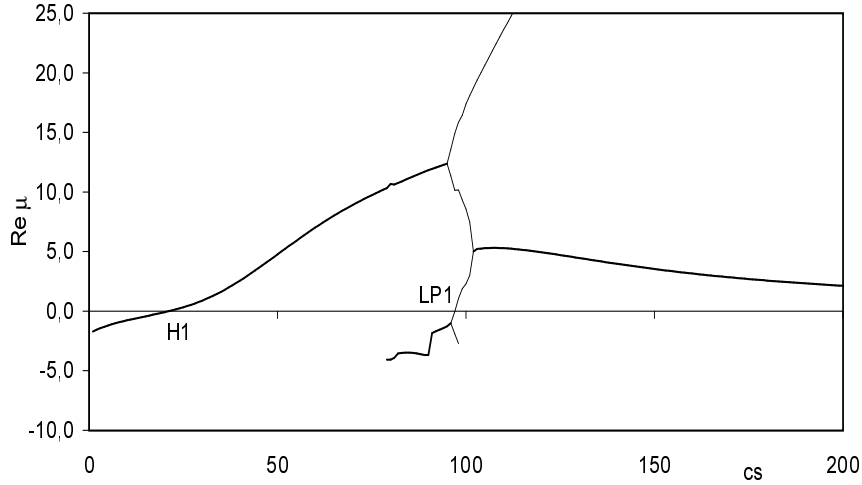


Figure 4: Eigenvalue movie of the unstable modes computed by Projected RPM

i.e. the following system of PDEs:

$$\frac{\partial v}{\partial t} = \frac{1}{5} \Delta v + \lambda(v - w) + \frac{1}{5} \lambda^2 e^v$$

$$\frac{\partial w}{\partial t} = \frac{1}{5} \Delta w + \lambda(v + w) + \frac{1}{5} \lambda^2 e^w$$

with Dirichlet boundary conditions

$$v(0, y) = v(a, y) = 0, \quad w(0, y) = w(a, y) = 0, \quad y \in (0, b),$$

$$v(x, 0) = v(x, b) = 0, \quad w(x, 0) = w(x, b) = 0, \quad x \in (0, a).$$

In all computations we set $a = 1$ and $b = 2$. The above system is discretized by finite differences with number of mesh points along x and y axis denoted by nx and ny . Table 2 shows CPU times and number of evaluations of the right-hand side G (nGCall) for problems with $nx = ny = 5$ and $nx = ny = 10$. Notice that the dimension of the resulting problem is 50 or 200, resp. Mind the paradoxical ratio of the CPU times for the cases $nx = ny = 5$ and $nx = ny = 10$. It is caused by the fact that the portions of the computed curves were not the same. The reason is the failure of both algorithms for $nx = ny = 10$. Fig. 6 depicts a solution curve computed by the Projected RPM for $nx = ny = 10$. Fig. 7 shows dependence of real part of the unstable modes μ_1, \dots, μ_m on the number of continuation steps cs . [h]

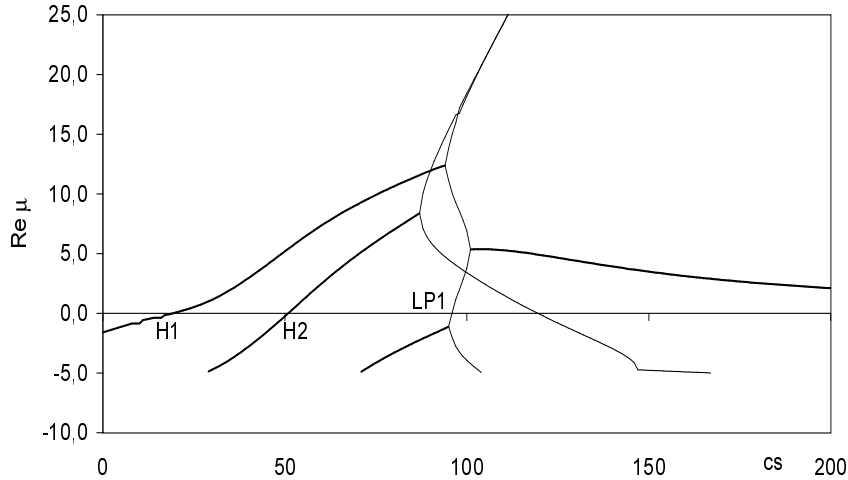


Figure 5: Eigenvalue movie of the unstable modes computed by Newton's method

	Original RPM		Projected RPM	
	$nx = 5$	$nx = 10$	$nx = 5$	$nx = 10$
CPU time [s]	639	547	173	189
nGCall	11 150 076	2 420 610	2 417 740	651 889

Table 2: CPU times for nonsymmetric system in 2-D

4 Conclusions

Numerical tests indicate that the Projected RPM is superior to the original version of the RPM. In our opinion it is due to the four following reasons:

- Solution of the dynamical system (12), (13) is bounded due to the Lemma. On the other hand the solution of the dynamical system (19), (20) may be unbounded whenever any unstable mode is present.
- In the Projected RPM the original system (5) is solved, especially Newton's step (16) is clearly defined. On the other hand the original version of the RPM relies on the fixed-point formulation which is not natural. In particular, the smallness of $\|u - F(u, \lambda)\|$ does not imply the smallness of $\|G(u, \lambda)\|$.
- Relation between the spectra $\sigma(G_u)$ and $\sigma(F_u)$ is not clear when a black-box solver is used. It is crucial for detection of Hopf bifurcation points.
- In usual cases when G arises from the discretization of PDEs the differential G_u is available explicitly. It is not true for F_u due to the machinery behind the fixed-point formulation.

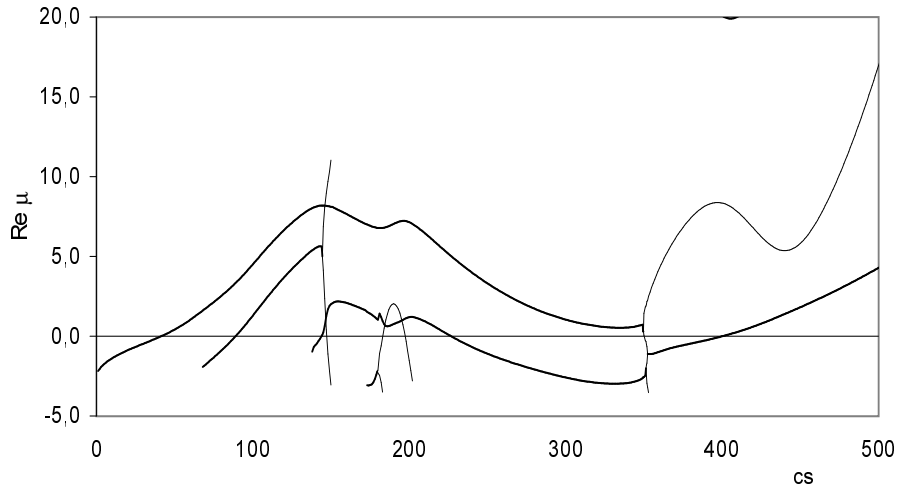
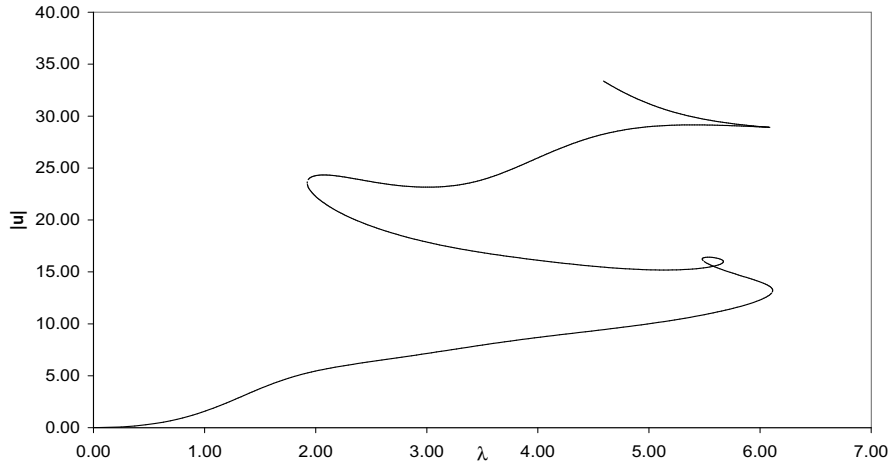


Figure 7: Eigenvalue movie of the unstable modes for nonsymmetric system in 2-D with $n_x=n_y=10$ computed by the Projected RPM

However both methods suffer from the same drawback: They seem to be sensitive to the accuracy with which we compute the basis Z . Unfortunately procedures maintaining the basis in both original and Projected RPM are essentially the same. We conclude that for any future effort to improve RPM this will be the key problem.

Acknowledgments: The authors gratefully acknowledge the support of Grant Agency of the Czech Republic (grant #201/98/0528) and grant MSM 113200007.

References

1. E. L. Allgower, K. Georg *Numerical continuation methods*, Springer Verlag, New York, 1990
2. W.-J. Beyn, W. Kless, V. Thümmer *Continuation framework for invariant subspaces and its application to travelling waves*, In: F. Keil, W. Mackens, H. Voss and J. Werther eds., Scientific Computing in Chemical Engineering II, pp 144–151, Springer, 1999
3. J. Bošek, V. Janovský *A note on the recursive projection method* Proceedings of GAMM96, ZAMM 1997, Berlin, pp.437-440
4. B. D. Davidson *Large-scale continuation and numerical bifurcation for partial differential equations*, SIAM J. Numer. Anal., 34(5)(1997), pp. 2001–2027
5. J. W. Demmel, L. Dieci, M. J. Friedman *Computing connecting orbits via an improved algorithm for continuing invariant subspaces*, to appear
6. T. J. Garratt, G. Moore, A. Spence *A generalised Cayley transform for the numerical detection of Hopf bifurcation points in large systems*, In Contributions in numerical mathematics, pp. 177–195, World Sci. Publ. 1993
7. W. Govaerts, *Numerical methods for bifurcation of dynamical equilibria*, SIAM, Philadelphia, 2000
8. W. Govaerts, A. Spence *Detection of Hopf points by counting sectors in the complex plane*, Numer. Math. 75(1996), pp. 43–58
9. J. Guckenheimer, M. Myers, B. Sturmfels *Computing Hops bifurcation I*, SIAM J. Numer. Anal. 34(1997), pp. 1–21
10. V. Janovský, O. Liberda *Recursive Projection Method for detecting bifurcation points*, Proceedings SANM'99, pp 121–134, Union of Czech Mathematicians and Physicists, 1999
11. V. Janovský, O. Liberda *Continuation of invariant subspaces via RPM*, in preparation
12. H. B. Keller *Numerical methods in bifurcation problems*, Springer Verlag, New York, 1987
13. G. M. Shroff, H. B. Keller, *Stabilization of unstable procedures: the Recursive Projection Method*, SIAM J. Numer. Anal., 30(4)(1993), pp. 1099–1120
14. M. Kubíček, M. Marek *Computational Methods in Bifurcation Theory and Dissipative Structures*, Springer(1983)
15. Š. Kubíček *Praktické implementace metod RPM1 a RPM2*, Diplomová práce, MFF UK Praha, 1997
16. K. Lust, D. Roose *Computation and bifurcation analysis of periodic solutions of large-scale systems*, IMA Preprint Series #1536, Feb 1998, IMA, University of Minnesota
17. R. Neubert *Predictor corrector techniques for detecting Hopf points*, Int. J. Bifurcation and Chaos 3 (1993), pp. 1311–1318
18. Y. Saad *Iterative methods for sparse linear systems*, PWS Publishing Company, Boston, 1996

The sweeping method for solving of boundary value problems for selfadjoint differential equations

Jiří Taufer

Department of Applied Mathematics
Faculty of Transportation Sciences
Czech Technical University in Prague
CZ Praha 1, Na Florenci 25

Abstract The idea of the transfer of conditions for a very general boundary value problem for a system of differential equations with inner and transition conditions originates in various methods which have been introduced in the papers [?,?], [?] and [?]. The present paper is devoted to a special problem and the method are chosen in order to exploit the additional information, above all the symmetry and some sign properties. The resulting method is very advantageous as to the effort expended and fulfills all of the numerical stability claims.

Mathematics Subject Classification (1991): 65L10

Keywords and phrases: ODE, Two point boundary value problem, Transfer of boundary condition, Selfadjoint differential equation.

1 Introduction

In this part we repeat the fundamental results of the methods based on the idea of the transfer of conditions for a two point boundary value problem for the system of N ordinary differential equations

$$x'(t) + A(t)x(t) = f(t) \quad \text{a.e. in } (a, b), \quad (1)$$

where $x(t)$ and $f(t)$ are $N \times 1$ vectors and $A(t)$ is $N \times N$ matrix. We suppose the entries of the matrix $A(t)$ and the components of the vector $f(t)$ to be Lebesgue-integrable functions on (a, b) (further $\in \mathcal{L}(a, b)$). The boundary conditions are supposed to be of the form

$$Ux(a) = u, \quad (2)$$

$$Vx(b) = v, \quad (3)$$

where U and V are rectangular matrices in general, with the number of columns equal to N . The number of the components of the vectors u and v equals the number of rows of the matrices U and V .

Definition 1 *The following problem will be called the problem ψ : The vector $x(t)$ absolutely continuous on $\langle a, b \rangle$ is sought which satisfies the following requirements:*

1. $x'(t) + A(t)x(t) = f(t)$ a.e. in (a, b) .
2. $Ux(a) = u$ and $Vx(b) = v$.

Now we will formulate the theorems of the transfer of the conditions for the problem ψ and we will define the basic algorithm for the solution of the problem. For the sake of definiteness let the matrices U and V have n_1 and n_2 rows, respectively.

Theorem 1 *Let $D(t)$ be an absolutely continuous $n_1 \times N$ matrix and $d(t)$ an absolutely continuous vector with n_1 components, satisfying the equations*

$$D'(t) = D(t)A(t) + Z_1(t, D(t), d(t))D(t) \quad \text{a.e. in } (a, b), \quad (4)$$

$$d'(t) = D(t)f(t) + Z_1(t, D(t), d(t))d(t) \quad \text{a.e. in } (a, b) \quad (5)$$

and the initial conditions

$$D(a) = K_1U, \quad (6)$$

$$d(a) = K_1u, \quad (7)$$

where $Z_1(t, D, d)$ is an $n_1 \times n_1$ matrix such that $Z_1(t, D(t), d(t)) \in \mathcal{L}(a, b)$ and K_1 is a nonsingular matrix of order n_1 .

Then

$$D(t)x(t) = d(t) \quad \text{for every } t \in \langle a, b \rangle \quad (8)$$

and for every solution of the problem ψ .

This theorem brings us to the transfer of the left boundary condition (2) on the whole interval $\langle a, b \rangle$. The equation (8) is called the transferred condition. We say that the matrix $D(t)$ and the vector $d(t)$ realize the transfer of the condition (2). Analogously we can formulate the theorem on the transfer of the right boundary condition.

Theorem 2 *Let $C(t)$ be an absolutely continuous $n_2 \times N$ matrix and $c(t)$ an absolutely continuous vector with n_2 components, satisfying the equations*

$$C'(t) = C(t)A(t) + Z_2(t, C(t), c(t))C(t) \quad \text{a.e. in } (a, b), \quad (9)$$

$$c'(t) = C(t)f(t) + Z_2(t, C(t), c(t))c(t) \quad \text{a.e. in } (a, b) \quad (10)$$

and the initial conditions (this time at the point b)

$$C(b) = K_2V, \quad (11)$$

$$c(b) = K_2v, \quad (12)$$

where $Z_2(t, C, c)$ is an $n_2 \times n_2$ matrix such that $Z_2(t, C(t), c(t)) \in \mathcal{L}(a, b)$ and K_2 is a nonsingular matrix of order n_2 .

Then

$$C(t)x(t) = c(t) \quad \text{for every } t \in \langle a, b \rangle \quad (13)$$

and for every solution of the problem ψ .

The proof of Theorem 1 and 2 is in [?,?]. Now we will introduce two algorithms to be applied to the boundary value problem for a selfadjoint equation of $2n$ th order.

Algorithm A. Let the problem ψ have a solution. We choose an absolutely continuous matrix $R(t)$ such that the matrix $(D(t)R(t))$ is nonsingular for all $t \in \langle a, b \rangle$. We look for the vector $r(t)$ solving the differential equation

$$r'(t) = R(t)f(t) + (R'(t) - R(t)A(t)) (D(t)R(t))^{-1} (d(t)r(t)) \quad (14)$$

from the right to the left with the initial condition at the point b

$$r(b) = R(b)p \quad (15)$$

where p is a solution of the equation

$$(D(b)R(b))p = (d(b)r(b)) \quad (16)$$

Then the solution $x(t)$ of the problem ψ is found from the system

$$(D(t)R(t))x(t) = (d(t)r(t)) \quad \text{for all } t \in \langle a, b \rangle. \quad (17)$$

Algorithm B. Let the problem ψ have a solution. We choose an absolutely continuous matrix $R(t)$ such that the matrix $(R(t)C(t))$ is nonsingular for all $t \in \langle a, b \rangle$. We look for the vector $r(t)$ solving the differential equation

$$r'(t) = R(t)f(t) + (R'(t) - R(t)A(t)) (R(t)C(t))^{-1} (r(t)c(t)) \quad (18)$$

from the left to the right with the initial condition at the point a

$$r(a) = R(a)p \quad (19)$$

where p is a solution of the equation

$$(R(a)C(a))p = (r(a)c(a)) \quad (20)$$

Then the solution $x(t)$ of the problem ψ is found from the system

$$(R(t)C(t))x(t) = (r(t)c(t)) \quad \text{for all } t \in \langle a, b \rangle. \quad (21)$$

The method described here is referred to as the sweeping method.